SECURITY CLASSIFICATION OF THIS PAGE *(When Data Entered)*

REPORT DOCUMENTATION PAGE

READ INSTRUCTIONS BEFORE COMPLETING FORM

1. REPORT NUMBER: AFWAL-TR-81-3059	2. GOVT ACCESSION NO.
3. RECIPIENT'S CATALOG NUMBER	
4. TITLE *(and Subtitle)*: A SOURCE-DOUBLET APPROACH TO MODELING TRIPLE EJECTOR RACK STORE CONFIGURATIONS AND FORCE CALCULATIONS	5. TYPE OF REPORT & PERIOD COVERED: Final Technical Report February 1979 - July 1980
	6. PERFORMING ORG. REPORT NUMBER
7. AUTHOR(s): Calvin L. Dyer, Charles B. Heath	8. CONTRACT OR GRANT NUMBER(s)
9. PERFORMING ORGANIZATION NAME AND ADDRESS: Flight Dynamics Laboratory (AFWAL/FIGC), Air Force Wright Aeronautical Laboratories (AFSC), Wright-Patterson Air Force Base, Ohio 45433	10. PROGRAM ELEMENT, PROJECT, TASK AREA & WORK UNIT NUMBERS: Program Element 62201F, 2403-0535
11. CONTROLLING OFFICE NAME AND ADDRESS: Flight Dynamics Laboratory (AFWAL/FIGC), Air Force Wright Aeronautical Laboratories (AFSC), Wright-Patterson Air Force Base, Ohio 45433	12. REPORT DATE: July 1981
	13. NUMBER OF PAGES: 93
14. MONITORING AGENCY NAME & ADDRESS *(if different from Controlling Office)*	15. SECURITY CLASS. *(of this report)*: UNCLASSIFIED
	15a. DECLASSIFICATION/DOWNGRADING SCHEDULE

16. DISTRIBUTION STATEMENT *(of this Report)*

Approved for public release; distribution unlimited.

17. DISTRIBUTION STATEMENT *(of the abstract entered in Block 20, if different from Report)*

18. SUPPLEMENTARY NOTES

19. KEY WORDS *(Continue on reverse side if necessary and identify by block number)*

Aerodynamic Interference
Flow Fields
Aerodynamic Loads
Store Separation
External Stores

20. ABSTRACT *(Continue on reverse side if necessary and identify by block number)*

The method presented in this reported extends the FDL Subsonic Store Separation Program to include the aerodynamic modeling of the separating store as well as adjacent stores and the ejector rack. In the work presented in AFFDL-TR-74-130 only the volume effects of the stores and ejector rack are accounted for and Slender Body theory is used to calculate forces and moments on the separating store. In this report, doublets are used to model the upwash and sidewash of adjacent stores and the ejector rack. The induced flow-field portion of the total aircraft flow-field is included in the boundary conditions.

DD FORM 1 JAN 73 1473 EDITION OF 1 NOV 65 IS OBSOLETE

SECURITY CLASSIFICATION OF THIS PAGE *(When Data Entered)*

Once the non-uniform flow-field has been modeled, three-dimensional point sources and doublets along the separating store axis are used to calculate loadings. Store loadings using Slender Body theory and the Source-Doublet method are compared to wind tunnel data.

It is hoped that this method might offer a viable alternative to a complete mutual interference solution such as a paneling approach.

FOREWORD

This report presents an extension of the ideas contained in Appendix III of AFFDL-TR-72-83, Volume I. This effort extends the formulation given in Appendix III to compressible flows and accounts for forces in non-uniform flow. Upwash and sidewash modeling has been included for the stores and ejector rack adjacent to the store for which loading calculations are being performed. Comparisons of results with experimental data are presented. This report covers work performed between February 1979 and July 1980 by Calvin L. Dyer and Charles B. Heath (AFWAL/FIGC).

TABLE OF CONTENTS

LIST OF ILLUSTRATIONS

LIST OF ILLUSTRATIONS (Cont'd)

LIST OF ILLUSTRATIONS (Concluded)

LIST OF SYMBOLS

C_{d_c}	Cross flow drag coefficient
C_n	Normal force coefficient due to integrated surface pressure
C_y	Side force coefficient due to integrated surface pressure
C_{ℓ_m}	Pitching moment coefficient due to integrated surface pressure
C_{ℓ_n}	Yawing moment coefficient due to integrated surface pressure
$C_{n_{(BY)}}$	Normal force coefficient due to buoyancy
$C_{y_{(BY)}}$	Side force coefficient due to buoyancy
$C_{\ell_{m_{(BY)}}}$	Pitching moment coefficient due to buoyancy
$C_{\ell_{n_{(BY)}}}$	Yawing moment coefficient due to buoyancy
$C_{n_{(CF)}}$	Normal force coefficient due to cross flow drag
$C_{y_{(CF)}}$	Side force coefficient due to cross flow drag
$C_{\ell_{m_{(CF)}}}$	Pitching moment coefficient due to cross flow drag
$C_{\ell_{n_{(CF)}}}$	Yawing moment coefficient due to cross flow drag
C_p	Pressure coefficient
D	Store reference diameter
$\hat{e}_x, \hat{e}_r, \hat{e}_\theta$	Unit vectors in the x, r, and θ directions
K	Control point number index
ℓ_R	Reference length, taken as the maximum store diameter

LIST OF SYMBOLS (Cont'd)

ℓ_S	Store length
M_∞	Free stream mach number
N	Number of sources, horizontal doublets, and vertical doublets
$\vec{n}$	Unit normal vector to body surface
$\vec{q}(x,r,\theta)$	Perturbation velocity vector
R(x)	Store radius as function of x
S_r	Reference area, taken as maximum store cross section area
u,v,w	Perturbation velocities in physical, compressible space in the x, y, and z directions
u', v', w'	Perturbation velocities in incompressible space in the x', y', and z' directions
$u_x(x,r,\theta)$, $v_r(x,r,\theta)$ $u_\theta(x,r,\theta)$	Perturbation velocities in the x, r, and o directions
u_{x_s}, u_{r_s}	Perturbation velocities due to the sources
$u_{x_{d,v}}$, $u_{r_{d,v}}$, $u_{\theta_{d,v}}$	Perturbation velocities due to horizontal doublets
$u_{x_{d,w}}$, $u_{r_{d,w}}$, $u_{\theta_{d,w}}$	Perturbation velocities due to vertical doublets
U(x), V(x), W(x)	Components of $\vec{V}(x, r, \theta)$ in the x, y, and z directions at one arbitrary field point
$\vec{V}(x,r,\theta)$	Velocity vector describing the non-uniform flow field
$\vec{V}_R$	Resultant velocity vector, sum of $\vec{V}$ and $\vec{q}$
x, y, z	Cartesian coordinates in physical, compressible space
x', y', z'	Cartesian coordinates in incompressible space
x_i	X location on the store axis of the i^{th} source, horizontal doublet, or vertical doublet

LIST OF SYMBOLS (Concluded)

x_k	X location on the store axis of the k^{th} control point
x_{mom}	X location on store axis about which moments are calculated
x_{sep}	X location on store axis at which separation is specified
x, r, θ	Cylindrical coordinates in physical, compressible space
x', r', θ'	Cylindrical coordinates in incompressible space
z_p	Distance in z direction between store center of gravity and carriage location
β	$\sqrt{1 - M_\infty^2}$
γ	Ratio of Specific Heats
μ	I^{th} Singularity Strength
∞	Denotes Freestream Condition

SECTION I

INTRODUCTION

This effort extends the FDL Subsonic Store Separation Program by changing the aerodynamic models for the separating and adjacent stores as well as the ejector rack model. The method presented here is an extension of the work described in Appendix III of Reference 1. The advantage of this approach is that it does not employ the slender body assumption of the linear form of the boundary condition.

SECTION II

FLOW TANGENCY BOUNDARY CONDITIONS ON THE BODY SURFACE

The coordinate systems used to calculate the source and doublet strengths and associated velocities, i.e., velocities used in boundary condition formulation and resultant velocities once the source and doublet strengths have been determined, are shown in Figure 1. The transformation of the non-uniform flow-field velocity vector from cartesian coordinates to cylindrical coordinates is given by

$$\vec{V}(x,r,\theta) = [V(x)\cos\theta + W(x)\sin\theta + W(x)\sin\theta]\,\vec{e}_r + [W(x)\cos\theta - V(x)\sin\theta]\,\vec{e}_\theta + U(x)\vec{e}_x \qquad (1)$$

where U(x), V(x) and W(x) are the components of the velocity vector in the x,y, and z directions, respectively.

If the body surface is specified by a function

$$F(x, r, \theta,) = 0 \qquad (2)$$

then the unit normal vector to the body surface is given by

$$\vec{n} = \frac{\text{grad } F}{|\text{grad } F|} \qquad (3)$$

Where $\text{grad } F = \frac{\partial F}{\partial r}\,\vec{e}_r + \frac{1}{r}\frac{\partial F}{\partial \theta}\,\vec{e}_\theta + \frac{\partial F}{\partial X}\,\vec{e}_x$

The perturbation flow field induced by the store body can be characterized by the perturbation velocity vector $\vec{q}(x, r, \theta)$, i.e.,

$$\vec{q}\,(x,r,\theta) = u_r(x,r,\theta)\vec{e}_r + u_\theta(x,r,\theta)\vec{e}_\theta + u_x(x,r,\theta)\vec{e}_x \qquad (4)$$

Where u_x, u_r, and u_θ are the perturbation velocities in the x, r, and θ directions (see Figure 1), then the flow tangency boundary condition is given by

$$\vec{V}_R \cdot \vec{n} = 0 \qquad (5)$$

where $\vec{V}_R$ (the resultant velocity) is the sum of $\vec{V}$, after the transformation given by Equation 1 has been applied, and $\vec{q}$, given by Equation 4. Expanding Equation 5 by using Equations 1 and 4 gives

$$[V(x)\cos\theta + W(x)\sin\theta + u_r(x,r,\theta)]\frac{\partial F}{\partial r} +$$

$$[W(x)\cos\theta - V(x)\sin\theta + u_\theta(x,r,\theta)]^1/r\frac{\partial F}{\partial \theta} +$$

$$[U(x) + u_x(x,r,\theta)]\frac{\partial F}{\partial x} = 0 \qquad (6)$$

$$\text{on } F(x,r,\theta) = 0 .$$

Equation 6 is the non-linear flow tangency condition for an arbitrary body immersed in a non-uniform flow-field. We are going to restrict ourselves to a closed body of revolution from this point on in this report. With this in mind, the local body radius (r) is a function of x alone. So,

$$r = R(x)$$

which can be rewritten

$$r - R(x) = 0 \qquad (7)$$

and since $F(x, r, \theta) = 0$ describes the body shape

$$r - R(x) = F(x,r,\theta)$$

which leads to

$$\frac{\partial F}{\partial r} = 1 \quad , \quad \frac{\partial F}{\partial x} = -\frac{dR(x)}{dx} \quad , \quad \frac{\partial F}{\partial \theta} = 0$$

Substituting into the flow tangency condition (Equation 6 yields

$$u_r(x,r,\theta) = [U(x) + u_x(x,r,\theta)]\frac{dR(x)}{\partial x} - V(x)\cos\theta - W(x)\sin\theta \qquad (8)$$

on the body surface.

The boundary conditions of Equation 8 will be split along the cartesian axes. This allows the problem to be handled as the superposition of three separate problems. The three problems are:

(1) Axisymmetric flow past a body of revolution with the flow field characterized by velocity U (x). This part of the problem will be modeled with three-dimensional point sources, hence the subscript s.

$$u_{r_s}(x,r) = [U(x) + u_{xs}(x,r)] \frac{dR(x)}{dx} \quad \text{on } r = R(x). \tag{9}$$

(2) Lateral flow past the body characterized by velocity V(x). This part of the problem will be modeled by horizontal doublets and is denoted by the subscript d,v.

$$u_{r_{d,v}}(x,r,\theta) = u_{x_{d,v}}(x,r,\theta) \frac{dR(x)}{dx} - V(x)\cos\theta \quad \text{on } r = R(x). \tag{10}$$

(3) Vertical flow past the body characterized by velocity W (x). This part of the problem will be modeled by vertical doublets and is denoted by the subscript D,W.

$$u_{r_{d,w}}(x,r,\theta) = u_{x_{d,w}}(x,r,\theta) \frac{dR(x)}{dx} - W(x)\sin\theta \quad \text{on } r = R(x) \tag{11}$$

SECTION III

TREATMENT OF COMPRESSIBILITY AND FORMULATION TO DETERMINE SINGULARITY STRENGTHS

At this point, the present work departs from that of Appendix III of Reference 1. The approach used to solve for the singularity strength is to transform the problem to an equivalent incompressible one, determine the incompressible singularity strengths, and then transform the resultant flow field back to the compressible case. In Reference 2, pages 568 through 581, Karamcheti discusses the various aspects of determining point singularities for incompressible flow past a body of revolution. The principal transformations used are

$$x' = \frac{x}{\beta} \quad , \quad y' = y \quad , \quad z' = z \tag{12}$$

$$u' = \beta^2 u \quad , \quad v' = \beta v \quad , \quad w' = \beta w \tag{13}$$

$$\text{where } \beta = \sqrt{1 - M_\infty^2}$$

The primes denote incompressible space. The unprimed quantities are in compressible space (physical space). These transformations are explained in Reference 3, pages 5 through 7. By applying these transformations, we can use the various incompressible velocity formulas given in Appendix III of Reference 1. In the equations that follow in this section, the primes have been dropped for convencience, i.e., x in the formulas should be x' and $r = r' = (y')^2 + (z')^2$, but since y' = y and z' = z, the prime on r is superfluous.

The axisymmetric problem may be modeled by a distribution of three-dimensional point sources along the store body axis. The incompressible velocity components produced by N sources, located on the X axis (Figure 1) at x_i, i=1, N, at a field point (x,r) are given by:

$$\left.\begin{aligned} u_{r_s}(x,r) &= \frac{1}{4\pi} \sum_{i=1}^{n} \mu_{s_i} \frac{r}{\left[(x - x_i)^2 + r^2\right]^{3/2}} \\ u_{x_s}(x,r) &= \frac{1}{4\pi} \sum_{i=1}^{n} \mu_{s_i} \frac{x - x_i}{\left[(x - x_i)^2 + r^2\right]^{3/2}} \end{aligned}\right\} \tag{14}$$

where the $^{\mu}s_i$'s are the as yet undetermined source strengths. By substituting Equation 14 into Equation 9 we get N equations for the N source strengths, $^{\mu}s_i$, if we can prescribe $^{u}x_s$ (x,r) (the perturbation velocity at the N control points).

$$\frac{1}{4\pi} \sum_{i=1}^{n} {}^{\mu}s_i \frac{R(x_k) - (x_k - x_i)\frac{dR(x_k)}{dx}}{\left[(x_k) - x_i)^2 + R^2(x_k)\right]^{3/2}} = U(x_k) \frac{dR(x_k)}{dx} \qquad (15)$$

$$0 \leq x_k \leq \ell_s; \quad k = 1,2,\ldots n-2$$

By using the method described in Reference 4, we can define $U(x_k,R)$ for the aircraft/store configuration of our choice. Two of the above equations will be deleted in order to enforce the existence of a stagnation point at the store nose, and assure that conservation of mass is satisfied. By setting x_k=0, which implies $R(x_k)$=0, in Equation 15 we force the store nose to become a stagnation point.

$$\frac{1}{4\pi} \sum_{i=1}^{n} \frac{{}^{\mu}s_i}{x_i^2} = U(0,0) \qquad (16)$$

The conservation of mass is satisfied by setting the sum of the sources strengths equal to zero:

$$\frac{1}{4\pi} \sum_{i=1}^{n} {}^{\mu}s_i = 0 \qquad (17)$$

This allows us to apply Equation 15 at N-2 points along the store body surface. Experience has shown that spacing the sources proportioned to the local body radius and applying Equation 15 at the midpoint between successive sources gives the best results. If Equation 15 was applied at midpoint between the N sources, there would be N-1 equations. Again, experience has shown that if we delete the fourth control point upstream

from the point on the body where the maximum radius is first reached, we get a favorable solution.

The second or sidewash problem is represented by a distribution of three-dimensional point doublets whose axes are aligned horizontally to oppose the sidewash, i.e. flow in the y direction in Figure 1. The incompressible velocity components produced by N doublets located on the store body axis (x axis Figure 1) are given by:

$$\left.\begin{aligned}
u_{r_{d,v}}(x,r,\theta) &= \frac{\cos\theta}{4\pi}\sum_{i=1}^{n}\frac{\mu_{d_i,v}}{\left[(x-x_i)^2+r^2\right]^{3/2}} \\
&\quad - \frac{3\cos\theta}{4}\sum_{i=1}^{n}\frac{\mu_{d_i,v}r^2}{\left[(x-x_i)^2+r^2\right]^{5/2}} \\
u_{\theta_{d,v}}(x,r,\ ) &= -\frac{\sin\theta}{4\pi}\sum_{i=1}^{n}\frac{\mu_{d_i,v}}{\left[(x-x_i)^2+r^2\right]^{3/2}} \\
u_{x_{d,v}}(x,r,\theta) &= -\frac{3\cos\theta}{4\pi}\sum_{i=1}^{n}\frac{d_{i,v}r(x-x_i)}{\left[(x-x_i)^2+r^2\right]^{5/2}}
\end{aligned}\right\} \quad (18)$$

Substituting Equations 18 into the boundary conditions given by Equation 10 gives:

$$\left.\begin{aligned}
&\frac{1}{4\pi}\sum_{i=1}^{n}\frac{-\mu_{d_i,v}}{\left[(x_k-x_i)^2+R^2(x_k)\right]^{3/2}} \\
&\quad\cdot\left[1-3R(x_k)\,\frac{R(x_k)-(x_k-x_i)\dfrac{dR(x_k)}{dx}}{(x_k-x_i)^2+R^2(x_k)}\right]=V(x_k)
\end{aligned}\right\} \quad (19)$$

$$0 \le x_k \le \ell_s; \quad k = 1,2,\ldots n$$

When x_k denotes the control point location and $R(x_k)$ is the body radius at x_k. The doublets' locations and control points are chosen to be at the midpoint between each source. This will provide N-1 locations, so the Nth doublet and control point were arbitrarily chosen to coincide with the last source location. Reference 4 is used to determine $V(x_k)$.

The third problem, upwash, is solved in the same manner as the sidewash problem. N vertical doublets are placed on the store body longitudinal axis. The incompressible velocity components are given by:

$$\left.\begin{aligned} u_{r_{d,w}}(x,r,\theta) &= \frac{\sin\theta}{4}\sum_{i=1}^{n}\frac{\mu_{d_i,w}}{\left[(x-x_i)^2+r^2\right]^{3/2}} \\ &\quad -\frac{3\sin\theta}{4\pi}\sum_{i=1}^{n}\frac{\mu_{d_i,w}r^2}{\left[(x-x_i)^2+r^2\right]^{5/2}} \\ u_{\theta_{d,w}}(x,r,\theta) &= \frac{\cos\theta}{4}\sum_{i=1}^{n}\frac{\mu_{d_i,w}}{\left[(x-x_i)^2+r^2\right]^{3/2}} \\ u_{x_{d,w}}(x,r,\theta) &= -\frac{3\sin\theta}{4\pi}\sum_{i=1}^{n}\frac{\mu_{d_i,w}r(x-x_i)}{\left[(x-x_i)^2+r^2\right]^{5/2}} \end{aligned}\right\} \quad (20)$$

Substituting Equations 20 into the boundary condition given by Equation 11 gives:

$$\frac{1}{4\pi}\sum_{i=1}^{n}\frac{-\mu_{d_i,w}}{\left[(x_k-x_i)^2+R^2(x_k)\right]^{3/2}} \cdot\left[1-3R(x_k)\,\frac{R(x_k)-(x_k-x_i)\frac{dR(x_k)}{dx}}{(x_k-x_i)^2+R^2(x_k)}\right] = W(x_k) \quad (21)$$

$$0 \le x_k \le \ell_s; \qquad k = 1,2,\ldots n$$

The nomenclature for the vertical doublets and control point locations is the same as for the horizontal doublets. The method of Reference 4 is used to calculate $W(x_k)$.

SECTION IV

SELECTION OF PRESSURE-VELOCITY RELATIONSHIP

Once the singularity strengths in Equations 14, 18, and 20 have been determined, they can be used to calculate the velocity at any point on the body surface. The surface velocity can be related to the surface pressure through various relationships. In Reference 1, the incompressible Bernoulli equation was used. This restricted the range of Mach numbers for which their results would be valid, but it has the nice feature that the analytical expressions for the circumferential pressure distribution could be integrated in closed form. In Reference 5 and other places, it has been found that the isentropic compressible Bernoulli equation relates theoretical prediction to experimental results better than the theoretically consistent linear relationship. In order to extend the present method to compressible speeds and take advantage of this improved correlation (Reference 5) the isentropic compressible Bernoulli equation was selected from Reference 6 as the pressure-velocity relationship for this application.

$$C_p = \frac{2}{\gamma M_\infty^2}\left\{\left[1 + \frac{\gamma-1}{2} M_\infty^2 \left(1 - \frac{u^2}{U_\infty^2}\right)\right]^{\gamma/(\gamma-1)} - 1\right\} \qquad (22)$$

The disadvantage to this approach is that the circumferential pressure distribution is not readily amenable to integration in a closed form. However, the pressures can be numerically integrated both circumferentially and longitudinally.

SECTION V

PROCEDURE FOR CALCULATING BODY FORCES AND MOMENTS

The forces and moments on the separating store are calculated by integrating the pressure circumferentially and longitudinally on the surface and adding a term to account for buoyancy when the store is in non-uniform flow. Aft of the point of flow separation a viscous cross-flow drag coefficient is used to calculate the forces.

The equations used to determine the forces and moments acting on the store are:

$$\left.\begin{aligned} C_N &= \int_0^{x_{sep}} \int_0^{2\pi} C_p(x,\theta)\,(-\sin\theta)\,r(x)\,d\theta\,dX \\ C_y &= \int_0^{x_{sep}} \int_0^{2\pi} C_p(x,\theta)\,(-\cos\theta)\,r(x)\,d\theta\,dX \\ C_{\ell_m} &= \int_0^{x_{sep}} \int_0^{2\pi} (X_{mom} - X)\,C_p(x,\theta)\,(-\sin\theta)\,r(x)\,d\theta\,dX \\ C_{\ell_N} &\int_0^{x_{sep}} \int_0^{2\pi} (X_{mom} - X)\,C_p(x,\theta)\,(-\cos\theta)\,r(x)\,d\theta\,dX \end{aligned}\right\} \quad (23)$$

Figure 1 shows the sign convention for theta. The buoyancy contribution to the forces and moments is given by:

$$\left.\begin{aligned} C_{n_{(BY)}} &= \frac{2\pi}{S_R} \int_0^{x_{sep}} r^2 \frac{d\left(\frac{w(x)}{u_\infty}\right)}{dx_s}\,dx_s \\ C_{y_{(By)}} &= \frac{2\pi}{S_R} \int_0^{x_{sep}} r^2 \frac{d\left(\frac{v(x)}{u_\infty}\right)}{dx_s}\,dx_s \\ C_{\ell_{m_{(BY)}}} &= \frac{2\pi}{S_R \ell_R} \int_0^{x_{sep}} (x_{mom} - x) r^2 \frac{d\left(\frac{w(x)}{u_\infty}\right)}{dx_s}\,dx_s \end{aligned}\right\} \quad (24)$$

$$C_{\ell_{N_{(BY)}}} = \frac{2\pi}{S_R \ell_R} \int_0^{x_{sep}} (x_{mom} - x) r^2 \frac{d(\frac{v(x)}{u_\infty})}{dx_s} \, dx_s \qquad \text{(24 Contd)}$$

From Reference 1, pages 27 and 28.

Potential flow is assumed along the body up to a specified point. After this point, the forces and moments are calculated using crossflow drag theory. The equations for the crossflow drag forces and moments are:

$$\left.\begin{aligned}
C_{N_{(CF)}} &= \frac{2C_{D_c}}{S_R} \int_{x_{sep}}^{\ell_s} r \left(\frac{v(x)}{u_\infty}\right)^2 + \left(\frac{w(x)}{u_\infty}\right)^2 \frac{w(x)}{u_\infty} \, dx_s \\
C_{F_{(CF)}} &= \frac{2C_{D_c}}{S_R} \int_{x_{sep}}^{\ell_s} r \left(\frac{v(x)}{u_\infty}\right)^2 + \left(\frac{w(x)}{u_\infty}\right)^2 \frac{v(x)}{u_\infty} \, dx_s \\
C_{\ell_{M_{(CF)}}} &= \frac{2C_{D_c}}{S_R \ell_R} \int_{x_{sep}}^{\ell_s} (X_{mom} - x) \, r \left(\frac{v(x)}{u_\infty}\right)^2 + \left(\frac{w(x)}{u_\infty}\right)^2 \frac{w(x)}{u_\infty} \, dx_s \\
C_{\ell_{N_{(CF)}}} &= \frac{2C_{D_c}}{S_R \ell_r} \int_{x_{sep}}^{\ell_s} (X_{mom} - x) \, r \left(\frac{v(x)}{u_\infty}\right)^2 + \left(\frac{w(x)}{u_\infty}\right)^2 \frac{v(x)}{u_\infty} \, dx_s
\end{aligned}\right\} \quad (25)$$

from Reference 1, page 29. Guidance is given on page 29 of Reference 1 for determining the point at which separation occurs for bodies in uniform flow. No generalized formula has yet been devised to determine the flow separation point on bodies in non-uniform flow fields.

SECTION VI

PROBLEMS ENCOUNTERED AND RESULTS OBTAINED BY INTRODUCING THE SOURCE-DOUBLET METHOD OF CALCULATING BODY FORCES AND MOMENTS

Method verification proceeded from the relatively simple case of uniform flow to the complex flow-field of a realistic aircraft/stores configuration. Comparisons were made with data from References 7, 8, and 9, to demonstrate the validity and improvement of the basic approach. Flow-field data as well as force and moment data were used to assess the method. Free-stream predictions were compared with data at angles of attack of 2°, 4°, 6°, and 8° at Mach numbers of .25 and .70. The realistic aircraft/stores configuration was built up from a simple wing-body configuration by the addition of various components, i.e. pylon, rack, stores, and engine inlets. Non-uniform flow-field predictions were compared with data at 0° and 6° angle of attack at Mach number of .70.

Several check cases were run for the ogive cylinder store (Figure 2a) in a uniform flow. In implementing this procedure, the first problem that occurred was negative pressures. By casting the boundary conditions for the sources in terms of the body slope (see Equation 9) instead of the body radius, the zero streamline is not necessarily on the body surface. The use of body slope boundary conditions was found to give the "best", i.e. smoothest body representation, see References 1 and 3. No matter what is used as the boundary conditions, the mathematical models (sources and sinks) are going to produce some waviness in the zero streamline. The problem is illustrated in Figure 2b. To resolve this problem at each place along the body where the surface pressure was required, the location of the zero streamline was calculated. The pressure calculations were then performed on the zero streamline.

Once the method was giving numerical results, several other questions arose. First, how many singularities are required to give a meaningful answer? Of course, there is a trade-off between the number of singularities and computational time. To answer this question, runs were made varying the number of singularities. But before this question could be resolved, a problem with the loading predictions on the aft end of the store was encountered as illustrated in Figure 3. Figure 3 shows the

distributed NORMAL force $\frac{dCn}{dx}$ along the store. Distributed loads obtained by integrating experimentally measured pressures are indicated by the points with circles around them. The dashed line shows theoretical prediction based on slender body theory as given by Equation 46, Reference 1. The solid lines represent the theoretical predictions based on the Source-Doublet method presented in this report. Below the horizontal axis is a silhouette of the store shape for which the calculations were performed. At the top of the figure are the Mach number and angle of attack for which the calculations were presented. The second line of the heading gives the number of circumferential segments the store was broken into for pressure calculations and integration in conjunction with the Source-Doublet predictions. Also on the second line is the number of singularities used to model the store, i.e. the number of sources and sinks or doublets. The axial division of the body was proportional to the body radius. This was found to enhance the fidelity of the volume modeling (source-sink) of the body in Reference 3. The control points for both the source-sinks and the doublets were located midway between the sources on the body surface. The doublets were located on the body axis at the same longitudinal location as the control points. The third line is the number of equal length body segments the store was divided into for the slender body theory calculations. Just below the header information is the legend for the various symbols on the plot. To the right of the legend is the integrated loads and measured loads from a strain-gauge balance inside the model. The reference area is the store maximum cross-sectional area. The reference length is the store maximum diameter. The moment reference center was chosen to be at the store midpoint. The pressure data was obtained independently of the strain-gauge balance data, so the question of how pressure lines bridging a balance affect the load is not a problem in this data set. The columns are normal force coefficient (C_n) and pitching moment coefficient (C_m). Note that the last pressure data point, i.e. the point at x = .531 ft, is on extrapolated value. This was done so Simpson's Rule could be used to integrate the loadings.

Two problems are evident in the aft end loading. The jump in loading at x = .48 feet is caused by shifting to the viscous cross flow method of predicting forces as prescribed by Equation 50, Reference 1. Based on the pressure data, and considering this same behavior was observed at lower Mach numbers and angles of attack, it was decided to assume the flow was attached over the whole length of the body. This assumption is used for all subsequent calculations in this report. Although the second problem, a large negative load, in predicting the loading on the aft end of the store is evident in Figure 3, it is shown much more graphically in Figure 4. This problem results from the way the body wake is being modeled. To satisfy the law of conservation of mass, the body must be closed. In References 1, 3, and 4, it had been common practice to close the bodies by modeling the wake with the same shape as the nose. This was our initial approach, but as can be seen in Figure 4, the resultant velocities near the aft end of the store were much higher than experimental results indicate. This problem was corrected by extending the body one diameter downstream and then closing it with a wake of the same shape as the nose. Figure 5a is typical of the loadings produced by extending body. Based on the results illustrated in Figure 5a and the other comparisons in the free-stream at other Mach numbers and angles of attack. In all subsequent calculations, the wake is modeled by extending the body one diameter downstream and closing the body with the same shape as the nose.

At this point, we are prepared to tackle the question of how many sources are required to adequately model the loading. As an aside to this question an investigation into type of integration and the number of circumferential segments required was also undertaken. Simpson's Rule and Trapezoidal Rule integration were both tried. It was found that twenty circumferential segments yielded converged solutions and that for twenty circumferential segments either method of integration produced essentially identical results, see Table 1. The Trapezoidal Rule was employed, since it was easier to implement, faster and less restrictive in point spacing. Figure 6 shows a plot of C_n versus the number of singularities. It can be seen that in the range of 60 to 70 singularities,

TABLE 1

C_n, C_m, VERSUS NUMBER OF SINGULARITIES

Mach Number = .25 Angle of Attack = 8.0°

20 Circumferential Segments

T = Trapezoidal Rule Integration

S = Simpson's Rule Integration

Number of Singularities	C_{n_T}	C_{m_T}	C_{n_S}	C_{m_S}
50	.26133	.84407	.26136	.84406
58	.26563	.85719	.26566	.85718
69	.26721	.86170	.26724	.86169
86	.26640	.86569	.26643	.86580
98	.26659	.86616	.26662	.86615

the solution becomes convergent for uniform flow. All subsequent calculations assume that the 60 to 70 singularities will yield converged solutions for non-uniform flow-fields as well.

Figure 5 presents comparisons for Mach numbers of .25 and .70 for angle of attack of 2°, 4°, 6°, and 8°. These comparisons are for the ogive-cylinder store, Figure 2, in a uniform flow-field. The pressure loadings were obtained with a single longitudinal row of pressure taps in a meridional plane. The model was rotated through 360 degrees in 10 degree increments. Then the pressures were integrated circumferentially to obtain the running loads that are plotted in Figure 5. The data point at x = .1386 feet is somewhat questionable. It is clear from the response to angle of attack and Mach number that the tap is not plugged. This problem could be caused by a local imperfection in the body surface or maybe a small leak in the pressure line which would be proportional to the pressure at the tap. It appears that the value of DC_n/DX for this tap should be reduced in magnitude to conform to the trend of the other data points. It is interesting to observe that reducing the value would degrade the normal force correlation between the pressure and strain-gauge data in every case presented in Figure 5. The reduction would improve pitching moment correlation between the two types of data for all angles of attack at Mach number of .25 but only at 8 degrees angle of attack at Mach number of .70.

The agreement between the two types of experimental data and theory is not as good as hoped for. The location of the center of pressure was calculated for both types of data trying to get some insight into the lack of data to data correlation. In some instances, the variation in center of pressure, based on the data, was greater than one body diameter. The disagreement between the two types of data is not understood.

Correlation between either theoretical method and either type of data was less than excellent. Both theoretical methods correlate better with the loads obtained by integrating the pressure data. Usually within 10 percent on normal force and 20 percent on pitching moment. The Source-Doublet method did predict some lift carry-over on to the body

aft of the nose due to its three-dimensional nature. It appears that on the upper surface of the body in the x = .17 to .20 foot range that there may be some recompressions on the upper surface which is not predicted by either theory. Of course, Slender Body Theory could not be expected to predict this, since for uniform flow it degenerates into a term which is only a function of the rate of change of cross-sectional area. The Source-Doublet method's pitching moment prediction correlated better with the strain-gauge data than do the Slender Body Theory predictions. Based on this and the fact that the normal force prediction of the Source-Doublet method were nearly as close to experimental values as the Slender Body Theory it was decided to continue on by using the Source-Doublet method in conjunction with Reference 4 to predict loads in the flow-field of a realistic aircraft/stores configurations.

The end product of this investigation is to try to improve store trajectory prediction. Store trajectory prediction is a three-faceted problem: (1) flow-field prediction, (2) force and moment prediction, and (3) integration of the equations of motion. The first two points are addressed in this report.

By using the method detailed in Reference 4 to prescribe U(x), V(x), and W(x) in Equations 15, 19, and 21, respectively, the procedures outlined in Sections III and V can be applied to predict loads in the flow-fields of realistic aircraft/stores. The method outlined up to this point has assumed that the flow-field is precisely known, and that the only problem is developing a method to predict the forces acting on the store. The flow-fields of real aircraft/stores configurations are not precisely known or predicted. There are many problems with flow-field measurement and theoretical predictions. With this in mind, both flow-field and force predictions need to be scrutinized. Wind-tunnel measured flow-fields offer the principal yardstick to assess theoretical prediction. Comparison with both flow-field and loading data will be presented to evaluate the method described in this report.

Figure 7 shows the various model components for which comparisons are presented. N1-B2 denotes the wing-body configuration shown in

Figure 7a. P(1/3) stands for the pylon shown in Figure 7b attached to N1-B2 at the 1/3 semispan position. TER is the triple ejector rack model shown in Figure 7c. S2-S3 represent dummy store on the shoulder stations of the TER. S2 and S3 both have the same shape as the ogive-cylinder store shown in Figure 2a. (All stores are attached to the TER so the store midpoint is aligned axially with the rack centerline.) The store loading plots in Figures 8, 9, 10, and 11 have essentially the same information on them as presented earlier for the uniform flow-field comparisons. Some additional information is presented in the form of ticks on the horizontal axis. From left to right they are: local wing leading edge, rack nose, pylon leading edge, pylon trailing edge, aft end of rack, and wing trailing edge. These are vertical projections made perpendicular to the fuselage reference axis down to the store centerline in the carriage position. The data presented in Figures 8, 9, 10, and 11 are for a longitudinal traverse along the store centerline in the carriage position. Figures 8 through 11 represent a configuration buildup, i.e. from a simplistic configuration to a realistic one.

The correlation between the integrated pressure data and the strain-gauge data for the non-uniform flow-field case presented are not good. This is consistent with what was observed for the uniform flow-field cases. If the pressure data can be used as an indication of what the load distribution looks like, then as would be expected, the prediction deteriorates as the configuration becomes more complex. It should be pointed out again that these predictions are in the most complex part of the flow-field, i.e. carriage position. Dix in Reference 10 has found out that large gradients in loads exist within a few tenths of an inch of carriage position. Dix also found that extreme fidelity in modeling the ejector rack hardware influenced captive loads. The loading presented in Figures 8, 9, 10, and 11 are dependent on the quality of the flow-field predictions from Reference 4. In Figures 11c, d, and e, the U(x) and W(x), predicted by Reference 4 and non-dimensionalized by the free-stream velocity, are compared to velocities measured in the wind tunnel. The velocities given by the solid lines were used to make the predictions presented in Figures 11a and b. Figures 11c, d, and e show that the flow-field predictions generally predict the trends of the data but the

magnitude is not well predicted. Flow-field comparisons were made corresponding to Figures 8, 9, and 10 also. They showed diminishing agreement between theory and experiment as aircraft/stores configuration became now complete. Other comparisons similar to those presented in Figures 8, 9, 10, and 11, including flow-fields, were made and the same general conclusion that configuration complexity causes agreement between theory and experiment to diminish. These additional comparisons will be published as a separate document. One thing that needs to be done that was not done is to make predictions similar to those shown in Figures 11a through e as a function of vertical displacement. These types of comparisons would indicate where flow-field prediction needs refinement versus refining the method of predicting forces. Based on the lack of agreement in flow-field prediction indicated in Figures 11c through e and supported by other comparisons, it was decided to try to improve the flow-field model in Reference 4.

SECTION VII

FLOW-FIELD MODELING EXTENSION

The method of flow-field prediction in Reference 4 accounts for "primary interference" which is defined on page 2 of Reference 1. Primary interference which can be termed gross interference effects and can be viewed as the first term in an iterative procedure. The primary interference approach fits somewhere in the spectrum between modeling each component, i.e. fuselage, wing, and pylon, as though it was in the free-stream and a full blown panel or inter-active approach where every component influences every other component. This approach was selected to try to keep the computer resources (both time and core) down to an economically manageable size. As part of the primary interference approach, stores adjacent to the separating store (the store on which loads are to be calculated) and the ejector rack are modeled by sources and sinks. This models only the volume effect and only for the free-stream case. The source and sink strengths are calculated for each individual body in a uniform free-stream. Then these models are positioned in close proximity to represent the complete aircraft/store configuration. This procedure is theoretically correct since the governing equation is the Laplace's equation which is linear, so linear superposition of solutions is perfectly valid. The method presented in Reference 4 does not attempt to model the upwash and sidewash caused by adjacent stores and the ejector rack. In an attempt to improve both the flow-field and force and moment predictions, a cross-flow model for the shoulder stores and ejector rack was introduced into the method of Reference 4.

Essentially the doublet equations described in Section III were used to generate a model of the cross-flow produced by the bodies that are in close proximity. Doublets were placed in the horizontal and vertical direction along the axis of each store and the ejector rack similar to the way they were used for the separating store in Section III. The computer program of Reference 4 was modified to allow the whole configuration (except the separation store whose cross-flow is being modeled) to

contribute to V(x) and W(x) in Equations 19 and 21, respectively. Once the horizontal and vertical doublet strengths were determined, then their contribution given by Equations 18 and 20 could be added to U(x), V(x), and W(x) in Equations 11, 19, and 21 to account for the cross-flow induced on the separating store.

SECTION VIII

COMPARISONS USING THE EXTENDED FLOW-FIELD MODEL

In November 1979, the Air Force Flight Dynamics Laboratory and the Naval Weapons Center sponsored a test at Arnold Engineering Development Center to study the mutual interference associated with the carriage of three MK-83 bombs on a TER under the left inboard pylon on the F-4C aircraft. This wind tunnel test is documented in References 11 and 12. Comparisons between theoretical prediction and wind tunnel data of force and moment coefficients are presented as a function of vertical distance from the carriage position. The aircraft configuration consisted of the F-4C, see Figure 12, and the left inboard pylon (denoted PI on the comparison plots), see Figure 13, and the TER shown in Figure 14. Some configurations will have dummy stores on the shoulder stations. The dummy stores shape is labeled "actual configuration" in Figure 15. The "actual configuration" had to be modified in the aft end to accept the balance and sting. The modified afterbody is also shown in Figure 15. The suffix MU after MK-83 on the comparisons indicates modified afterbody-unfinned, while MF denotes modified afterbody-finned. The method described in this report only predicts forces acting on the body. The method described in Reference 1 is used to predict the fin forces. However, velocities induced by the doublets of adjacent stores and the ejector rack were included in the fin force calculations.

After the computer coding associated with the flow-field model extension described in Section VII had begun the Flight Control Division of the Air Force Wright Aeronautical Laboratories decided to discontinue work in the area of store separation prediction. The comparisons presented here are not to the detail needed for thorough method evaluation. The results are only to illustrate that the coding is working, hopefully correctly, and possibly provide the foundation for someone else to continue this investigation.

All comparisons presented in this section are for a Mach number of 0.60. One of the main purposes of the effort described in this report is to include compressibility. For a thorough method evaluation comparisons

must be made at higher Mach numbers. Data was taken at various Mach numbers during the test described in Reference 12. The main variables in the comparisons presented here are parent aircraft configuration and angle of attack. The group number on each figure can be used in conjunction with Reference 12 to fully define all test parameters.

Figures 16, 17, and 18 present results for a given configuration at angles of attack of 1, 5, and 9 degrees respectively. The configuration consists of the F-4C with a TER rack mounted on the left inboard pylon. A modified afterbody MK-83 is moved vertically (perpendicular to the aircraft waterlines) through the aircraft flow-field from its carriage position, i.e. ZP/D, to a vertical distance equal to 6 diameters below the carriage position. The first data point is not at exactly ZP/D=0.0 because of mechanical interferences associated with the test hardware. The configuration used for comparisons is the least complex configuration tested for which the method in Section VII would be applicable, i.e. if the method does not show some improved prediction capability for this case, provided the flow-field predicted by Reference 4 and Section VII is reasonable then the method should be scrapped. The legend for the various symbols on the plots are given in the upper right-hand corner of each plot. The dots with circles around them are data. SBT stands for slender body theory which denotes the application of the method of Reference 4 unmodified. S.D. stands for Source-Doublet and is used to denote the application of the method outlined in Sections III and IV in conjunction with the flow-field model of Reference 4. The suffix CFLOW indicates application of the two previously described methods for force and moment prediction with the addition of the cross-flow modeling described in Section VII to the flow-field modeling of Reference 4.

In all three applications, Figures 16, 17, and 18, the Source-Doublet method improved the correlation between predicted and measured moment coefficients (both pitching and yawing moment) over slender body theory as described in Reference 4 with or without the flow-field modeling of Section VIII. For yawing moment, the Source-Doublet method with cross-flow modeling of Section VII gave the best correlation between theory

and experiment of all four of the methods. The Source-Doublet method without the cross-flow model gave the best prediction for pitching moment. A substantial improvement in both pitching and yawing moment coefficient prediction is obtained by applying the methods of Sections III, IV, and VII in conjunction with Reference 4 over using Reference 4 alone. Adding the cross-flow model does not necessarily improve the Source-Doublet predictions as indicated in Figures 16b, 16d, and Figure 17b. The Source-Doublet method with and without the cross-flow model slightly degrades the force coefficient predictions shown in all three figures (16, 17, and 18). Including the cross-flow model has little effect on the slender body theory predictions.

In Figure 19, the cross-flow model contribution to the flow-field was terminated at ZP/D=2.0. From Figures 16, 17, and 18, it can be seen that the cross-flow contribution to the prediction is very small below two store diameters. Figure 19 is for the most complex TER loading, i.e. two shoulder stores with fins are present. The angle of attack of parent aircraft is 5.0 degrees. The Source-Doublet method with cross-flow model does an outstanding job predicting yawing moment, see Figure 19d, and does a good job predicting normal force, Figure 19a. Pitching moment and side force predictions are both poorly predicted.

Figure 20 presents results for a finned modified after body store and one shoulder store on the ejector rack. The shoulder store has fins and is on the outboard station of the rack. The fins on the shoulder store cannot be modeled by the method described in Reference 4. This configuration is at 5 degrees angle of attack and is of intermediate complexity, i.e. it is less complex than the one used to calculate the results presented in Figure 19, but more complex than the one used for comparisons in Figure 18. As was mentioned earlier, the methods presented in this report cannot predict fin forces. Therefore, the increment in force due to the fins predicted by Reference 4 has been added to the body forces predicted by the methods described in this report to obtain the total forces acting on the store. For the force prediction all four methods yielded essentially the same prediction. Normal force predictions are good, but side force predictions leave a little to be desired. The Slender Body and Source-Doublet methods

both give excellent agreement with experiment when the cross-flow model is included in the flow-field prediction method. The Source-Doublet method shows very good agreement with the yawing moment data both with and without the cross-flow model. Slender Body theory gives very poor prediction of the yawing moment.

Figure 21 is for the most complex configuration for which data in the joint Air Force/Navy test. The F-4c is at 5 degrees angle of attack with two finned stores on the shoulder station of the ejector rack. The Source-Doublet theory with the cross-flow model shows excellent agreement with the experimentally measured normal force. Agreement within the first two diameters below the carriage position for pitching moment is poor for all four methods with Slender Body theory being slightly better than the Source-Doublet predictions. Side force prediction is poor for all four methods. Again the Source-Doublet method does a very good job of predicting the yawing moment, certainly much better than Slender Body theory. In all comparisons, which include several not presented, the yawing moment prediction was consistently well predicted by the Source-Doublet method.

SECTION IX

CONCLUSIONS

The Source-Doublet method presented here has shown enough potential to warrant further investigation. The flow-field prediction of Reference 4, with the method described in Section VII, needs to be studied. Flow-field data from the joint AFFDL/NWC test, References 11 and 12, could be used. The method seems to consistently predict moments better than forces.

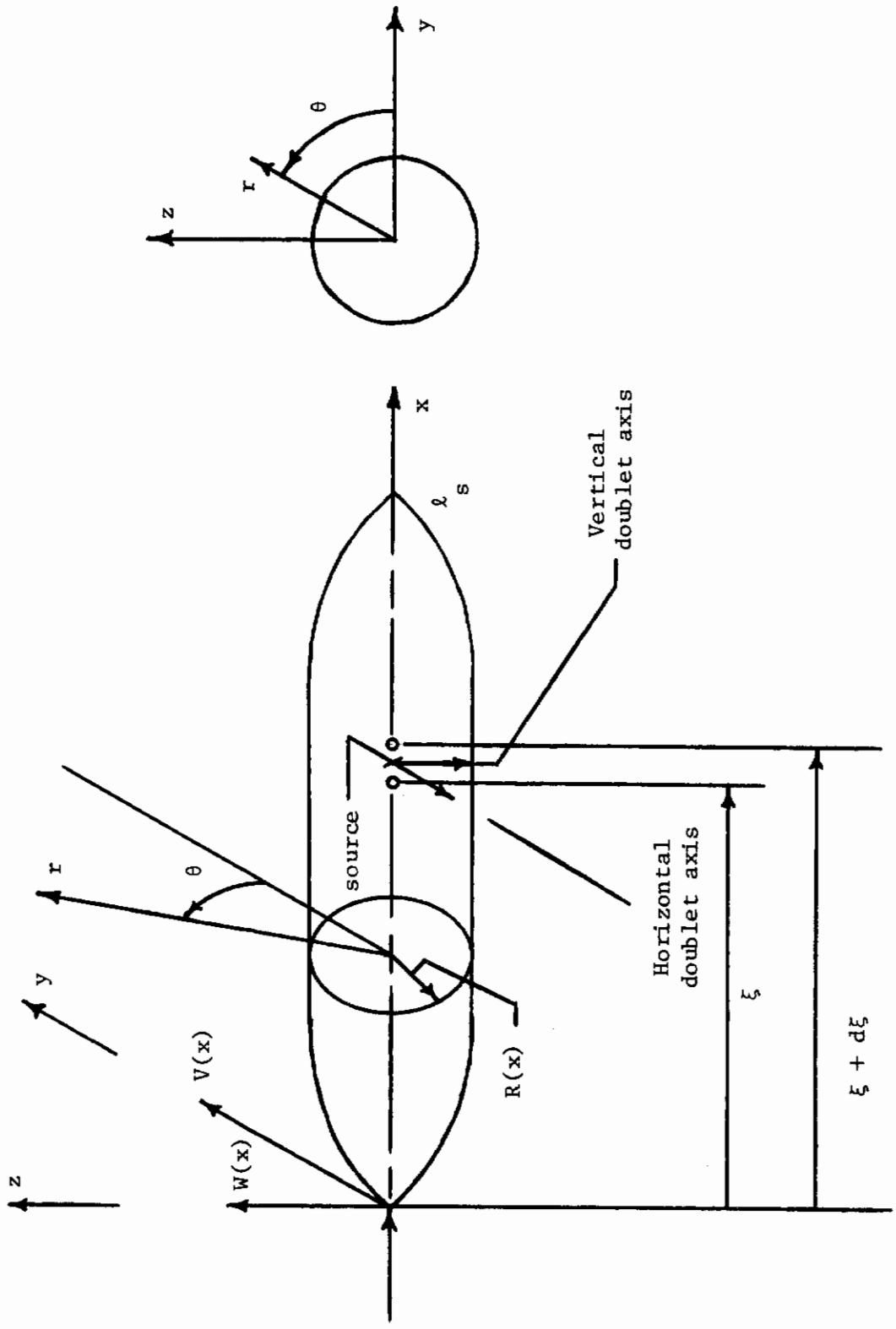

Figure 1. Coordinate Reference Frames Used in Source-Doublet Store Model

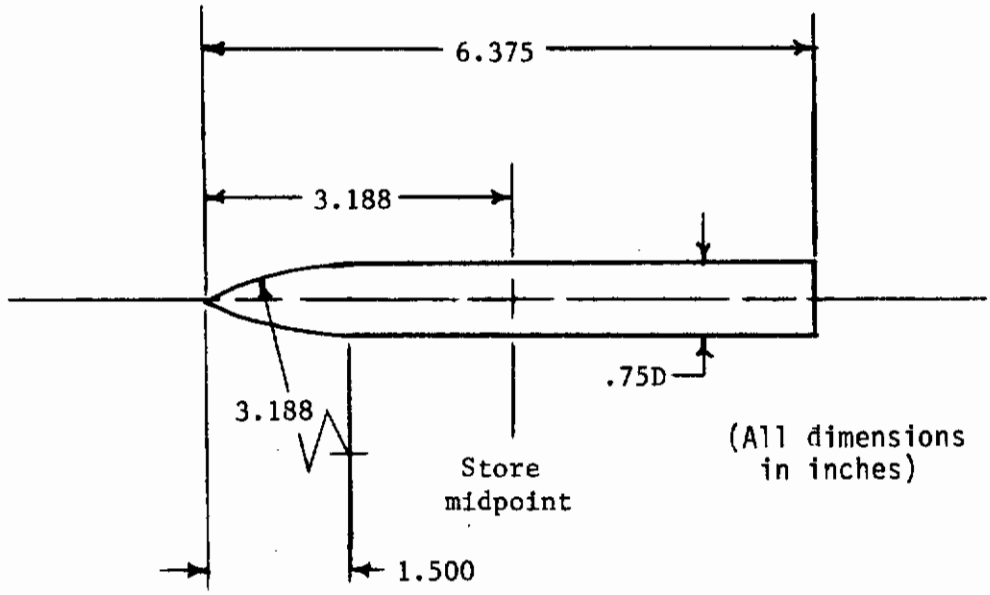

(a) Ogive cylinder store

(b) Zero streamline superimposed on
actual body radius.

Figure 2. Ogive Cylinder Pressure Store

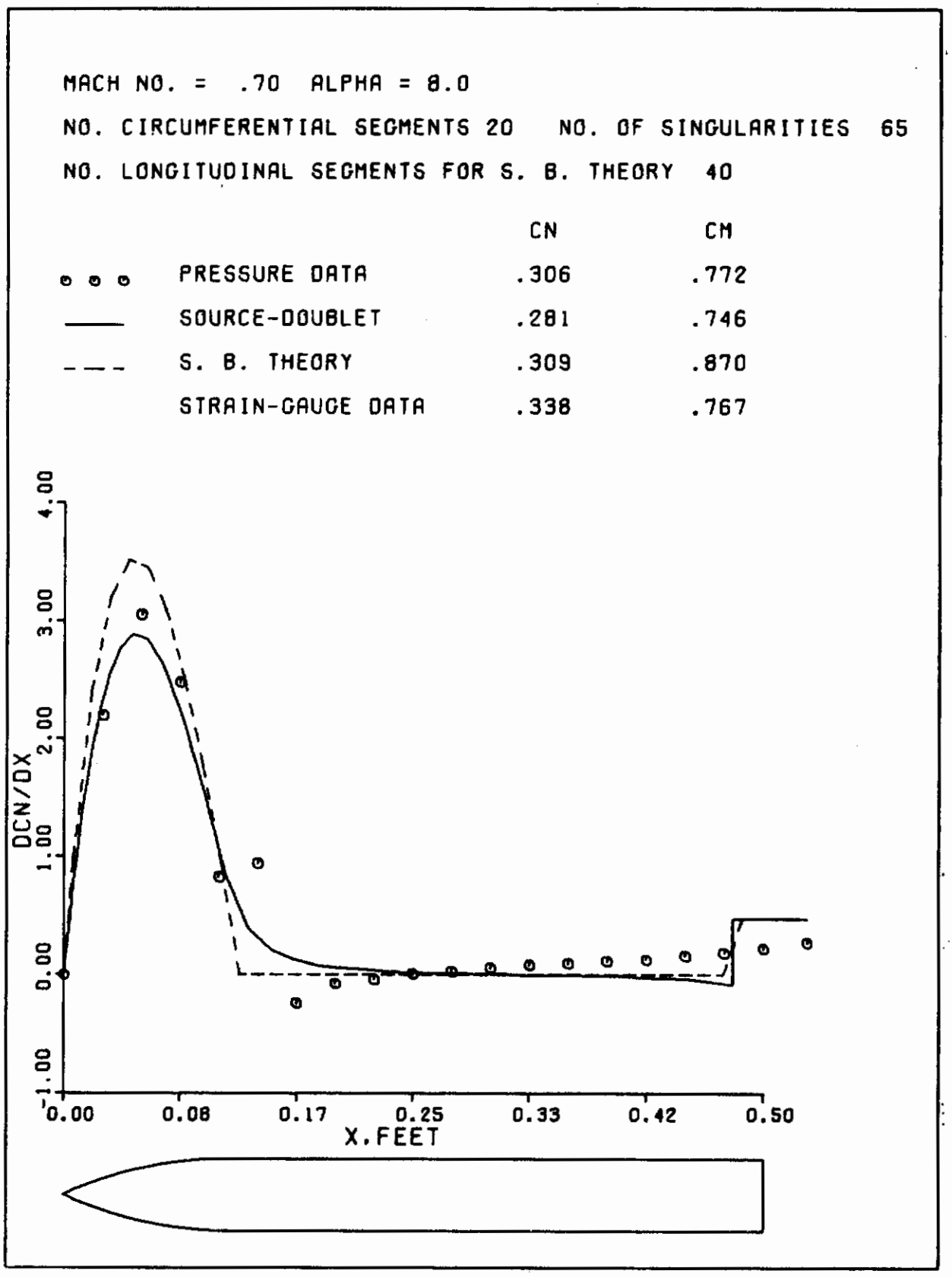

Figure 3. Short Wake Model Separation at .9 x/ℓ

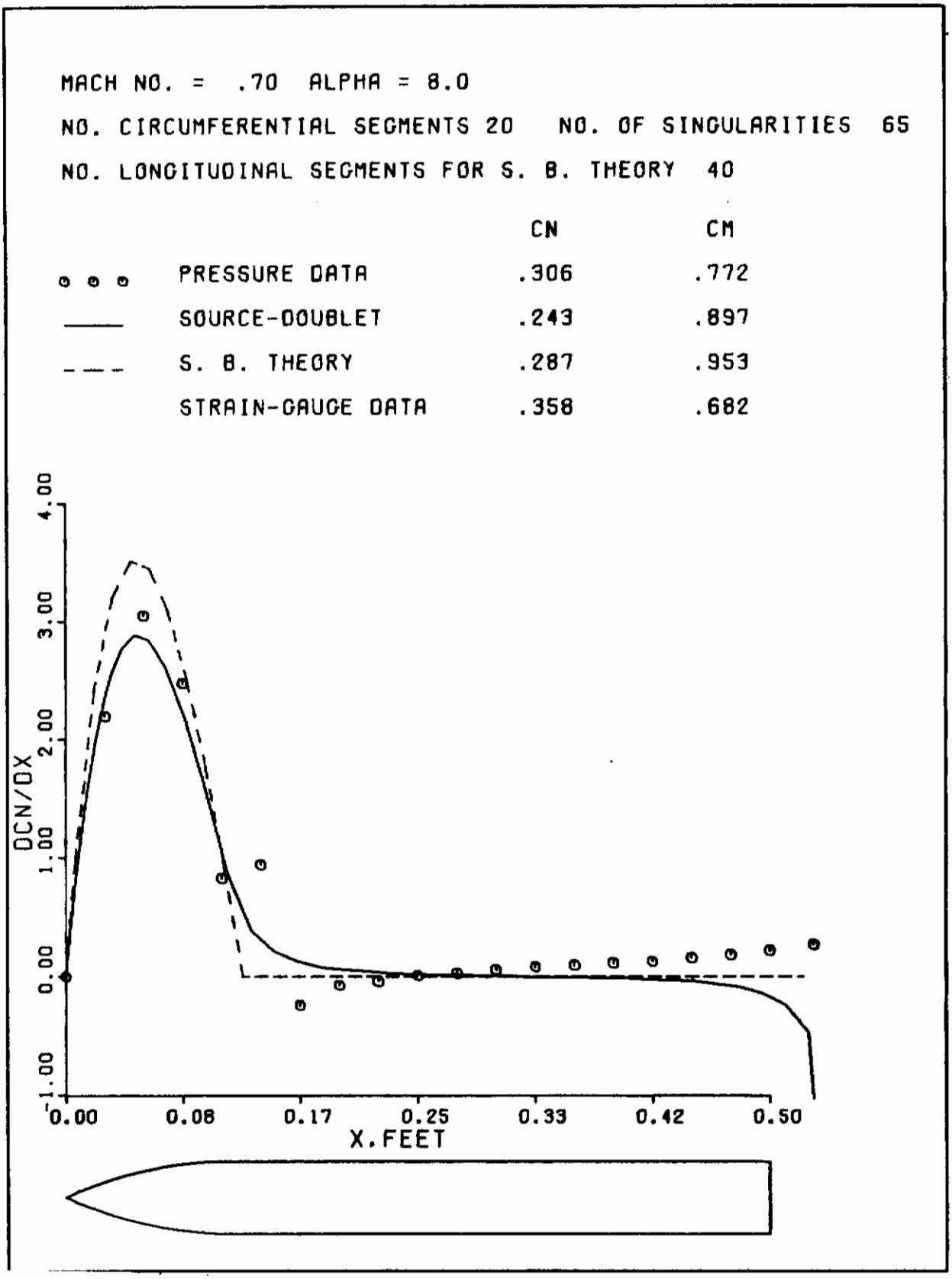

Figure 4. Short Wake Model Separation at 1.0 x/ℓ

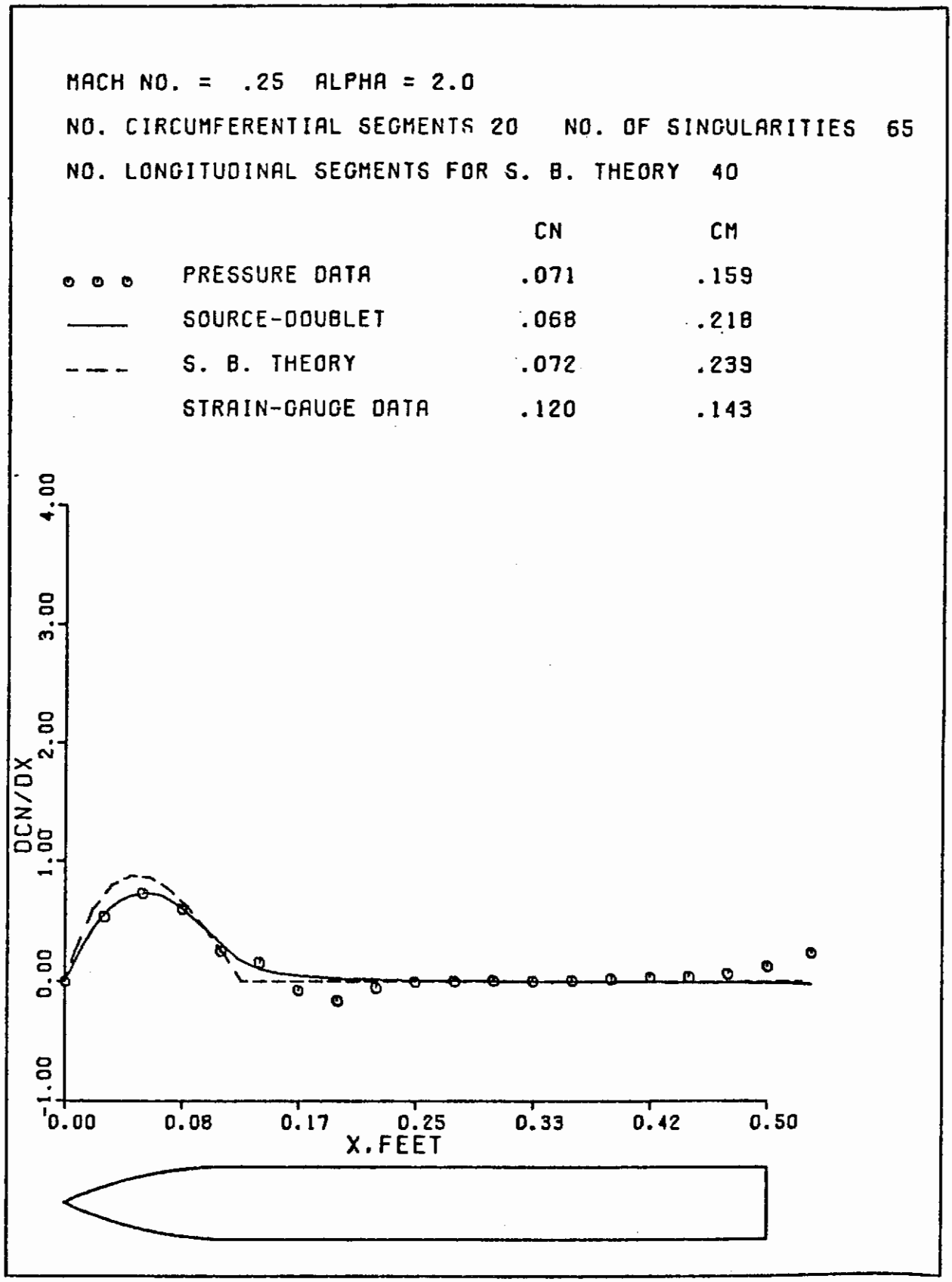

Figure 5. (Contd) Long Wake Model Separation at 1.0 x/ℓ
(a) Alpha=2° Mach Number=.25

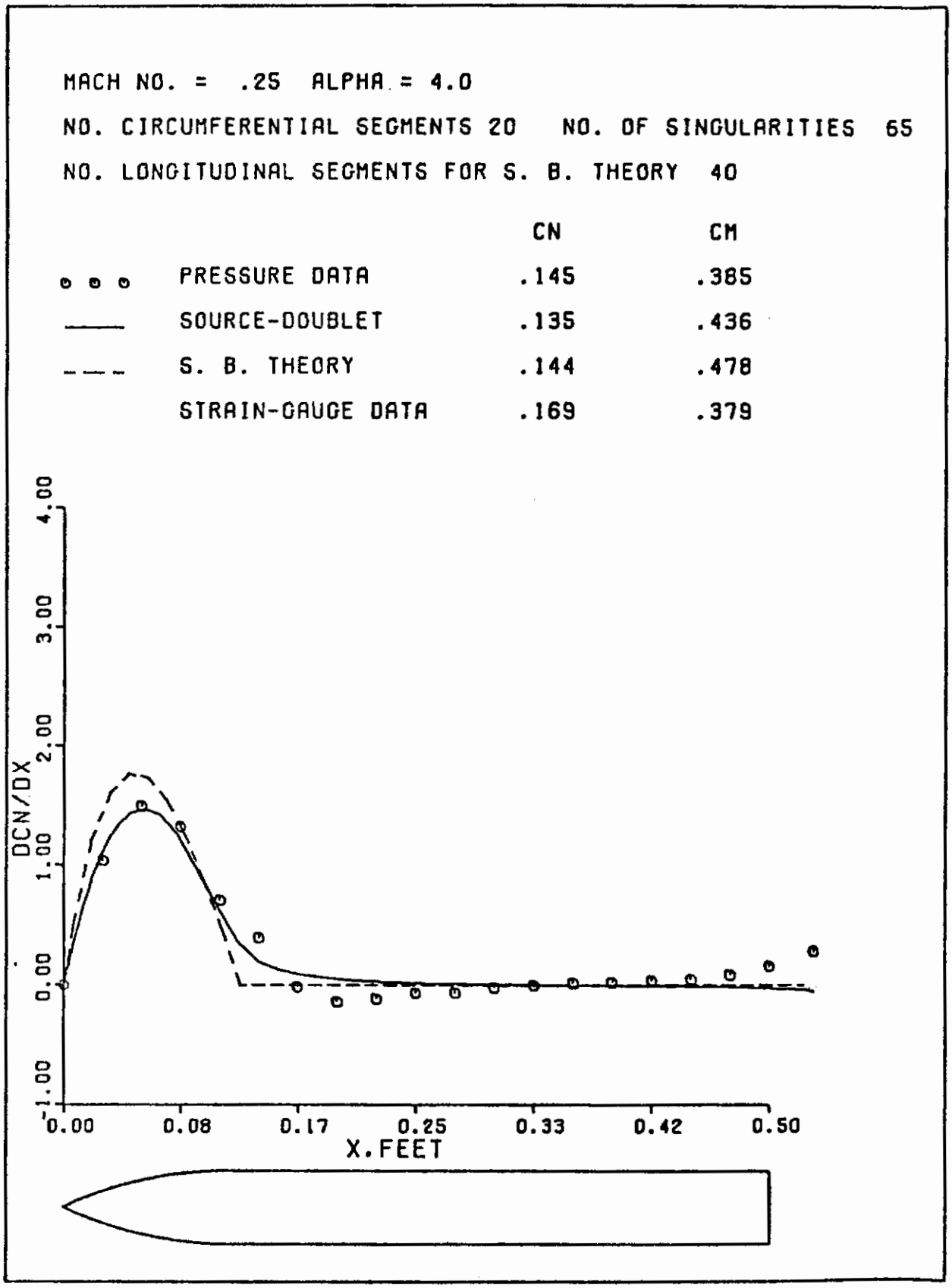

Figure 5 (Contd). Long Wake Model Separation at 1.0 x/ℓ
(b) Alpha=4° Mach Number=.25

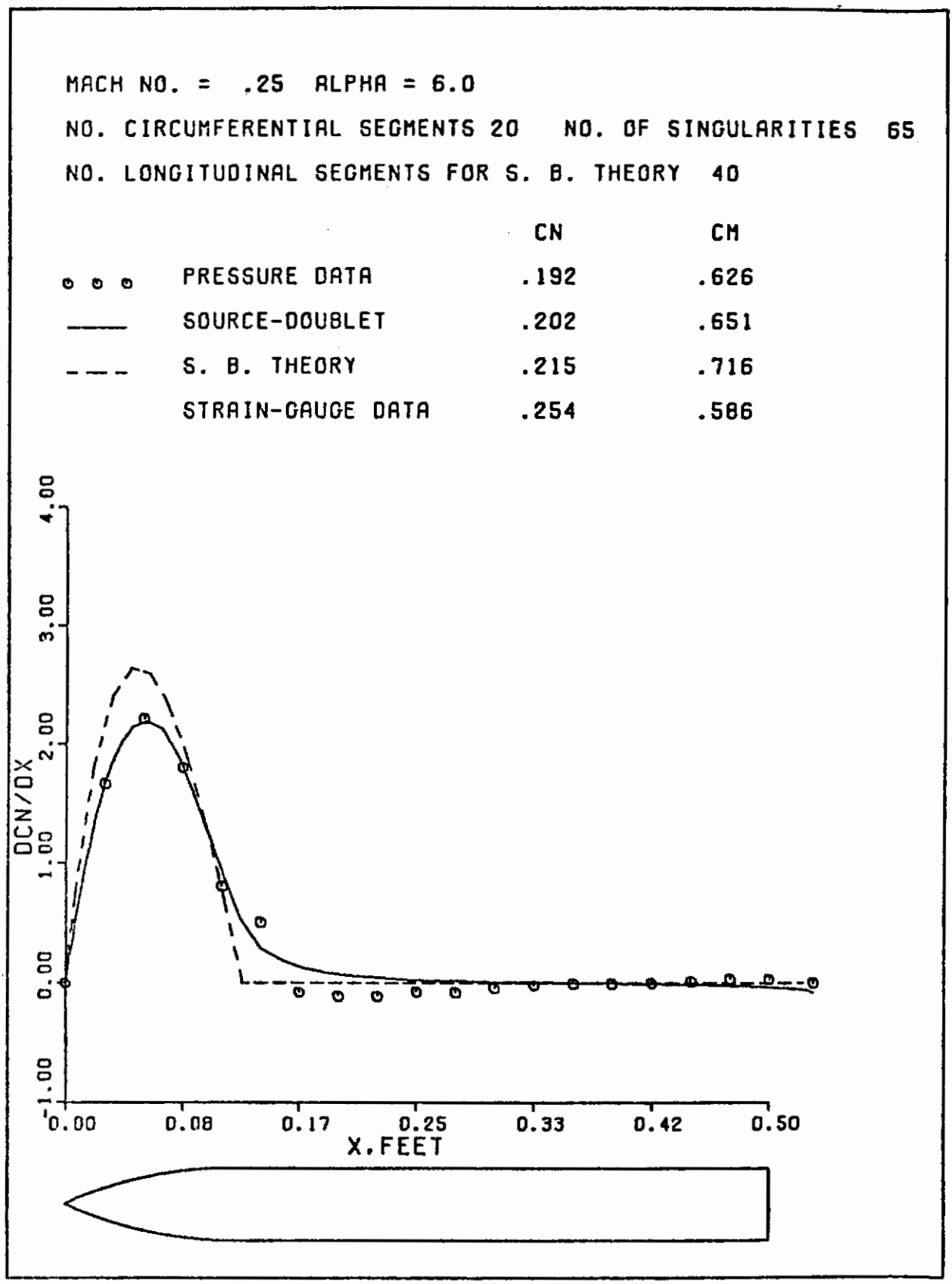

Figure 5 (Contd). Long Wake Model Separation at 1.0 x/ℓ
(c) Alpha=6° Mach Number=.25

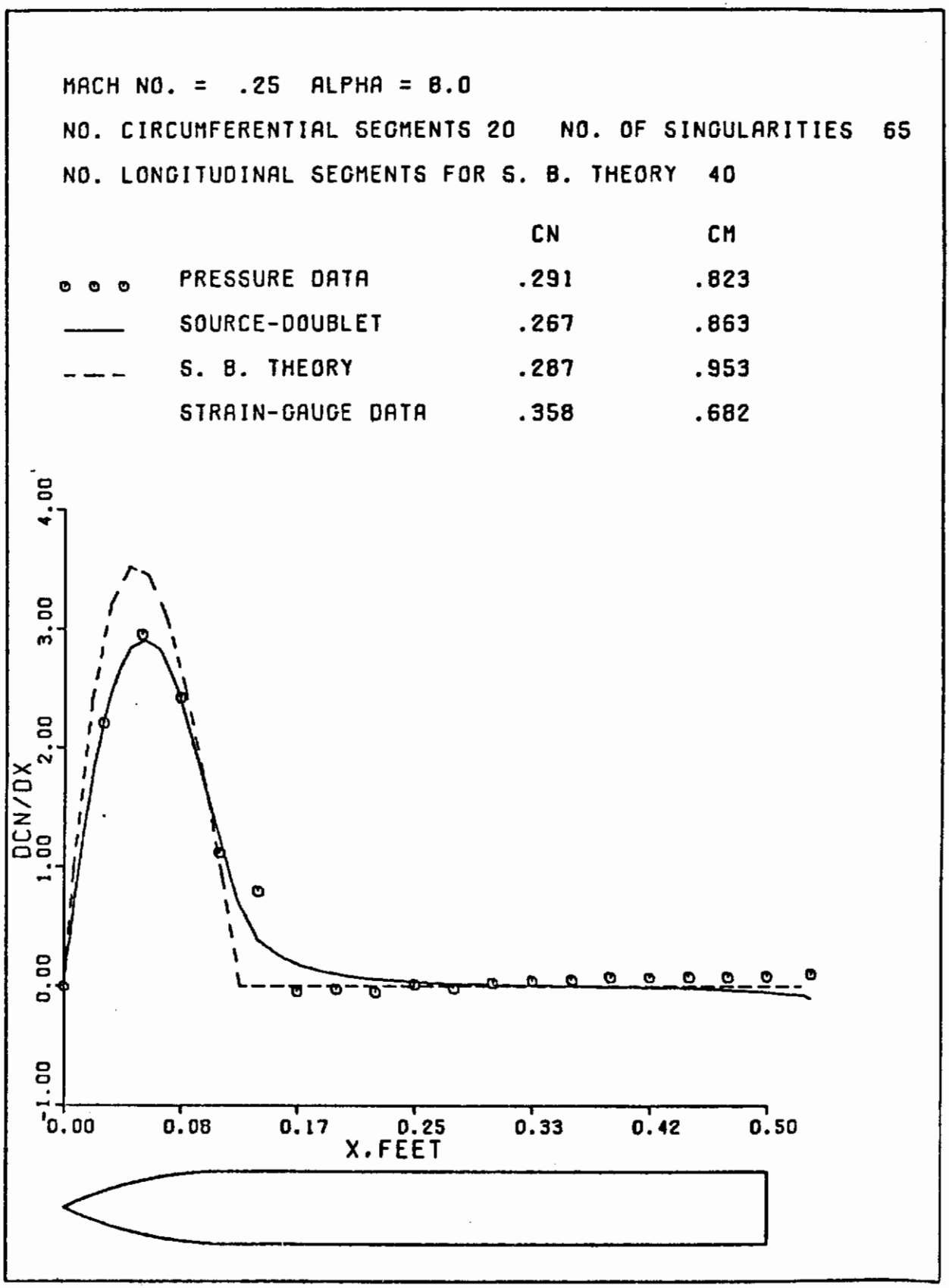

Figure 5 (Contd). Long Wake Model Separation at 1.0 x/ℓ
(d) Alpha=8° Mach Number=.25

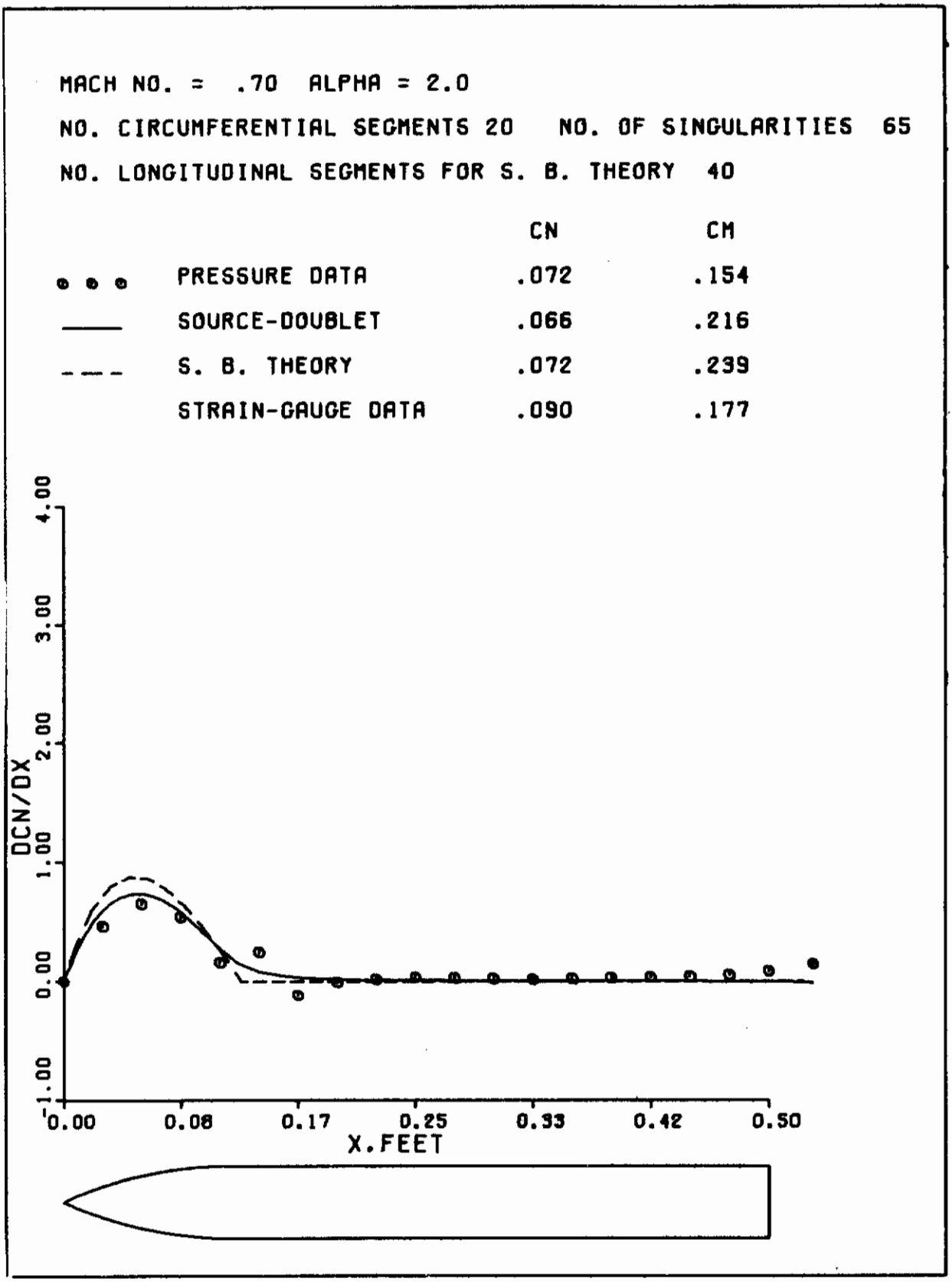

Figure 5 (Contd). Long Wake Model Separation at 1.0 x/ℓ
(e) Alpha=2° Mach Number=.70

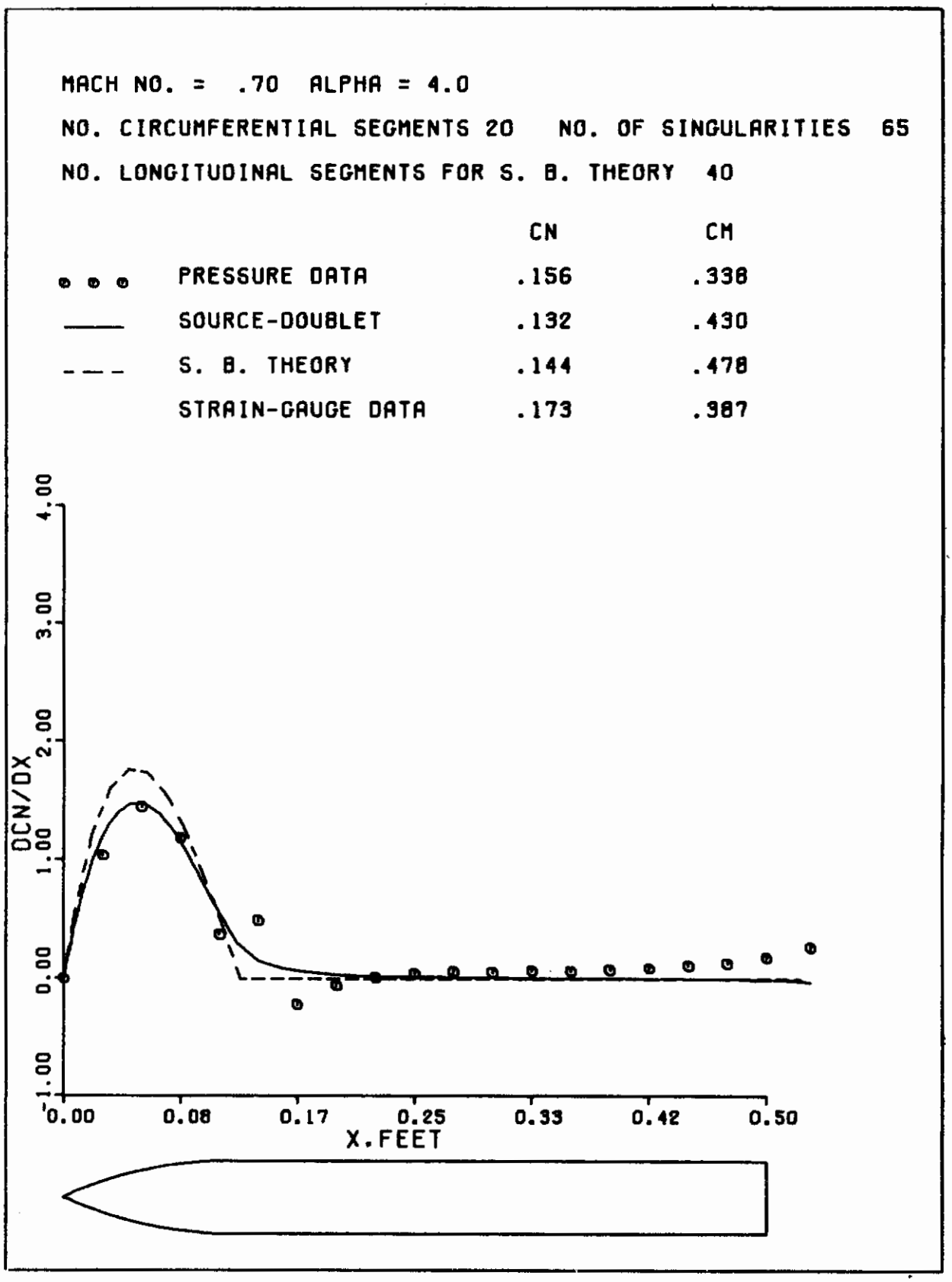

Figure 5 (Contd). Long Wake Model Separation at 1.0 x/ℓ
(f) Alpha=4° Mach Number=.70

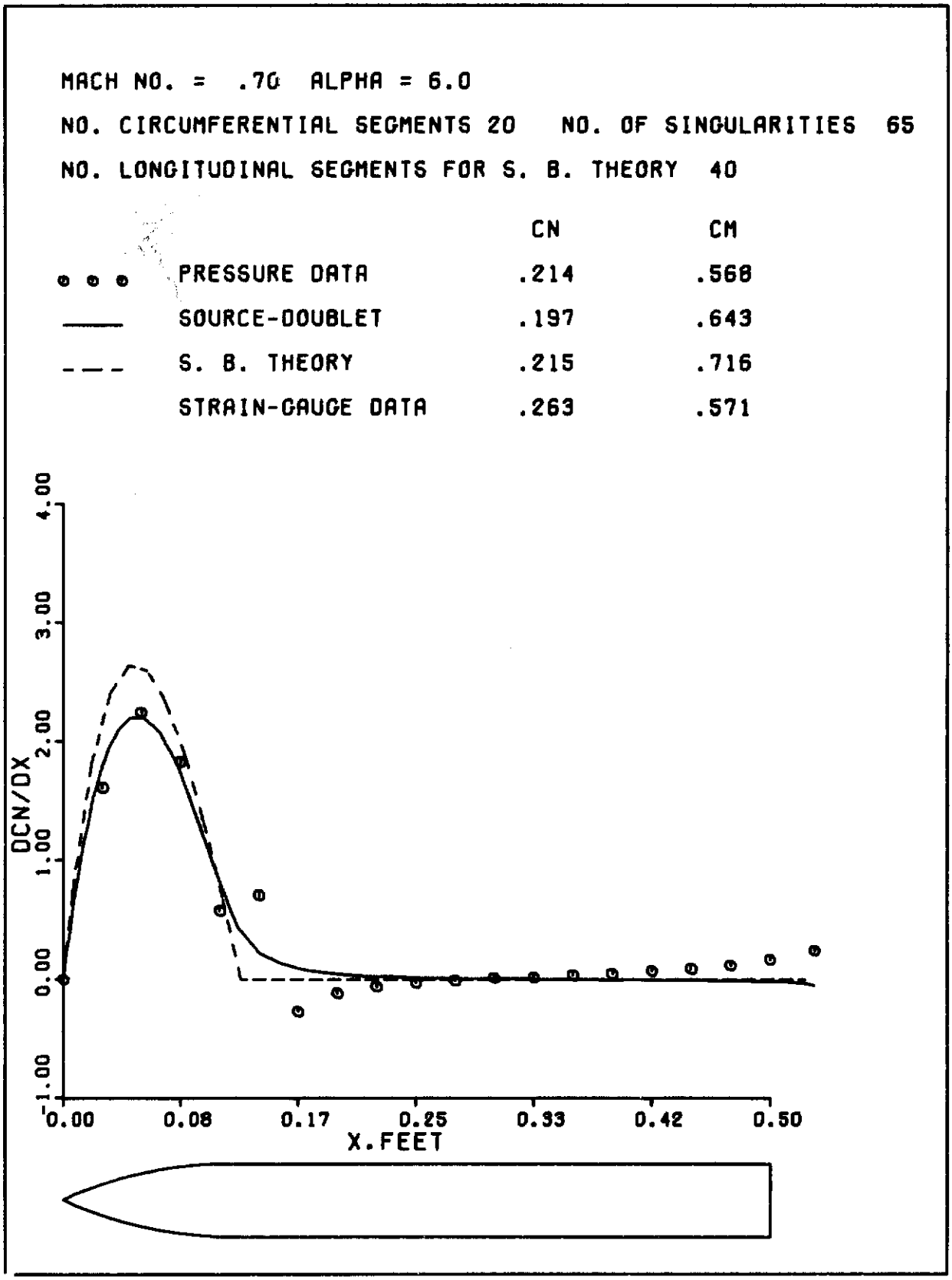

Figure 5 (Contd). Long Wake Model Separation at 1.0 x/ℓ
(g) Alpha=6° Mach Number=.70

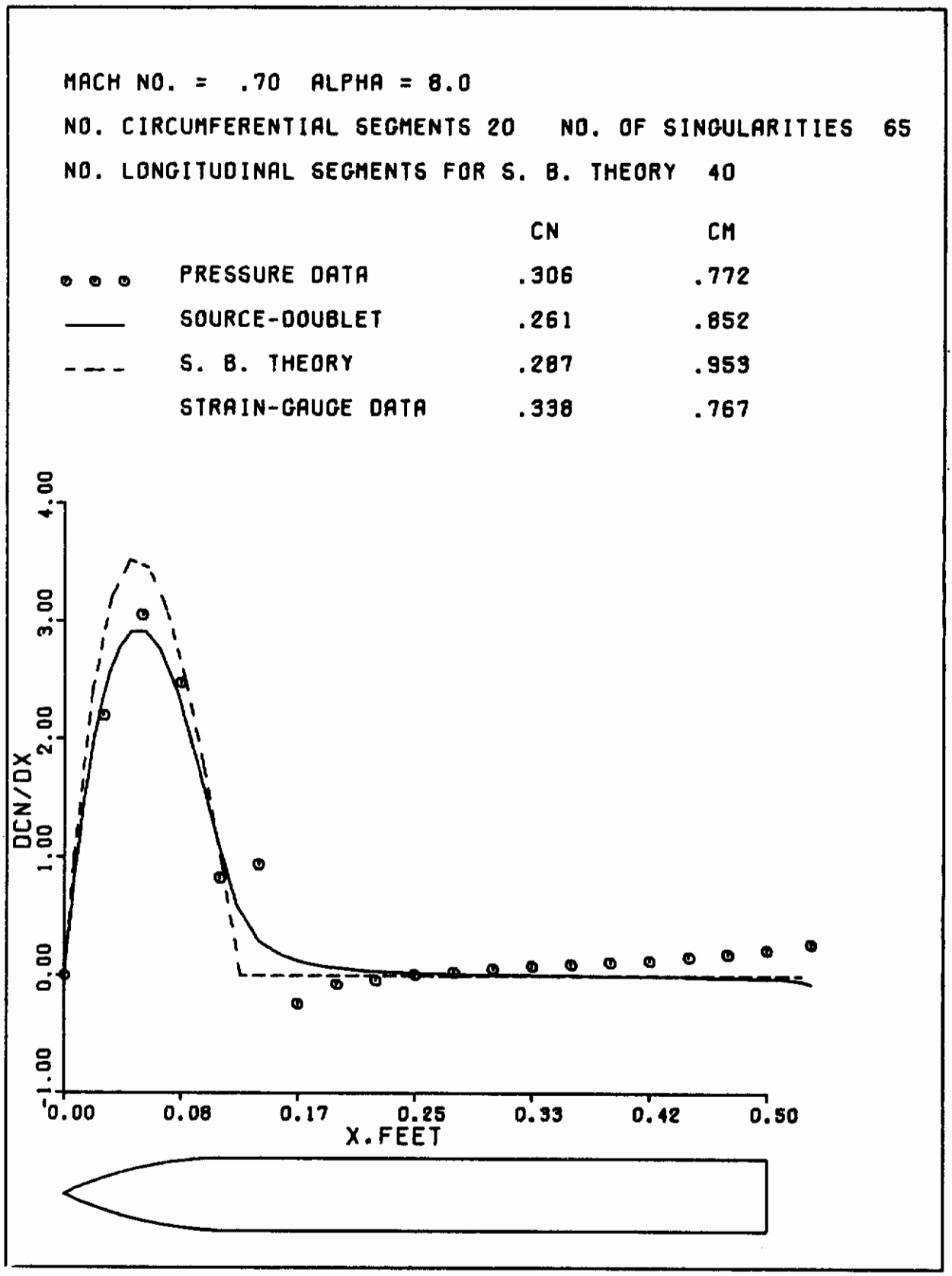

Figure 5 (Concluded). Long Wake Model Separation at 1.0 x/ℓ
(h) Alpha=8° Mach Number=.70

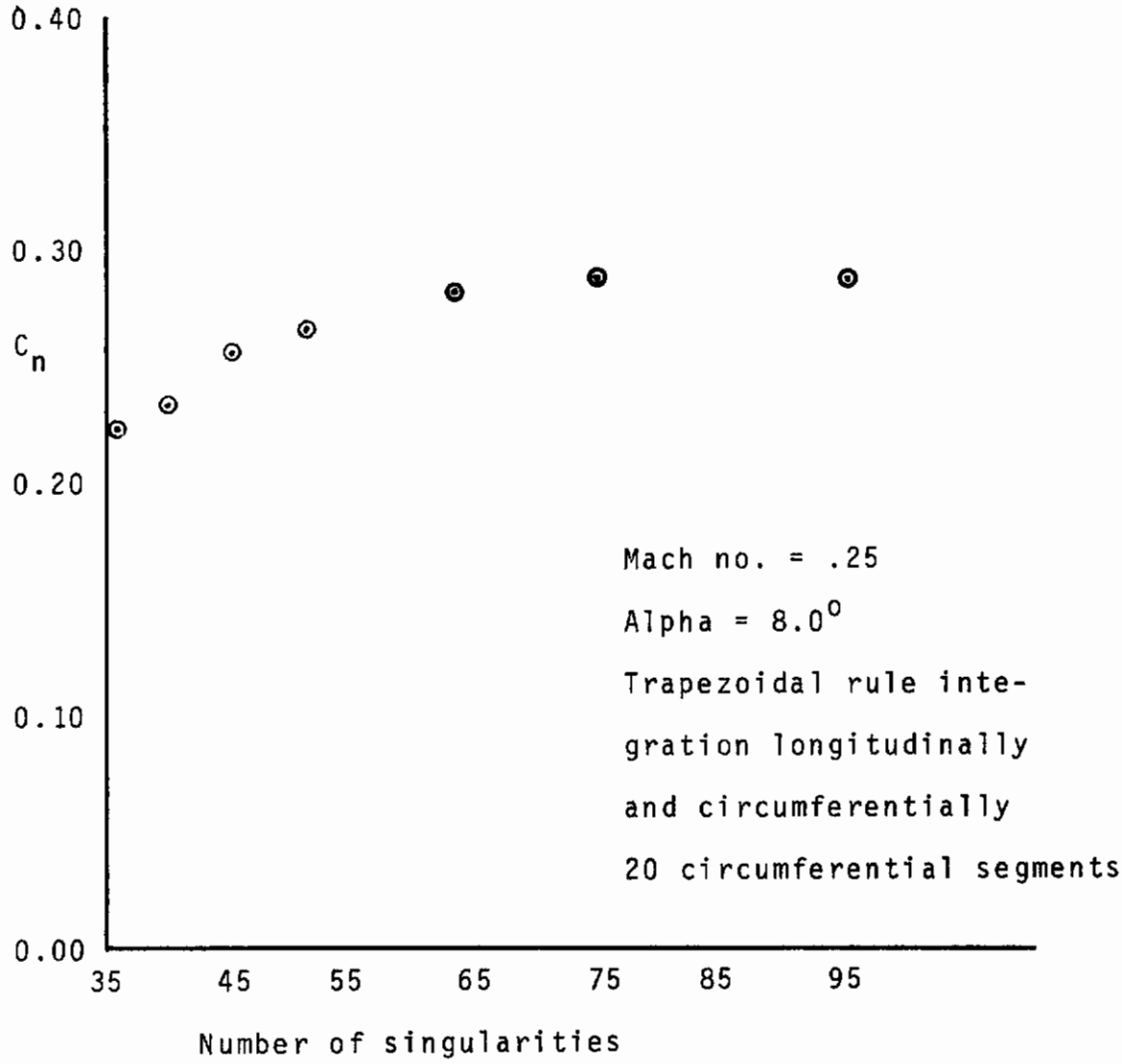

Figure 6. C_n as a Function of Number of Singularities

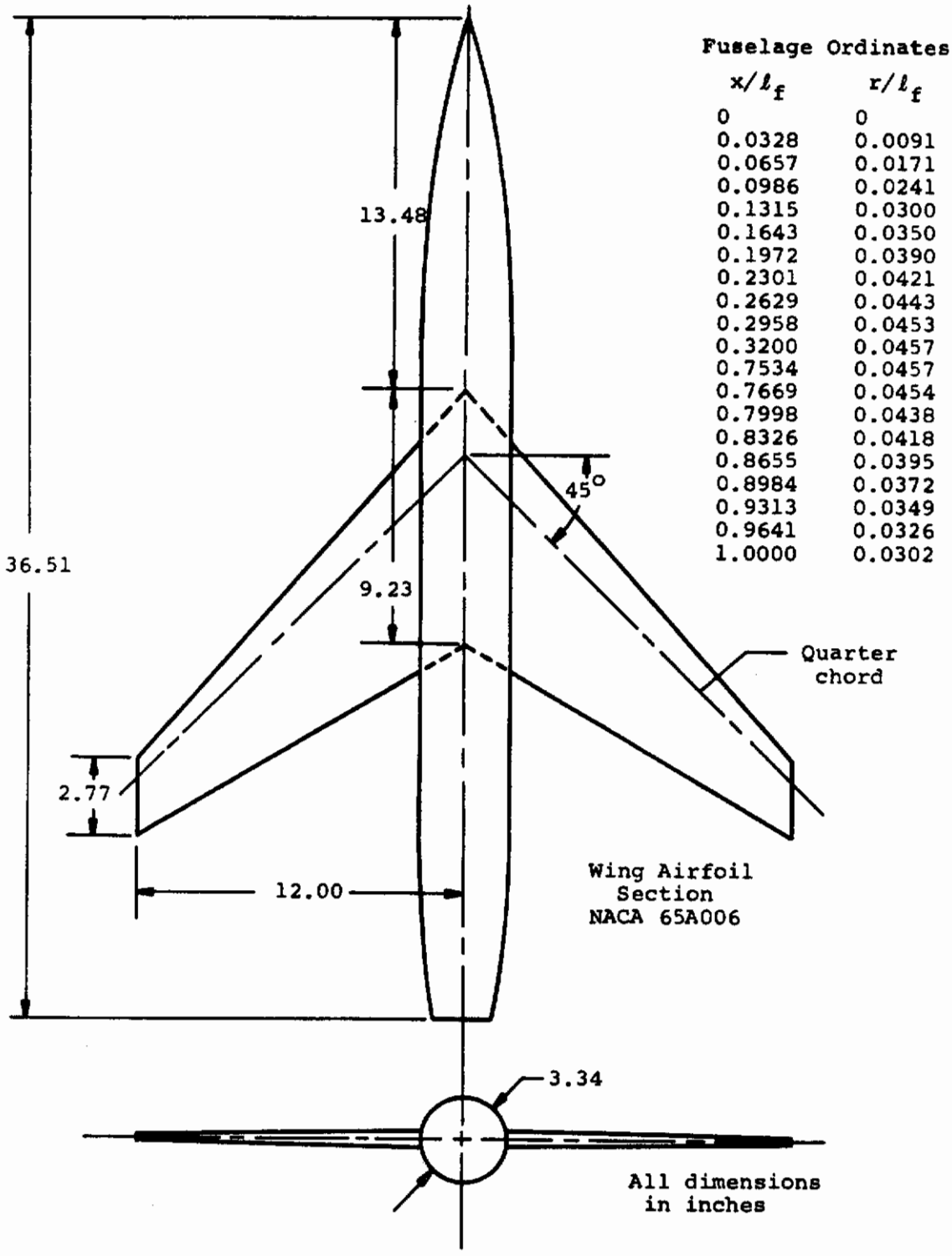

Figure 7. Wind-Tunnel Models Used in Sample Calculations
(a) Wing-Fuselage Combination

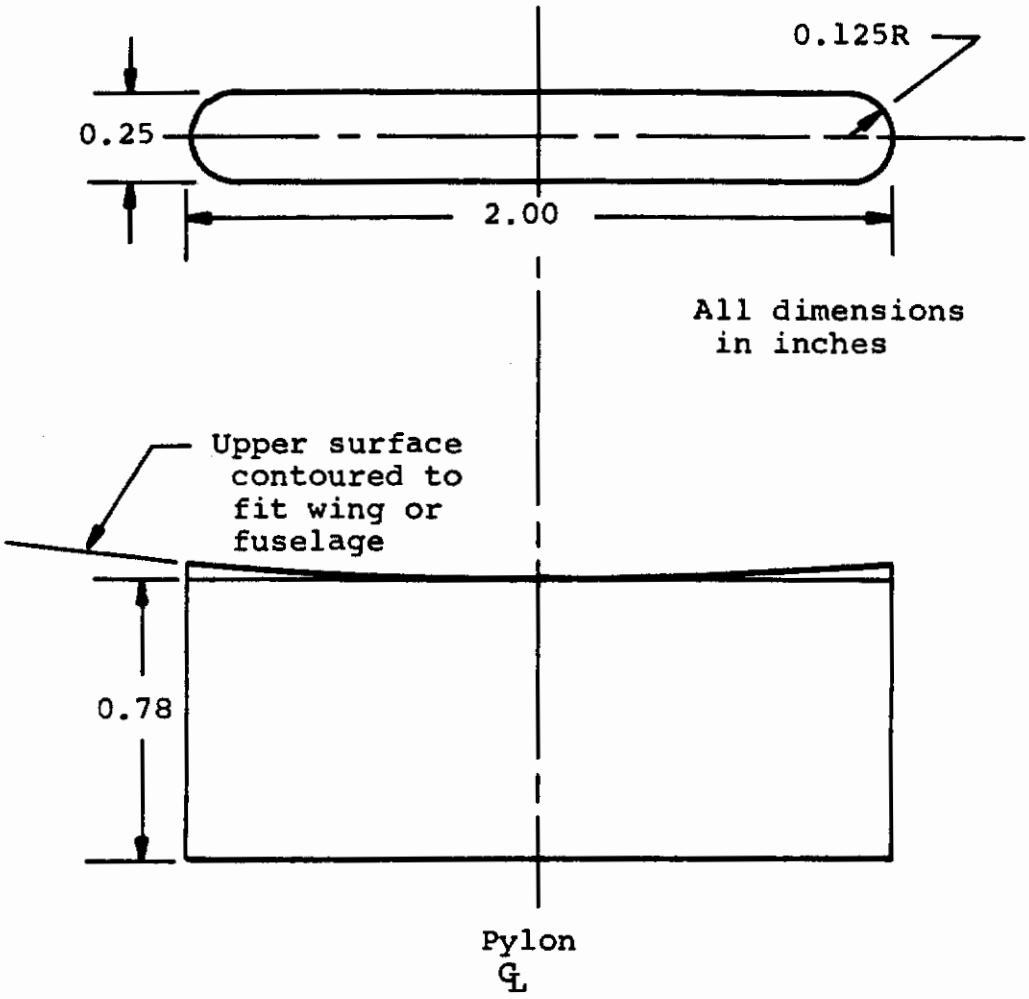

For wing pylons, pylon centerline located at 40% wing chord.

For fuselage pylon, pylon centerline located 19.43 inches aft of fuselage nose.

Figure 7. (Contd) Wind-Tunnel Models Used in Sample Calculations
(b) Pylon Used With Single Store and Triple Ejector Rack (TER)

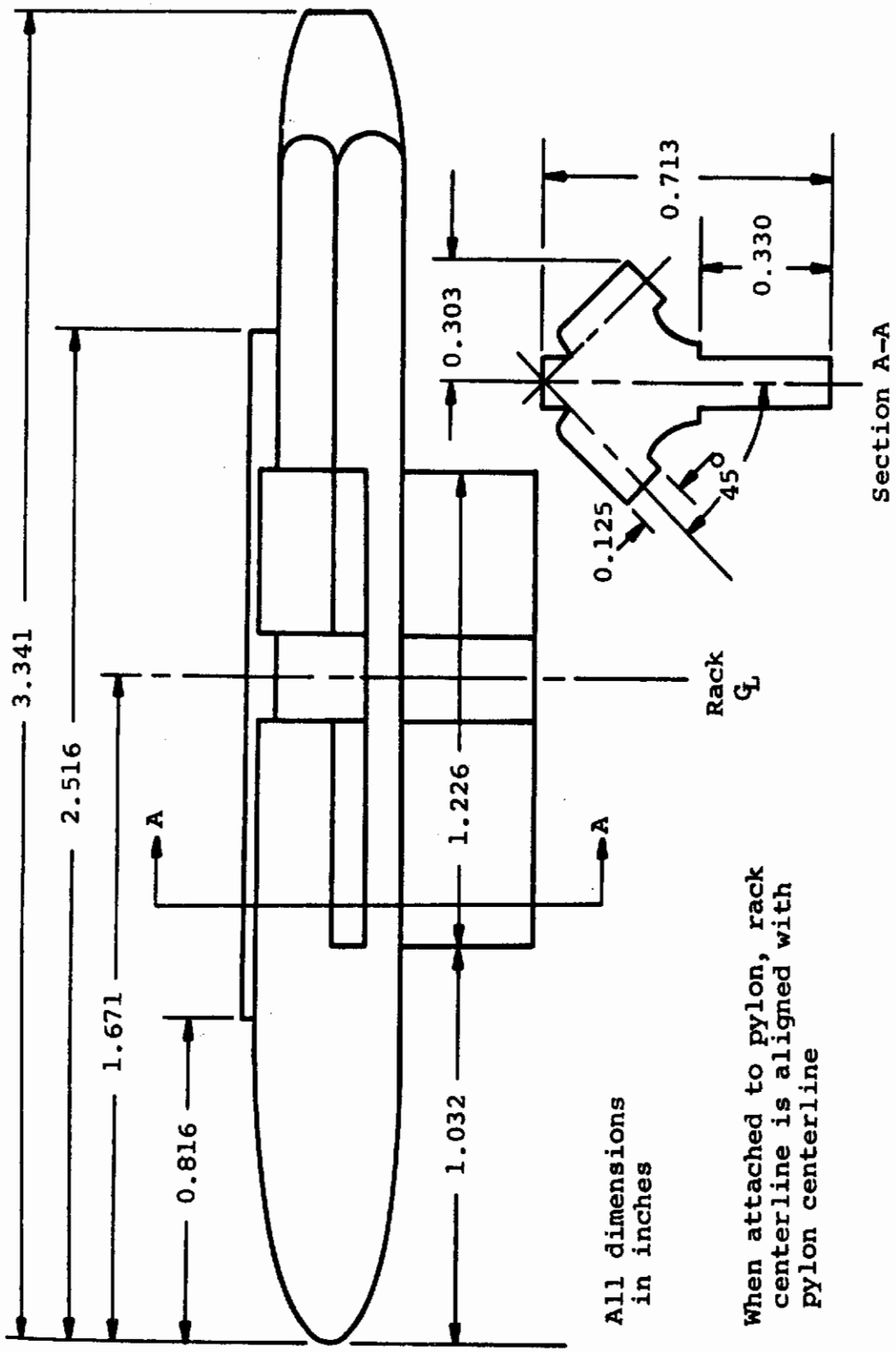

Figure 7. Wind-Tunnel Models Used in Sample Calculations
(Concluded) (c) Details of TER

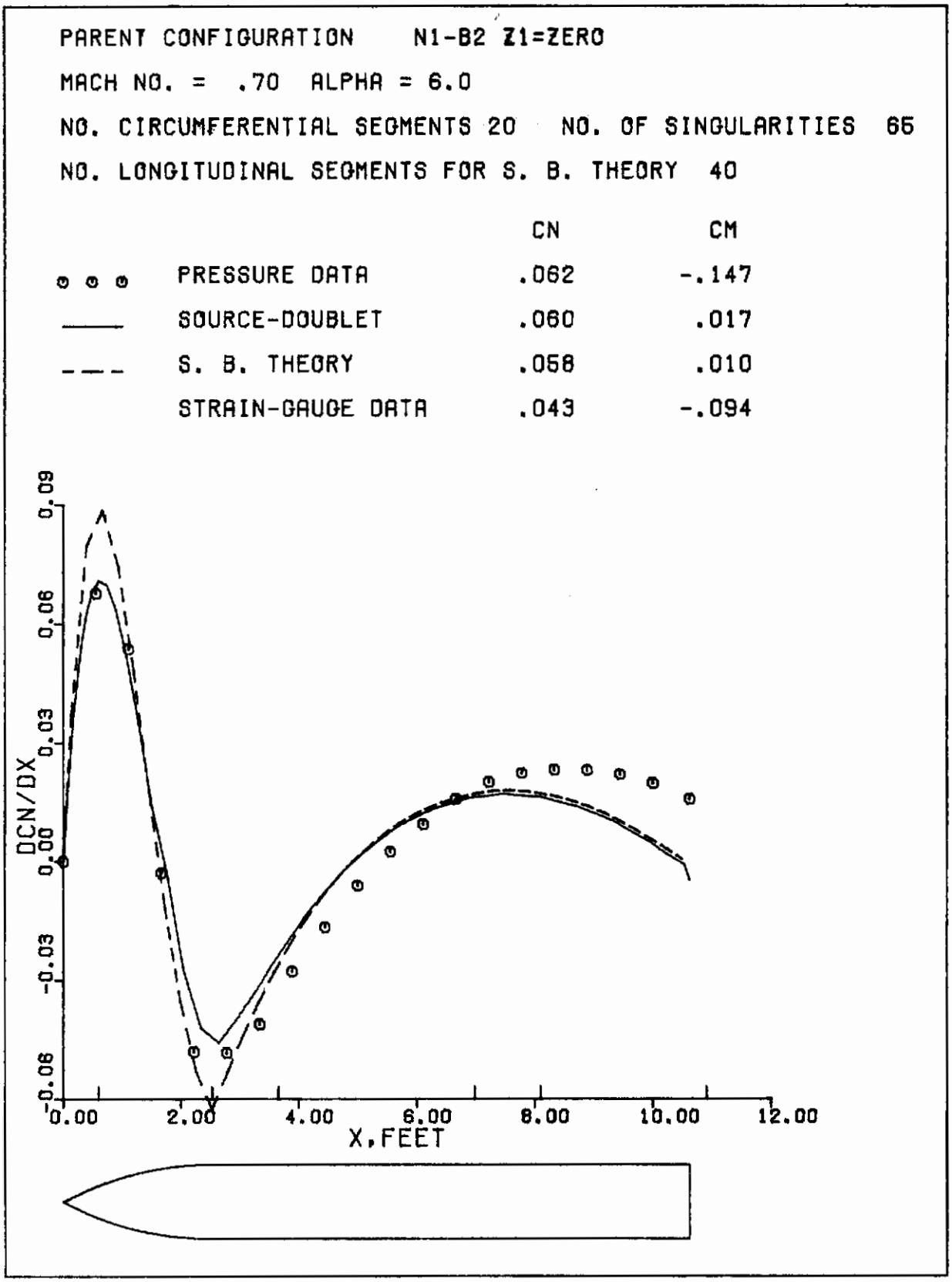

Figure 8. Wing-Body Forces and Moments (a) $^{dCn}/dx$ vs x

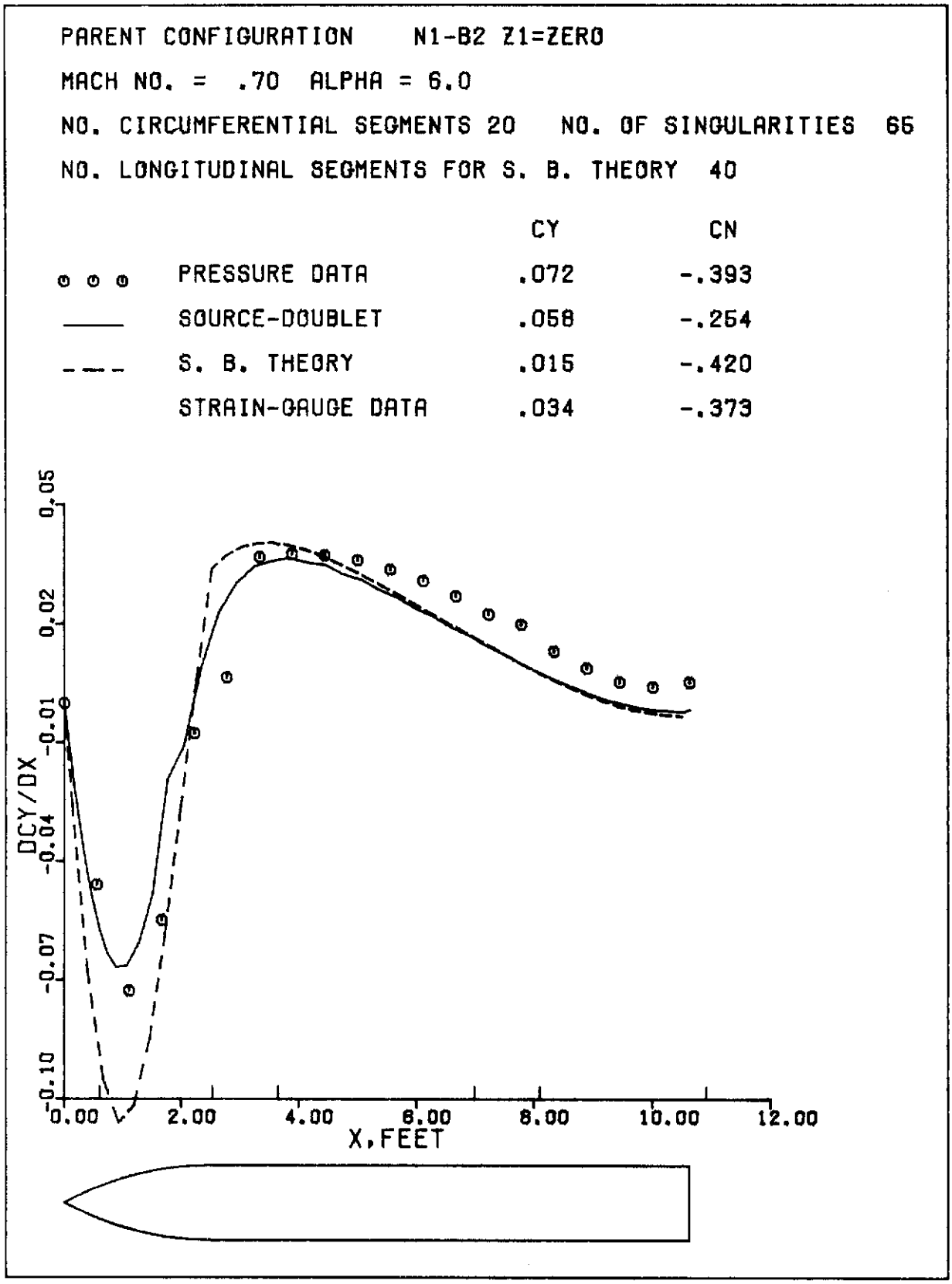

Figure 8 (Concluded). Wing-Body Forces and Moments (b) $^{dCy}/_{dx}$ vs x

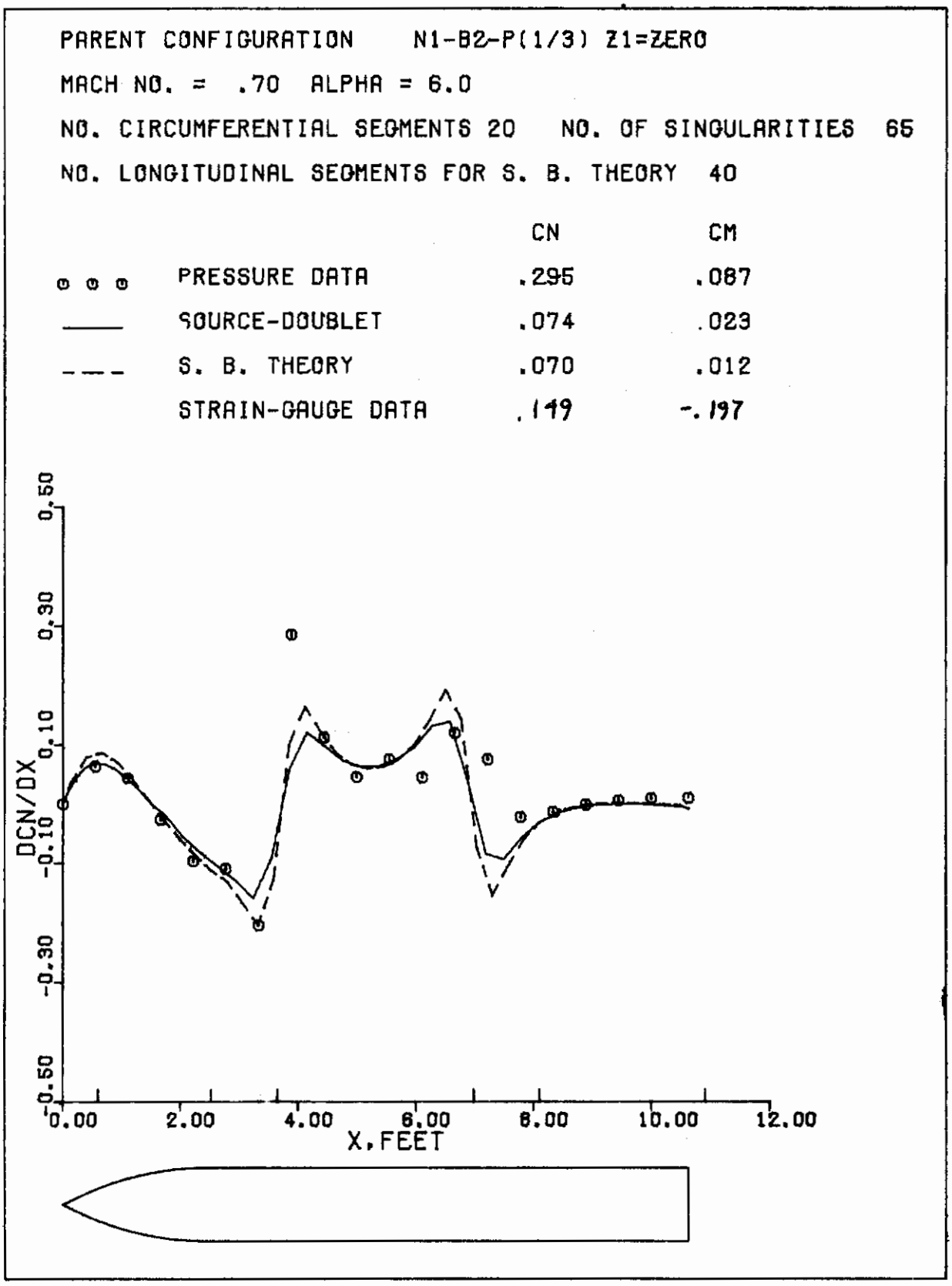

Figure 9. Wing-Body-Pylon Forces and Moments
(a) $^{dCn}/_{dx}$ vs x

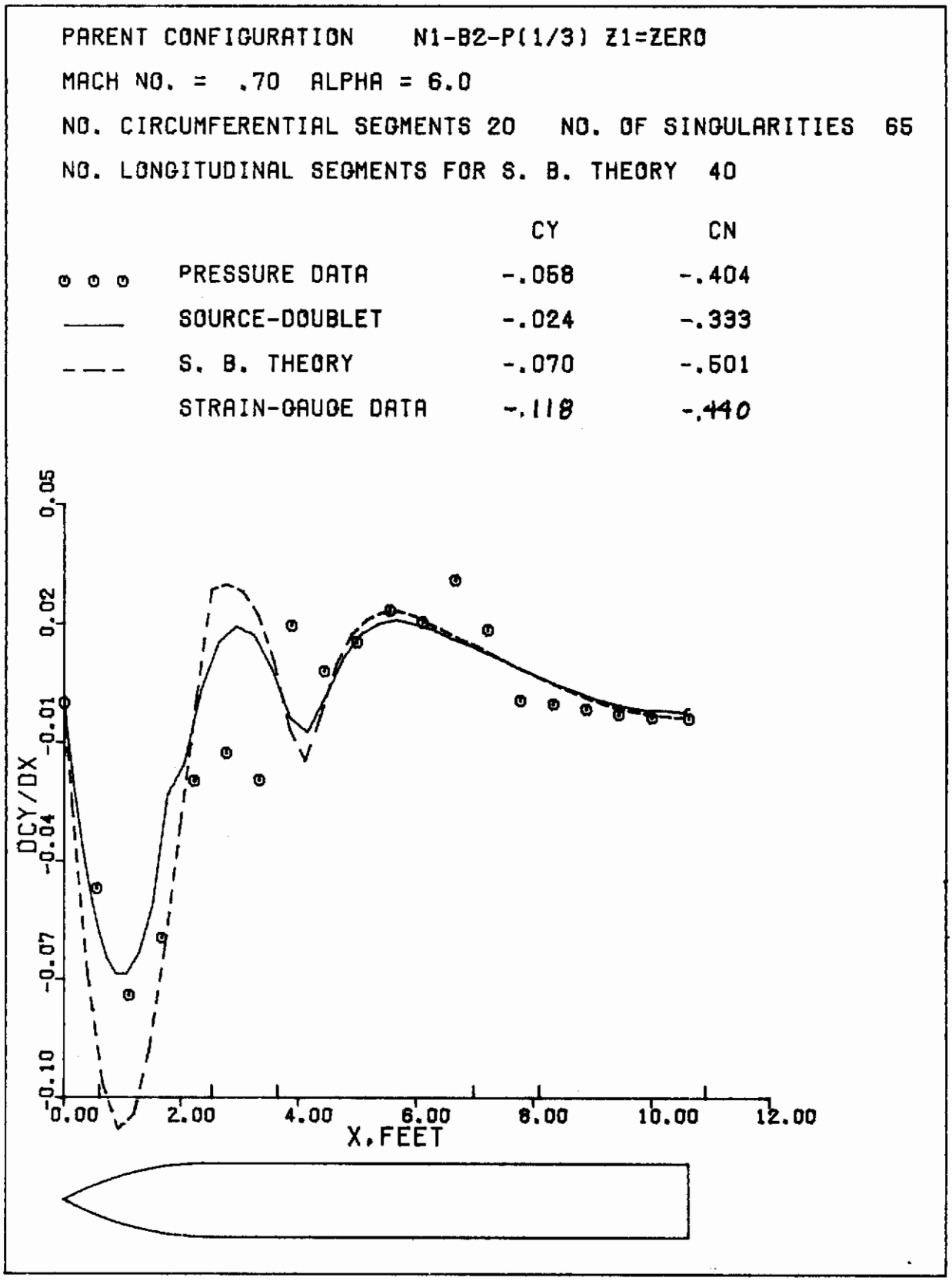

Figure 9. Wing-Body-Pylon Forces and Moments (Concluded) (b) dC_y/dx vs x

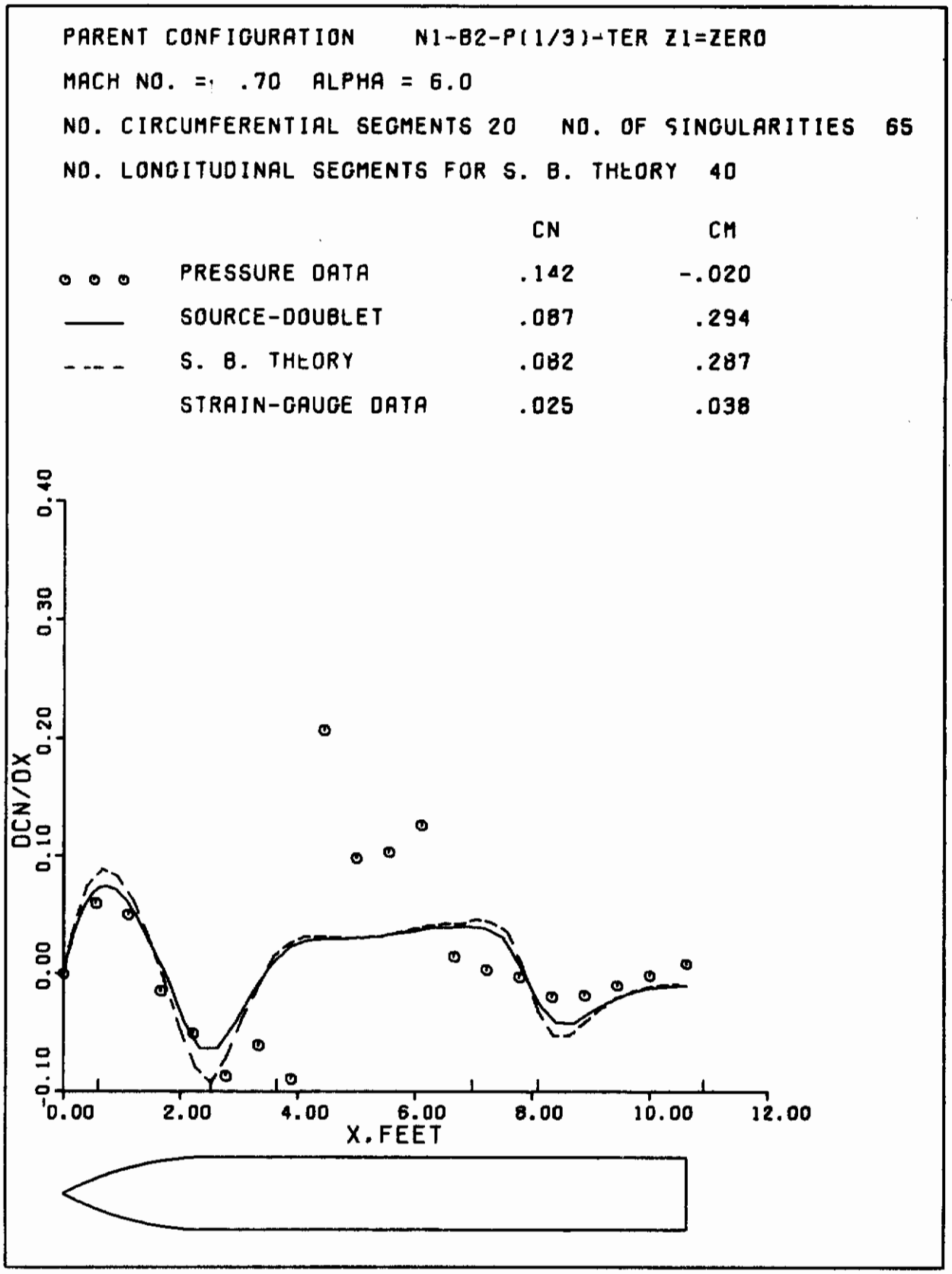

Figure 10. Wing-Body-Pylon-TER Forces and Moments

(a) dCn/dx vs x

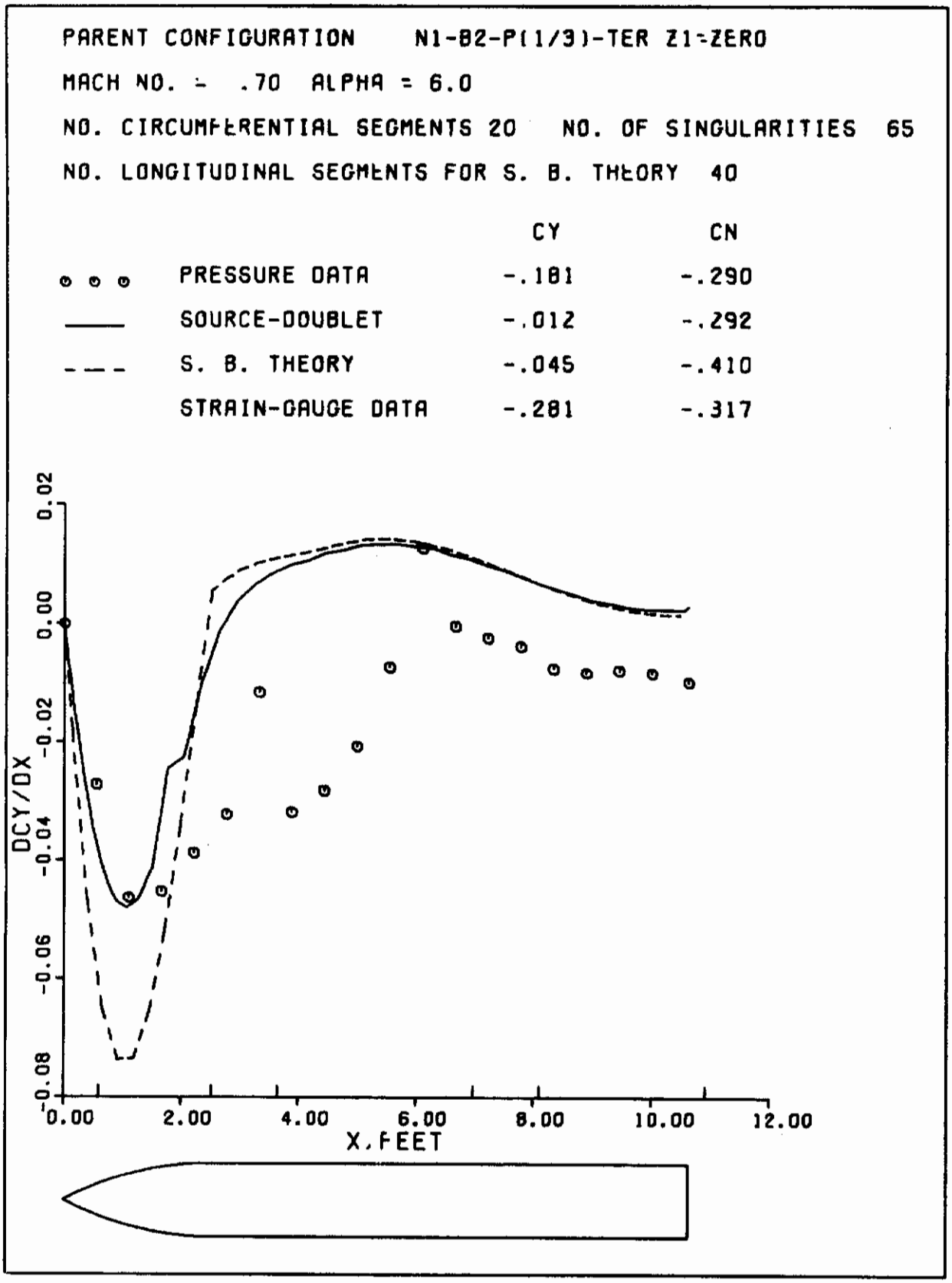

Figure 10. Wing-Body-Pylon-TER Forces and Moments (Concluded)

(b) dC_y/dx vs x

PARENT CONFIGURATION N1-B2-P(1/3)-TER-S2-S3 Z1=ZERO

MACH NO. = .70 ALPHA = 6.0

NO. CIRCUMFERENTIAL SEGMENTS 20 NO. OF SINGULARITIES 65

NO. LONGITUDINAL SEGMENTS FOR S. B. THEORY 40

		CN	CM
o o o	PRESSURE DATA	.352	-.514
———	SOURCE-DOUBLET	.304	.547
_ _ _	S. B. THEORY	.252	.413
	STRAIN-GAUGE DATA	.314	-.503

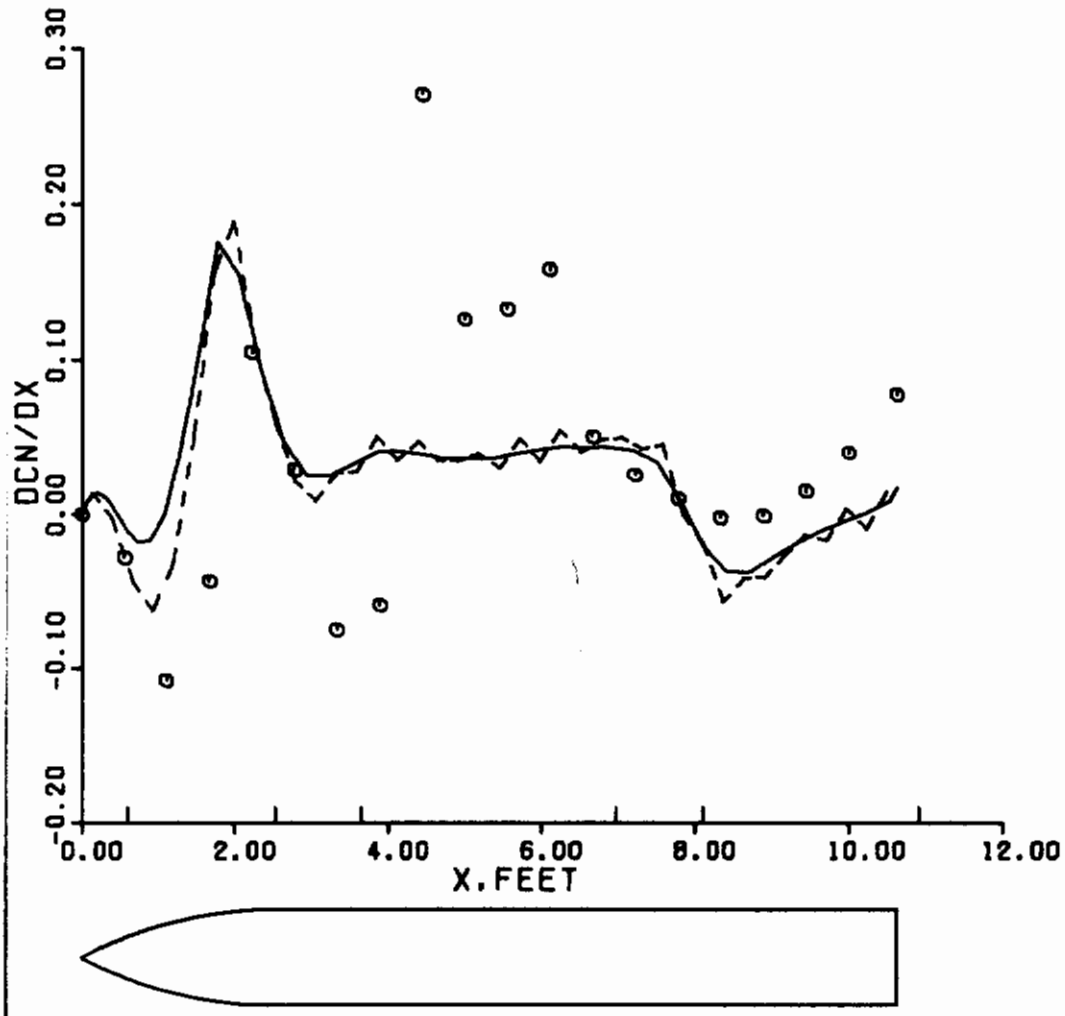

Figure 11. Wing-Body-Pylon-TER-Shoulder Stores Forces and Moments and Flow-Field Data (a) $^{dCn}/dx$ vs x

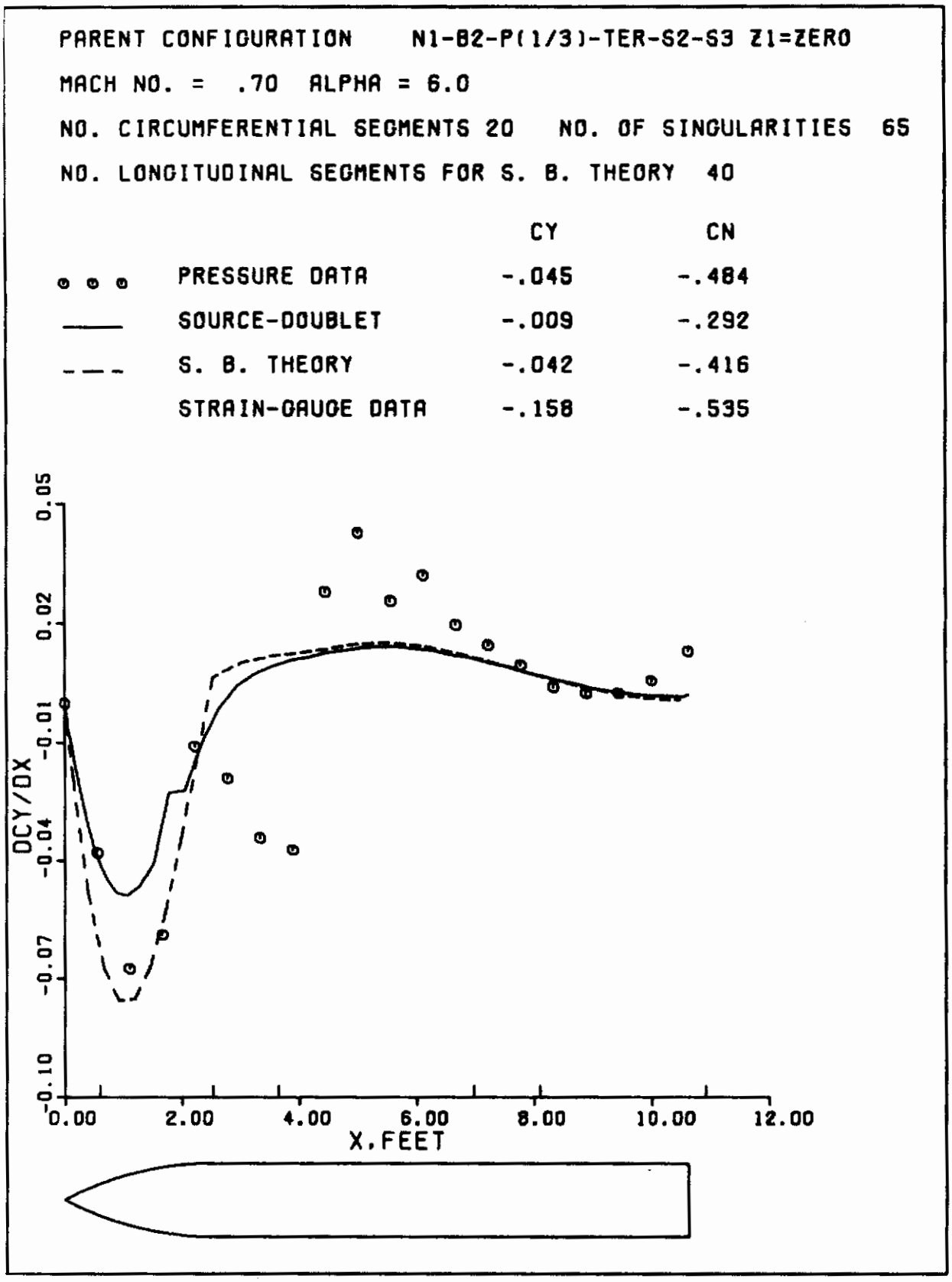

Figure 11. Wing-Body-Pylon-TER-Shoulder Stores Forces and Moments and (Contd)

Flow-Field Data (b) dCy/dx vs x

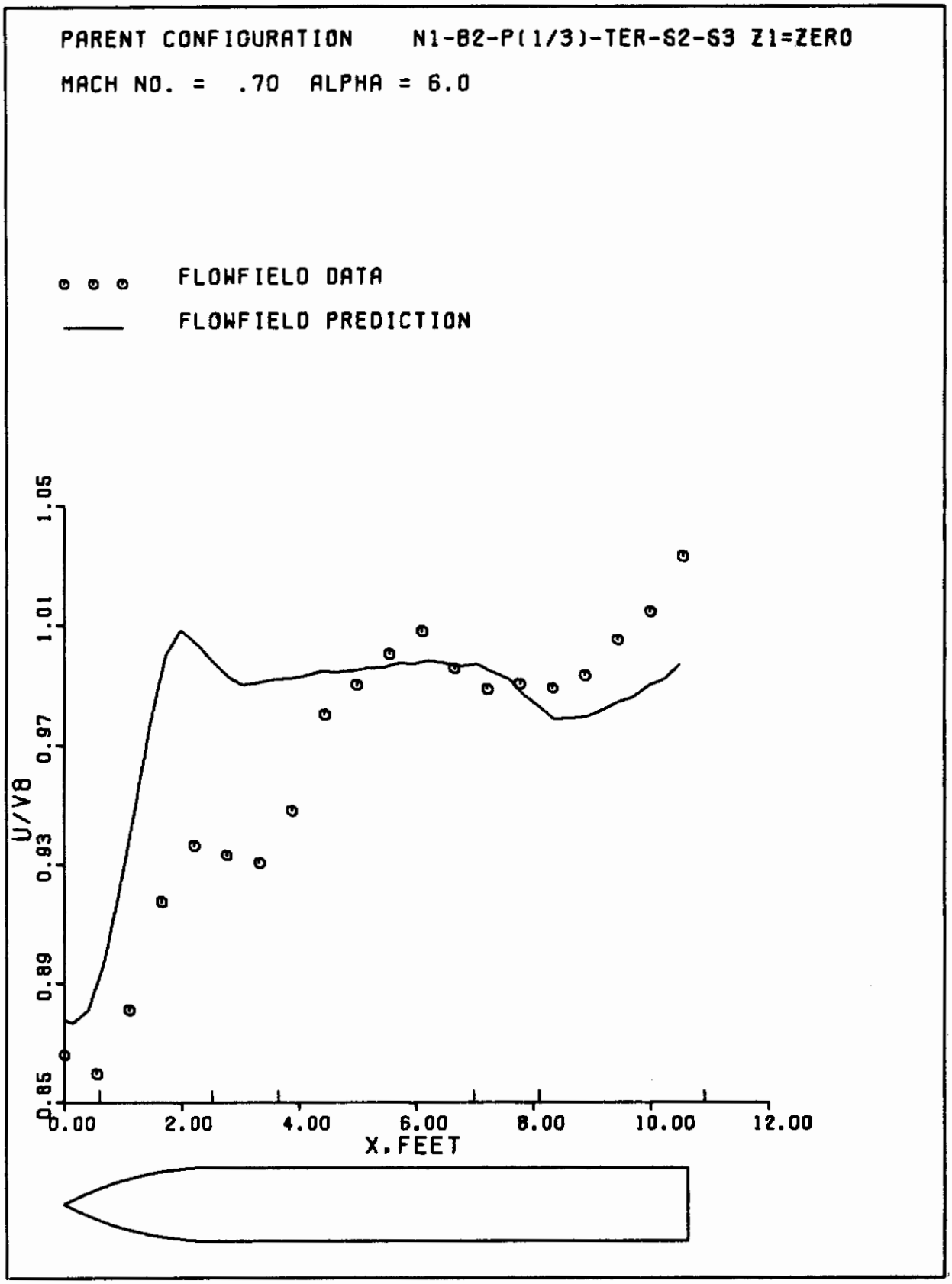

Figure 11. Wing-Body-Pylon-TER-Shoulder Stores Forces and Moments and (Contd)
Flow-Field Data (c) u Flow-Field Velocity

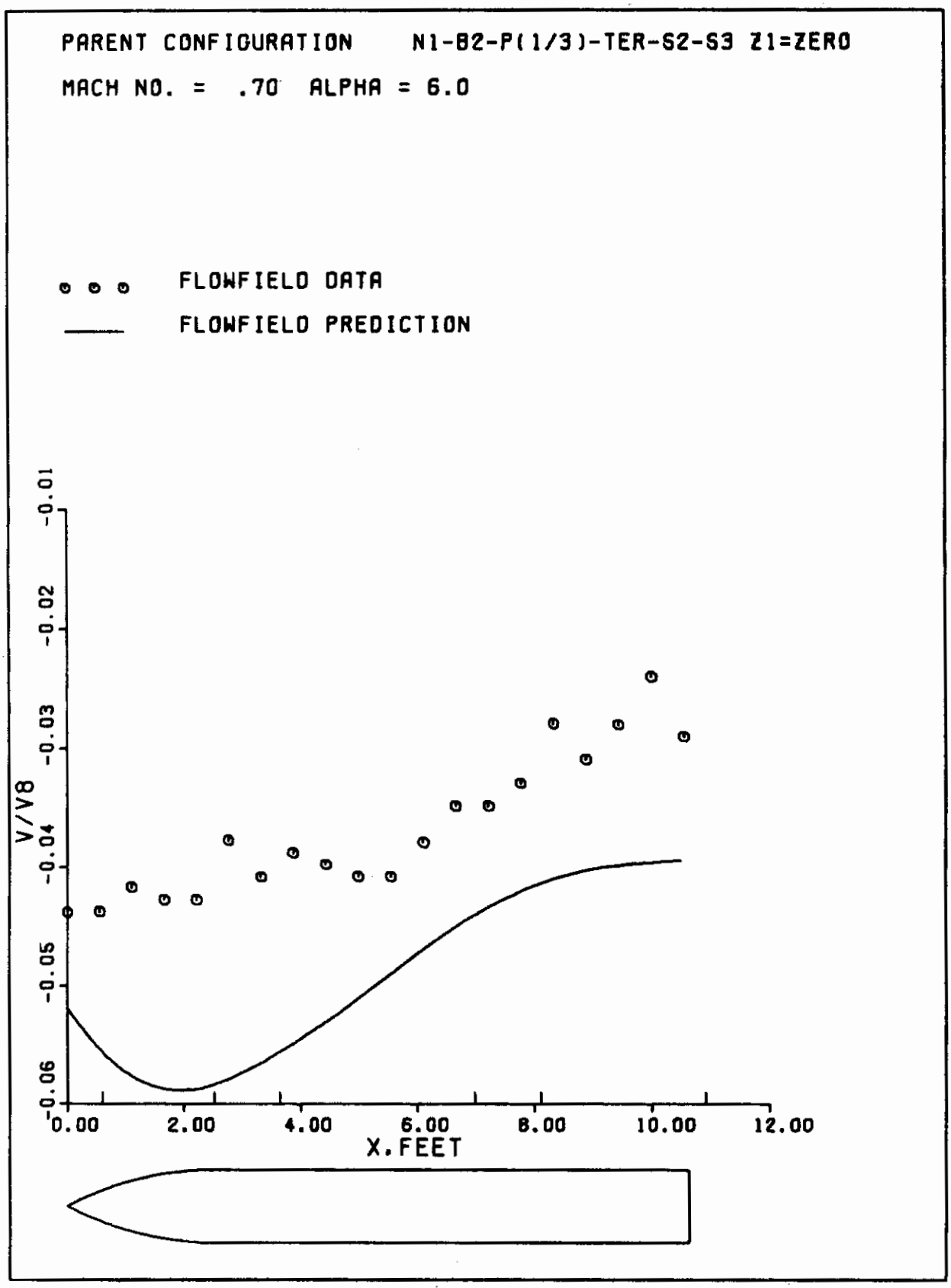

Figure 11. Wing-Body-Pylon-TER-Shoulder Stores Forces and Moments and (Contd) Flow-Field Data (d) v Flow-Field Velocity

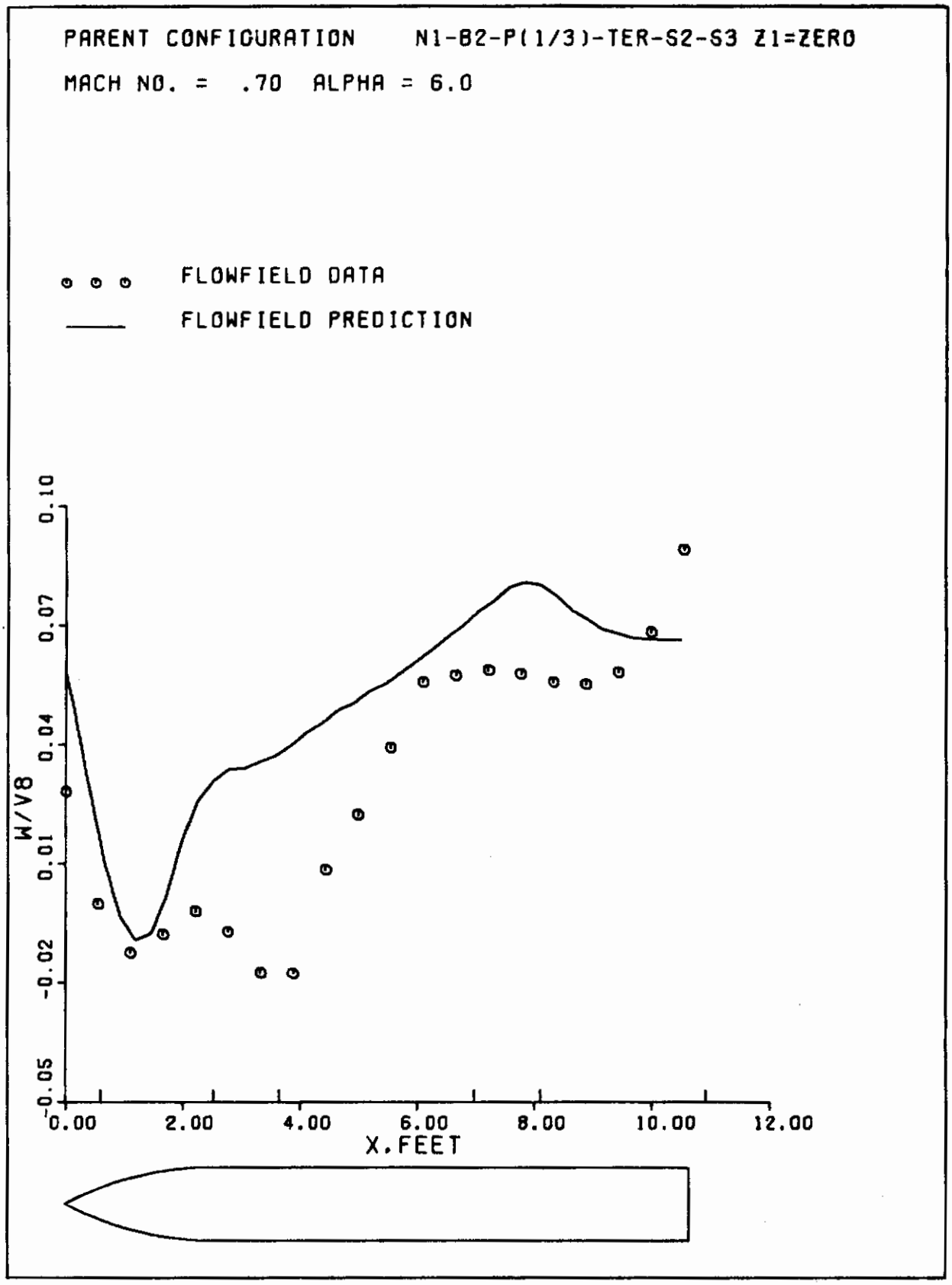

Figure 11. (Concluded) Wing-Body-Pylon-TER-Shoulder Stores Forces and Moments and Flow-Field Data (e) w Flow-Field Velocity

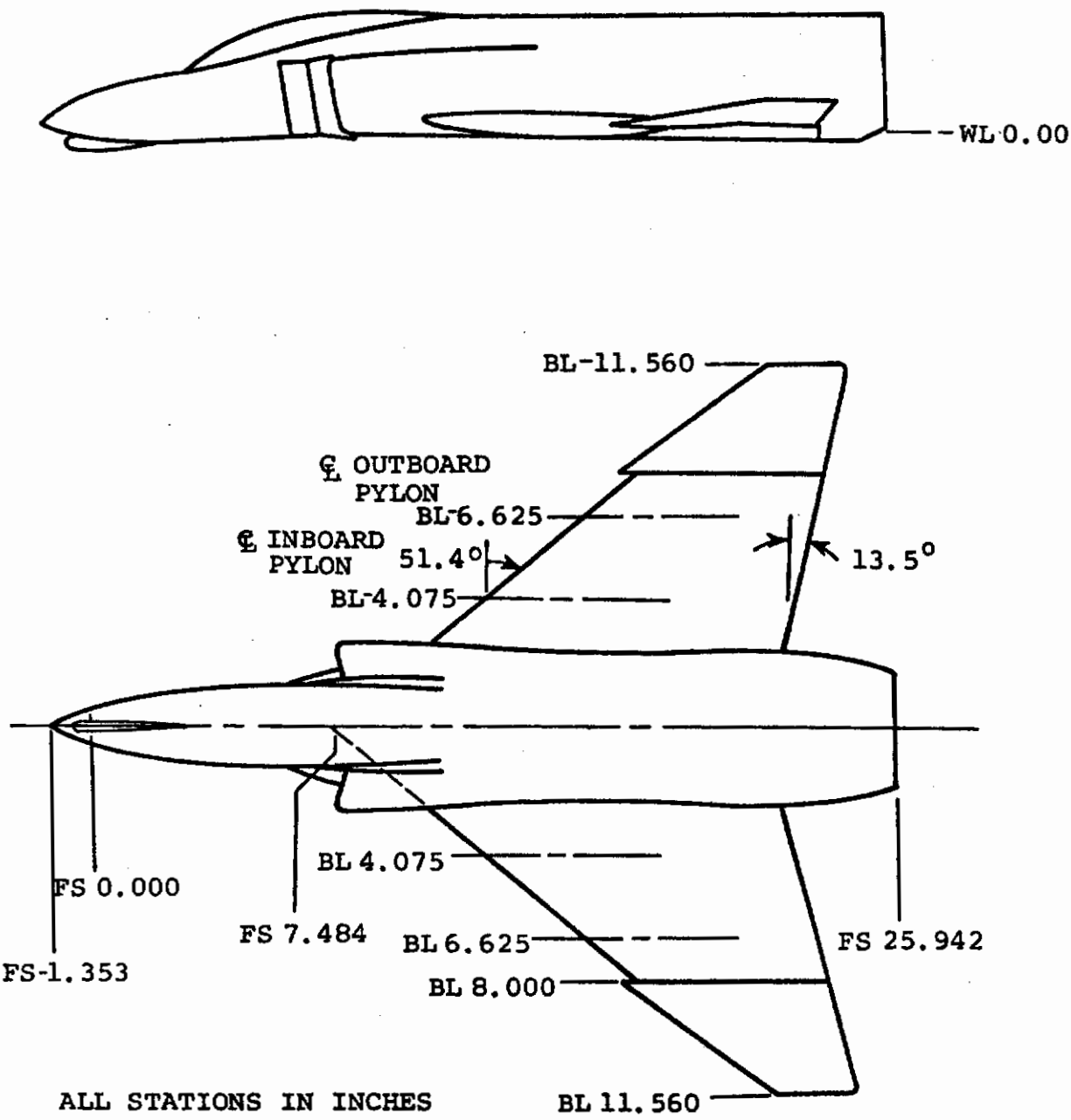

Figure 12. F4-C Aircraft Model

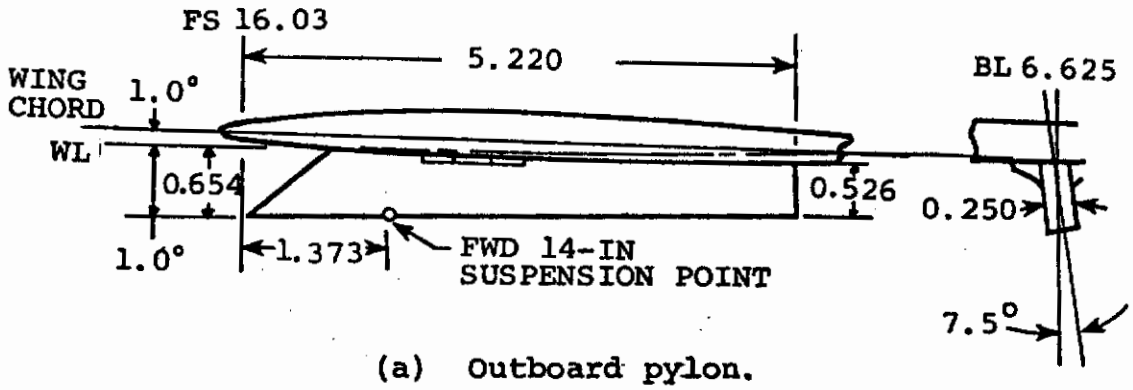

(a) Outboard pylon.

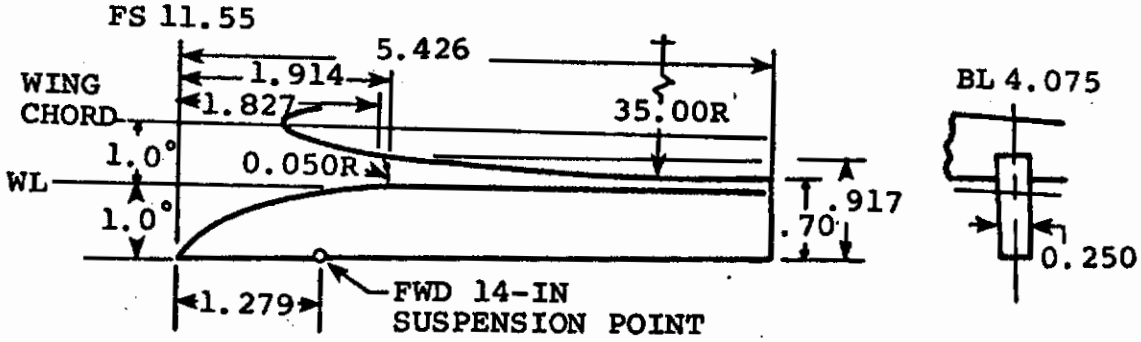

(b) Inboard pylon.

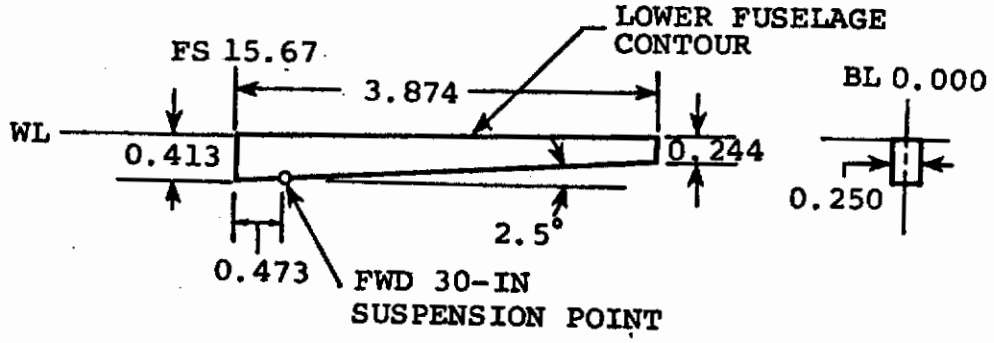

ALL DIMENSIONS IN INCHES

(c) Center pylon.

Figure 13. F4-C Pylon Models

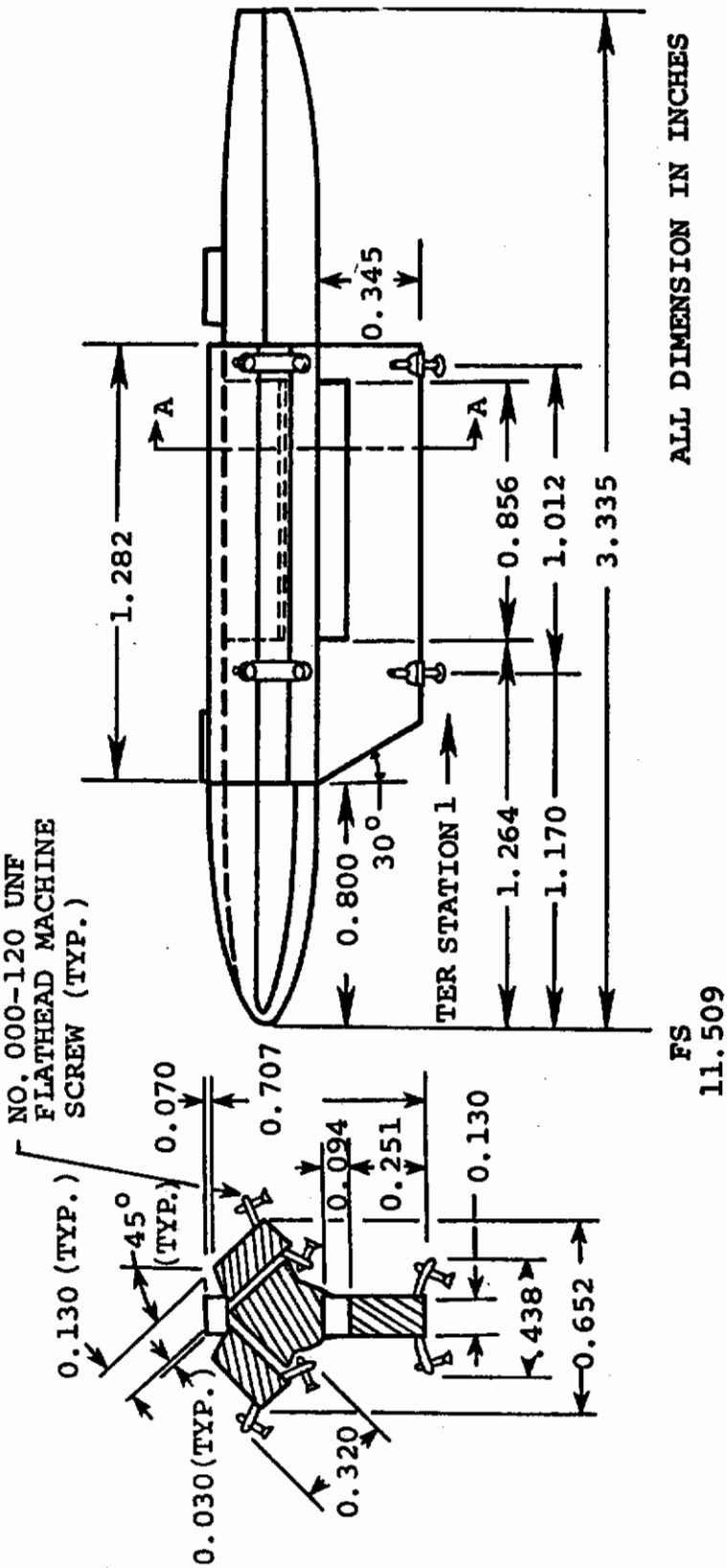

Figure 14. Modified Triple Ejector Model

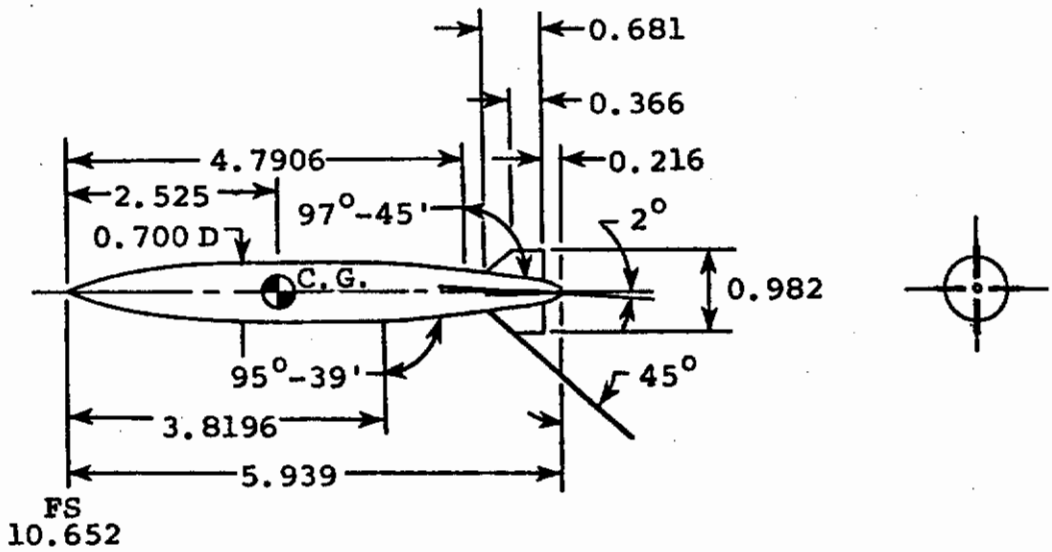

(a) Actual configuration.

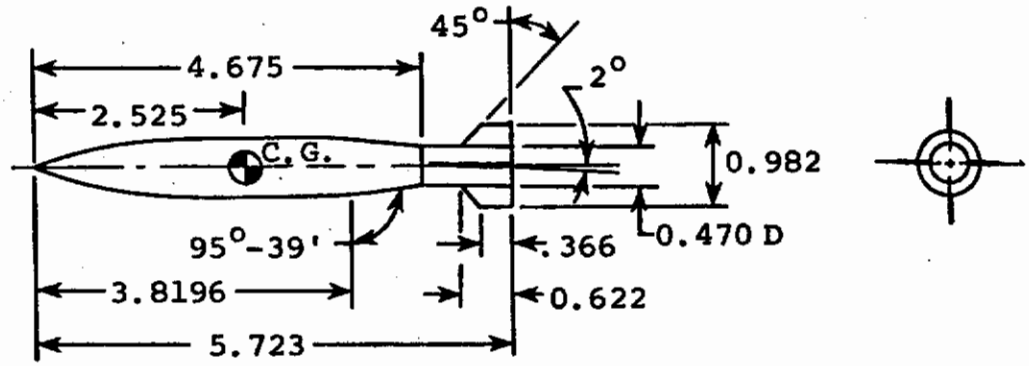

ALL DIMENSIONS IN INCHES

(b) Configuration modified for sting support.

Figure 15. Finned MK-83 Bomb Model

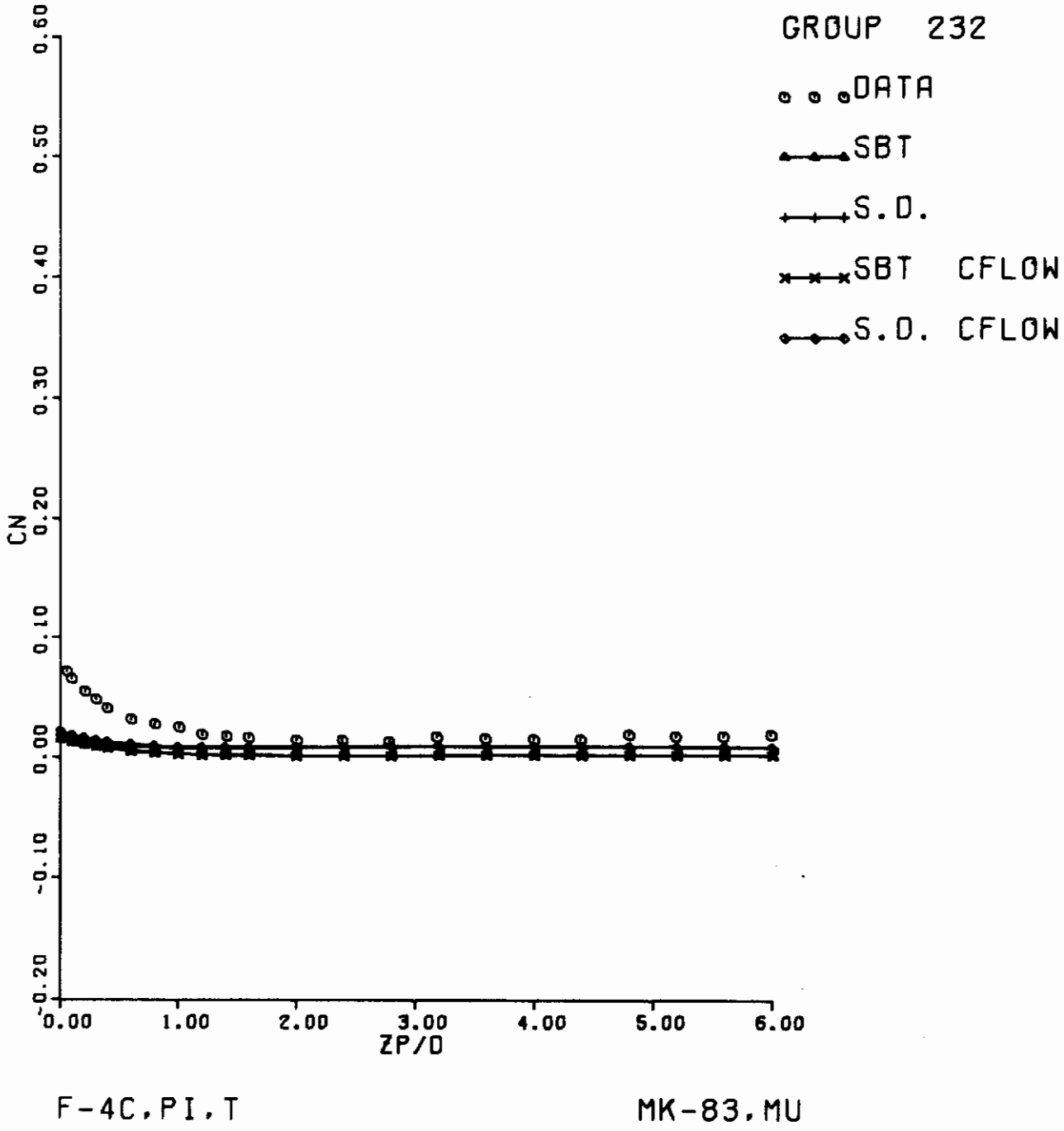

Figure 16. F-4C-Inboard Pylon-TER Loads at $Alpha_{store}=0^{o}$ with the Modified Unfinned MK-83 (a) C_n vs $Z_{P/D}$

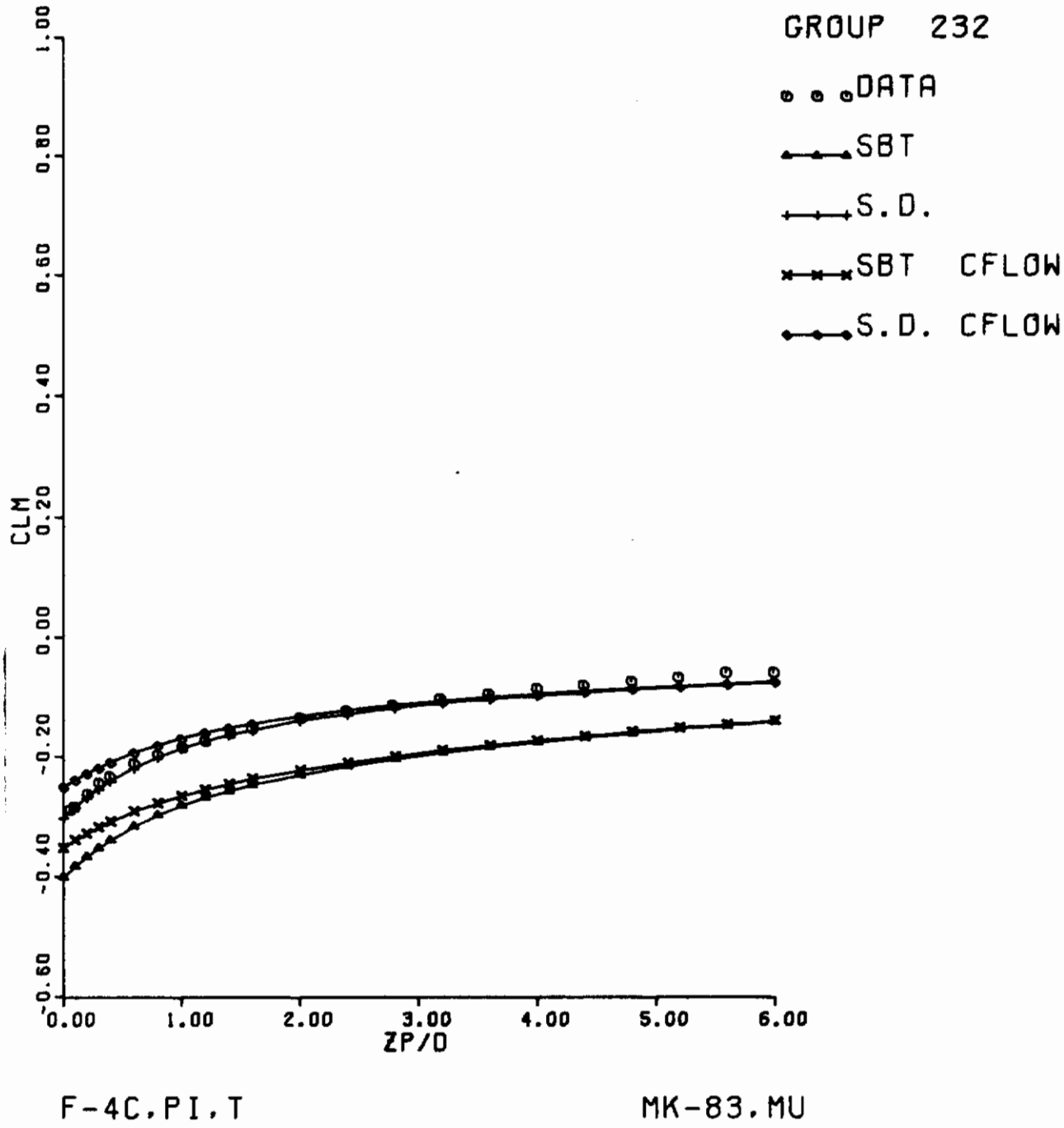

Figure 16. (Contd) F-4C-Inboard Pylon-TER Loads at $Alpha_{store}=0^{o}$ with the Modified Unfinned MK-83 (b) C_{ℓ_m} vs $Z_{P/D}$

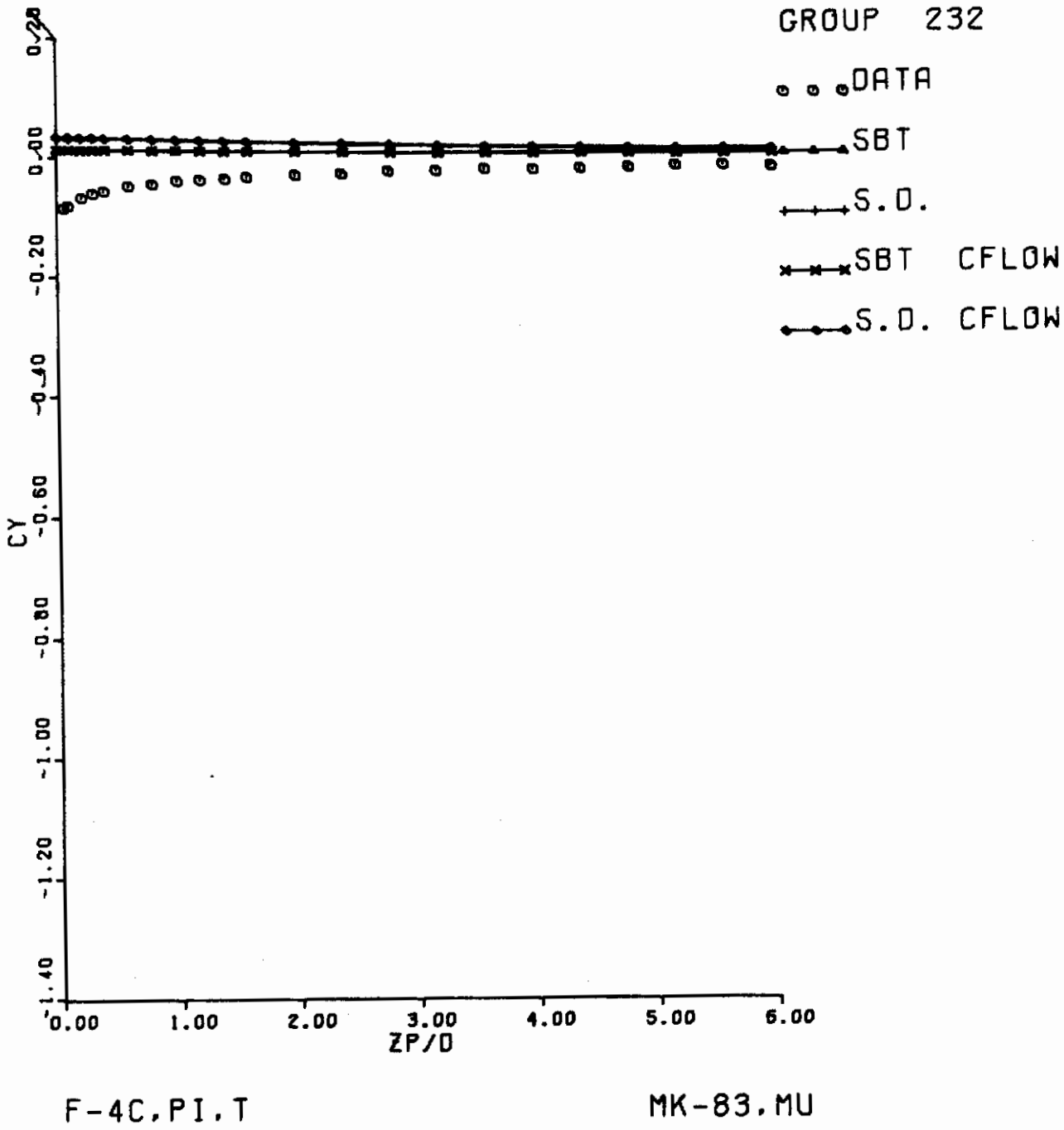

Figure 16. (Contd) F-4C-Inboard Pylon-TER Loads at $Alpha_{store}=0^{o}$ with the Modified Unfinned MK-83 (c) C_y vs $Z_{P/D}$

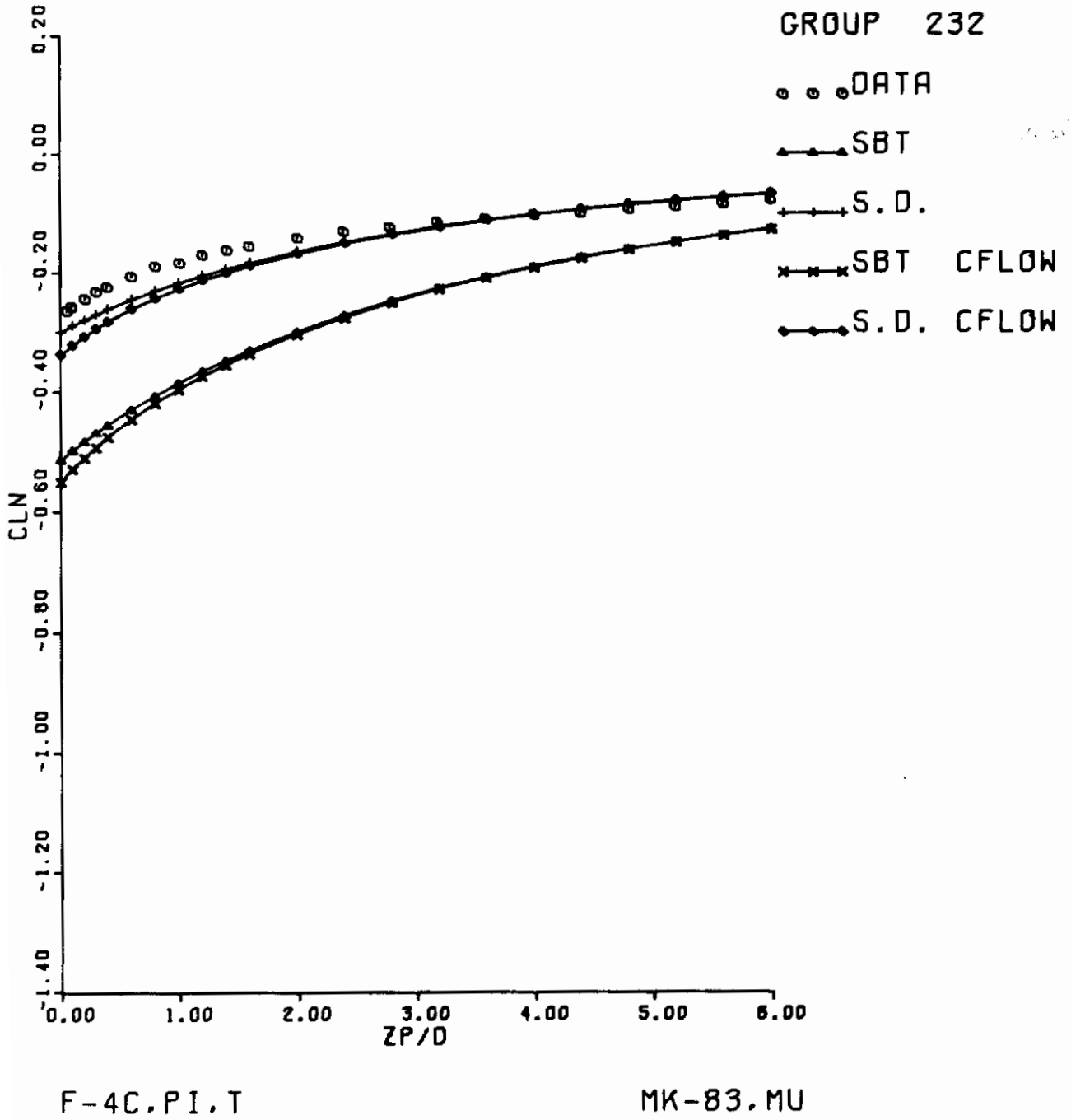

Figure 16. (Concluded) F-4C-Inboard Pylon-TER Loads at $Alpha_{store}=0^{o}$ with the Modified Unfinned MK-83 (d) C_{ℓ_n} vs $Z_{P/D}$

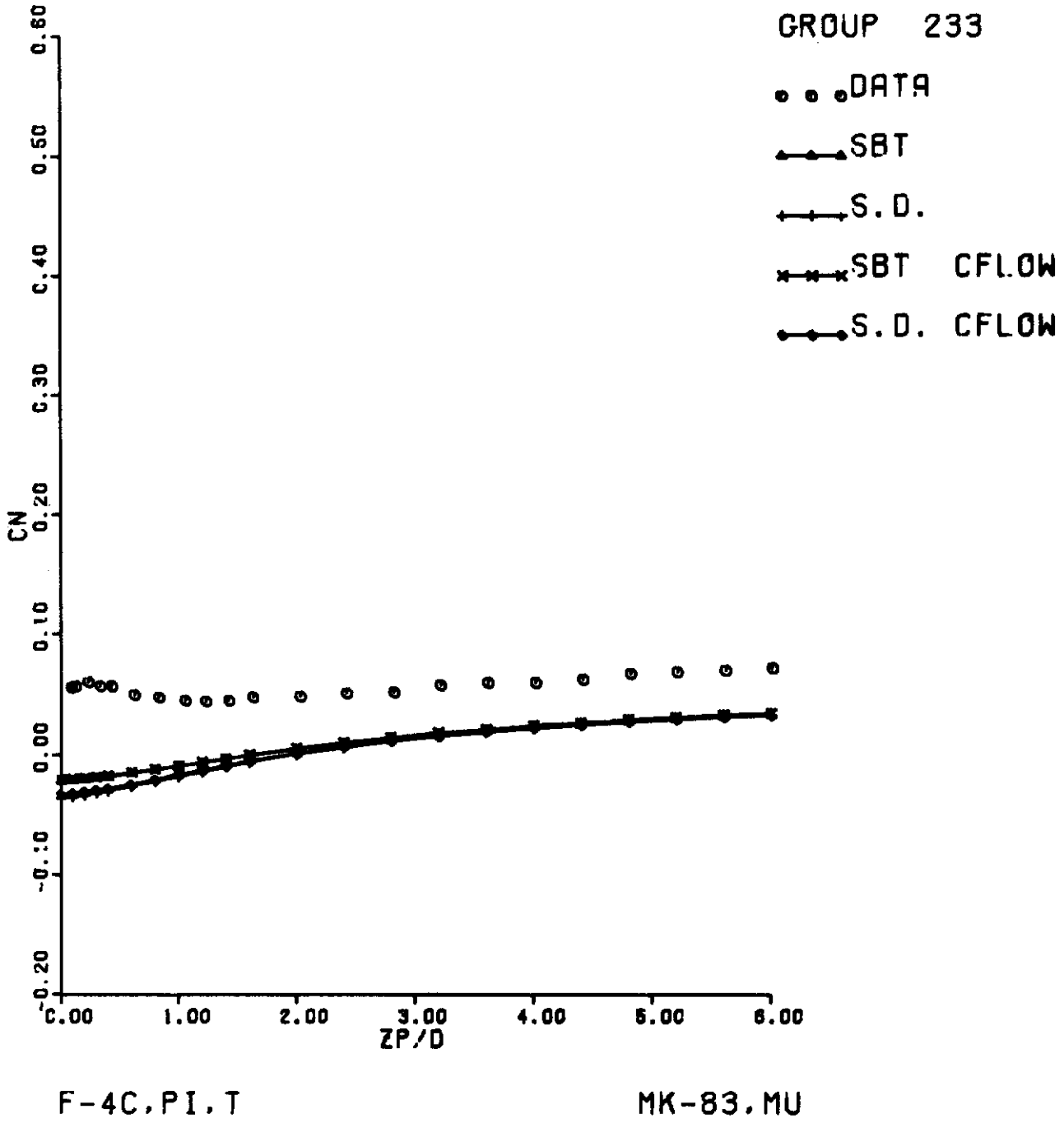

Figure 17. F-4C-Inboard Pylon-TER Loads at $Alpha_{store}=4^{o}$ with the Modified Unfinned MK-83 (a) C_n vs $Z_{P/D}$

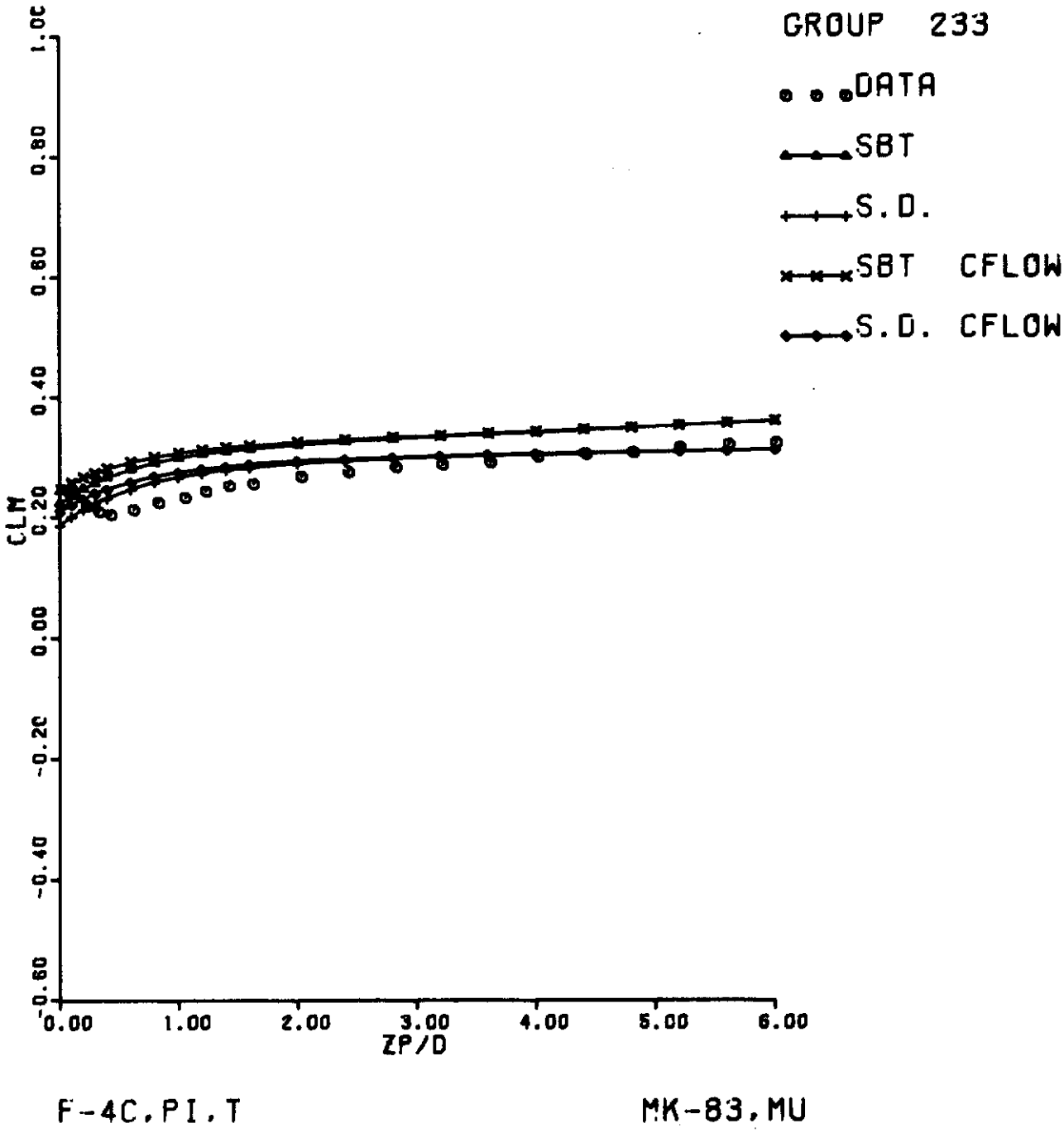

Figure 17. (Contd) F-4C-Inboard Pylon-TER Loads at $Alpha_{store}=4^{o}$ with the Modified Unfinned MK-83 (b) C_{ℓ_m} vs $Z_{P/D}$

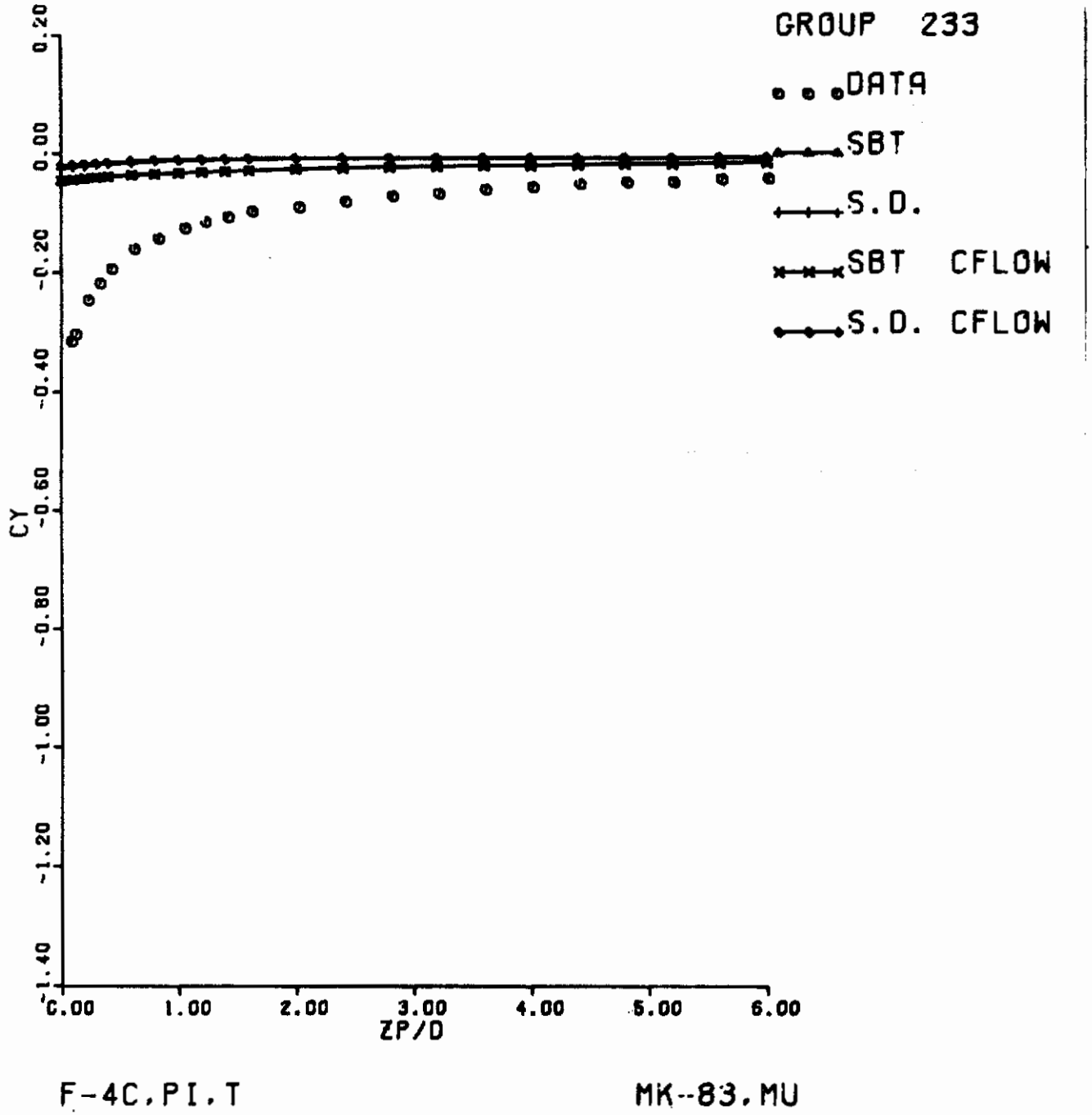

Figure 17. (Contd) F-4C-Inboard Pylon-TER Loads at $Alpha_{store}$=4° with the Modified Unfinned MK-83 (c) C_y vs $Z_{P/D}$

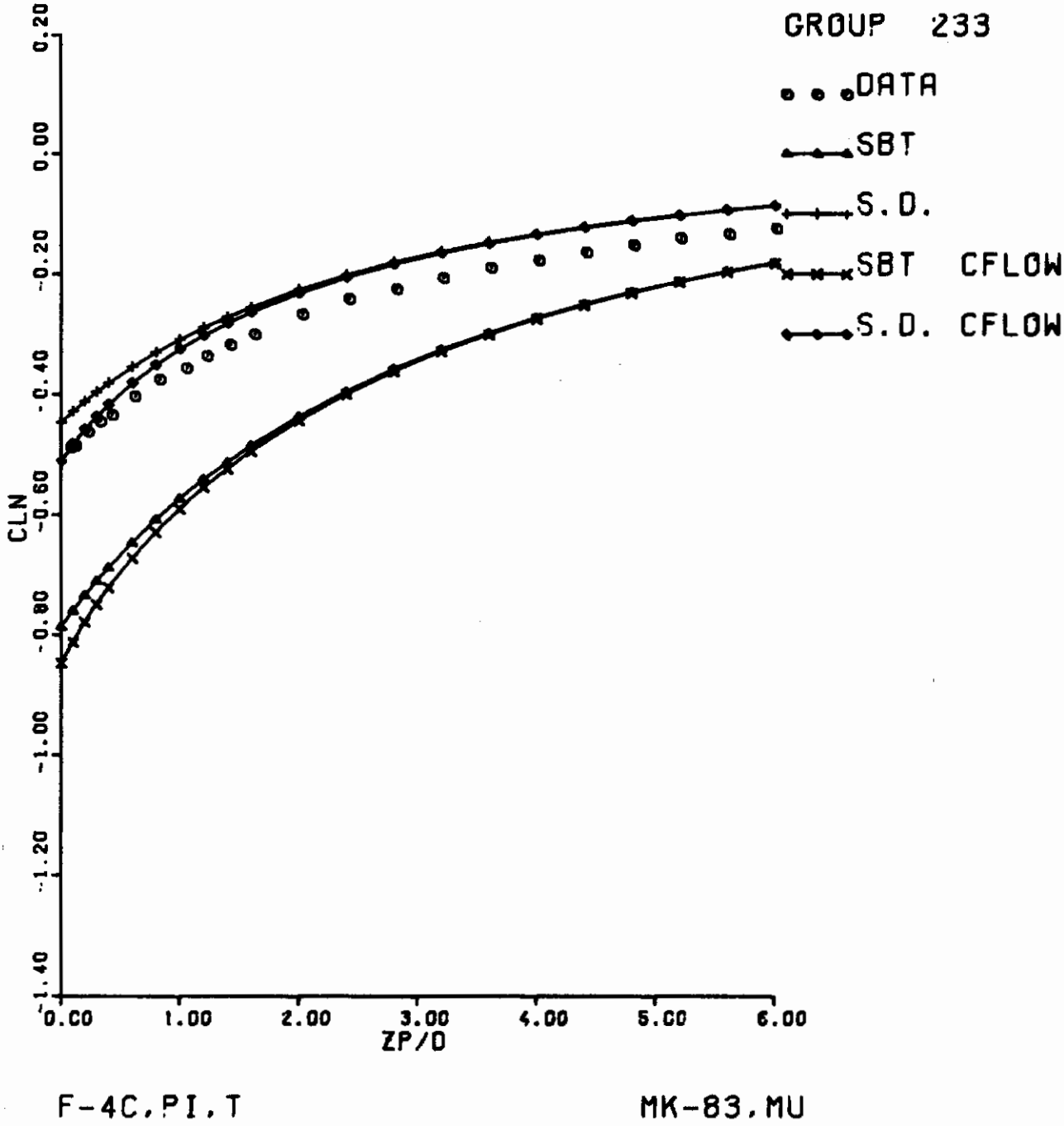

Figure 17. (Concluded) F-4C-Inboard Pylon-TER Loads at $Alpha_{store}=4^{o}$ with the Modified Unfinned MK-83 (d) C_{ℓ_n} vs $Z_{P/D}$

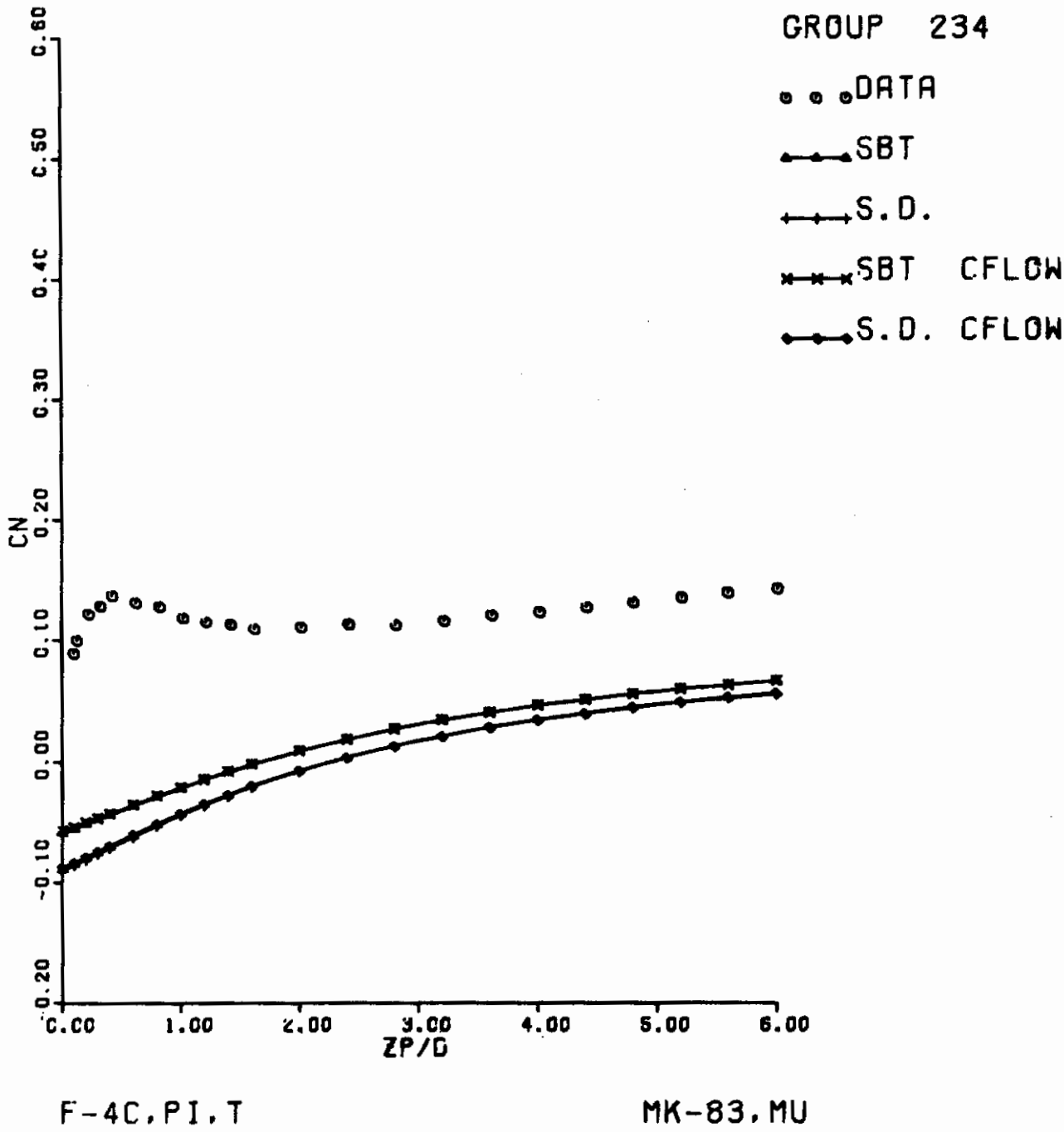

Figure 18. F-4C-Inboard Pylon-TER Loads at $Alpha_{store}=8^{o}$ with the Modified Unfinned MK-83 (a) C_n vs $Z_{P/D}$

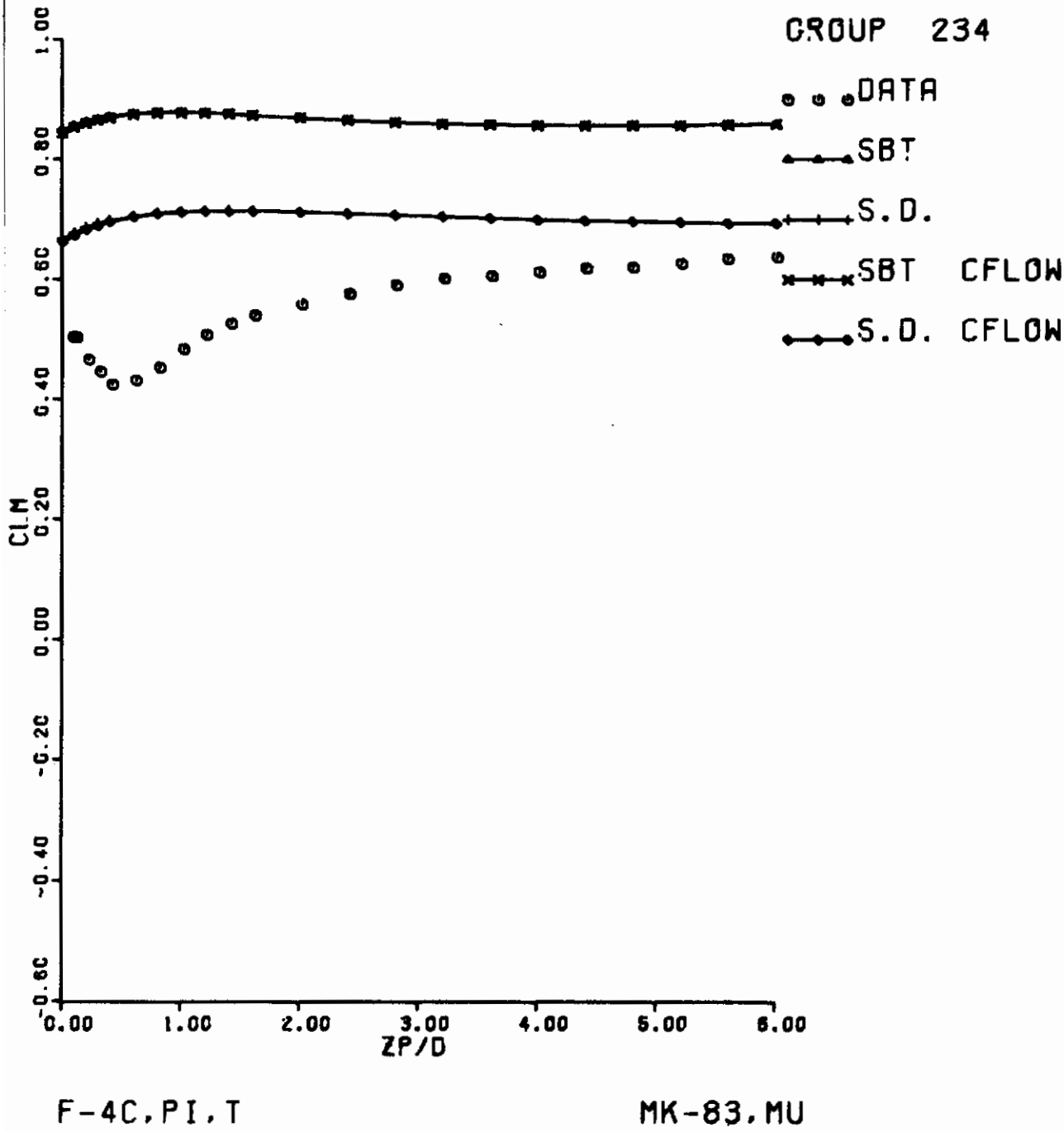

Figure 18. (Contd) F-4C-Inboard Pylon-TER Loads at $Alpha_{store}=8^{o}$ with the Modified Unfinned MK-83 (b) C_{ℓ_m} vs $Z_{P/D}$

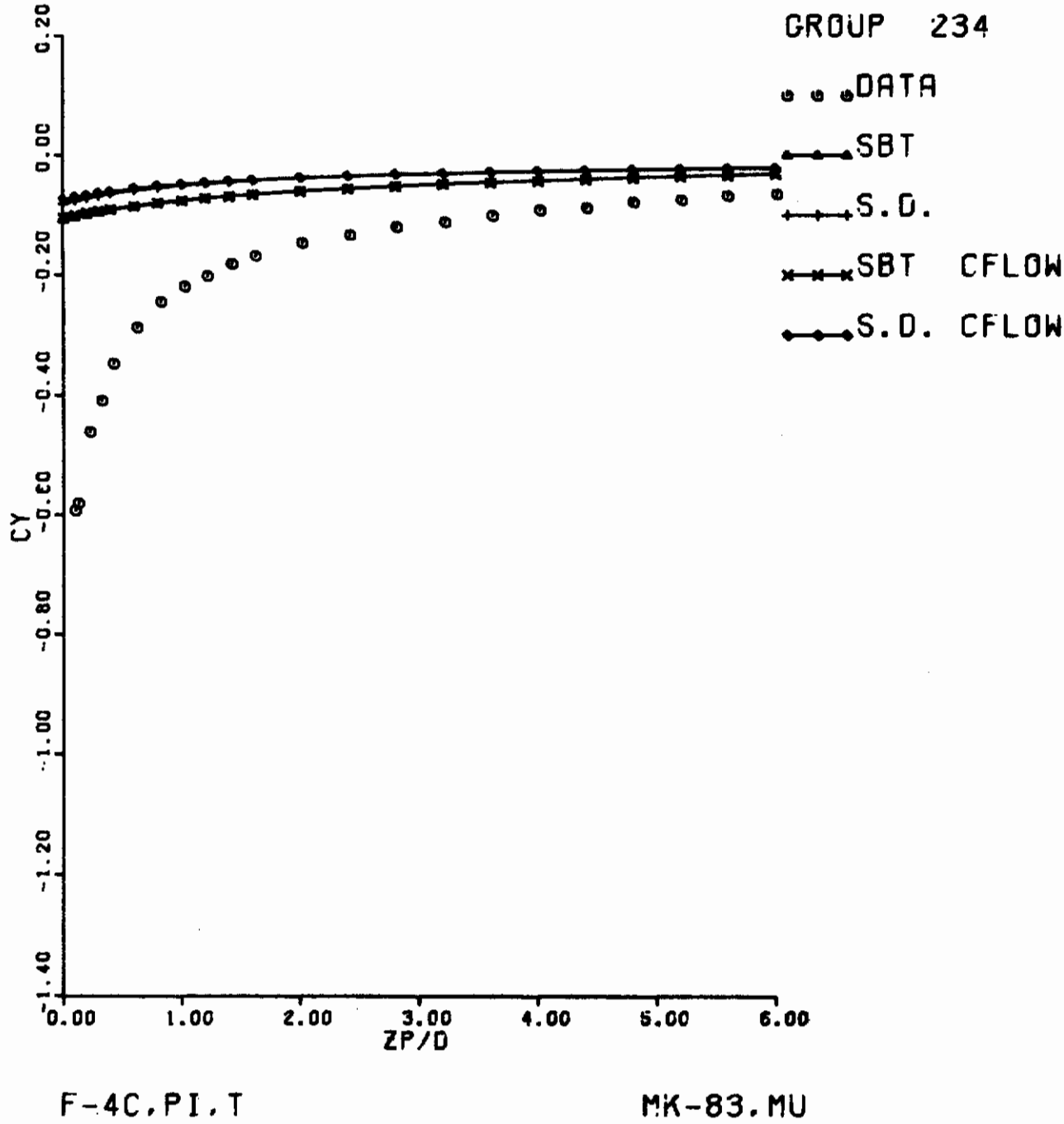

Figure 18. (Contd) F-4C-Inboard Pylon-TER Loads at $Alpha_{store}=8^{o}$ with the Modified Unfinned MK-83 (c) C_y vs $Z_{P/D}$

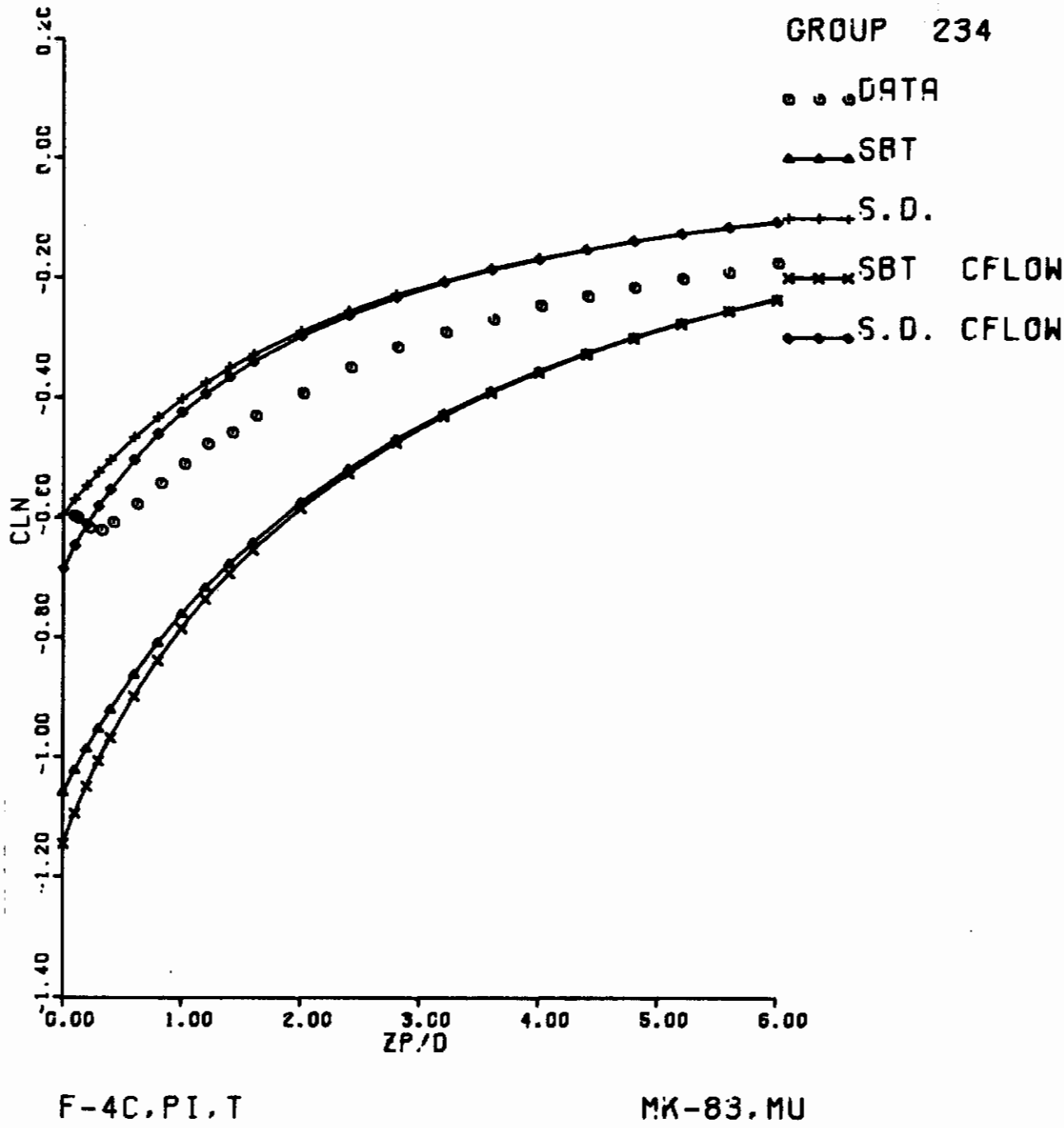

Figure 18. (Concluded) F-4C-Inboard Pylon-TER Loads at $Alpha_{store}=8^{o}$ with the Modified Unfinned MK-83 (d) C_{ℓ_n} vs $Z_{P/D}$

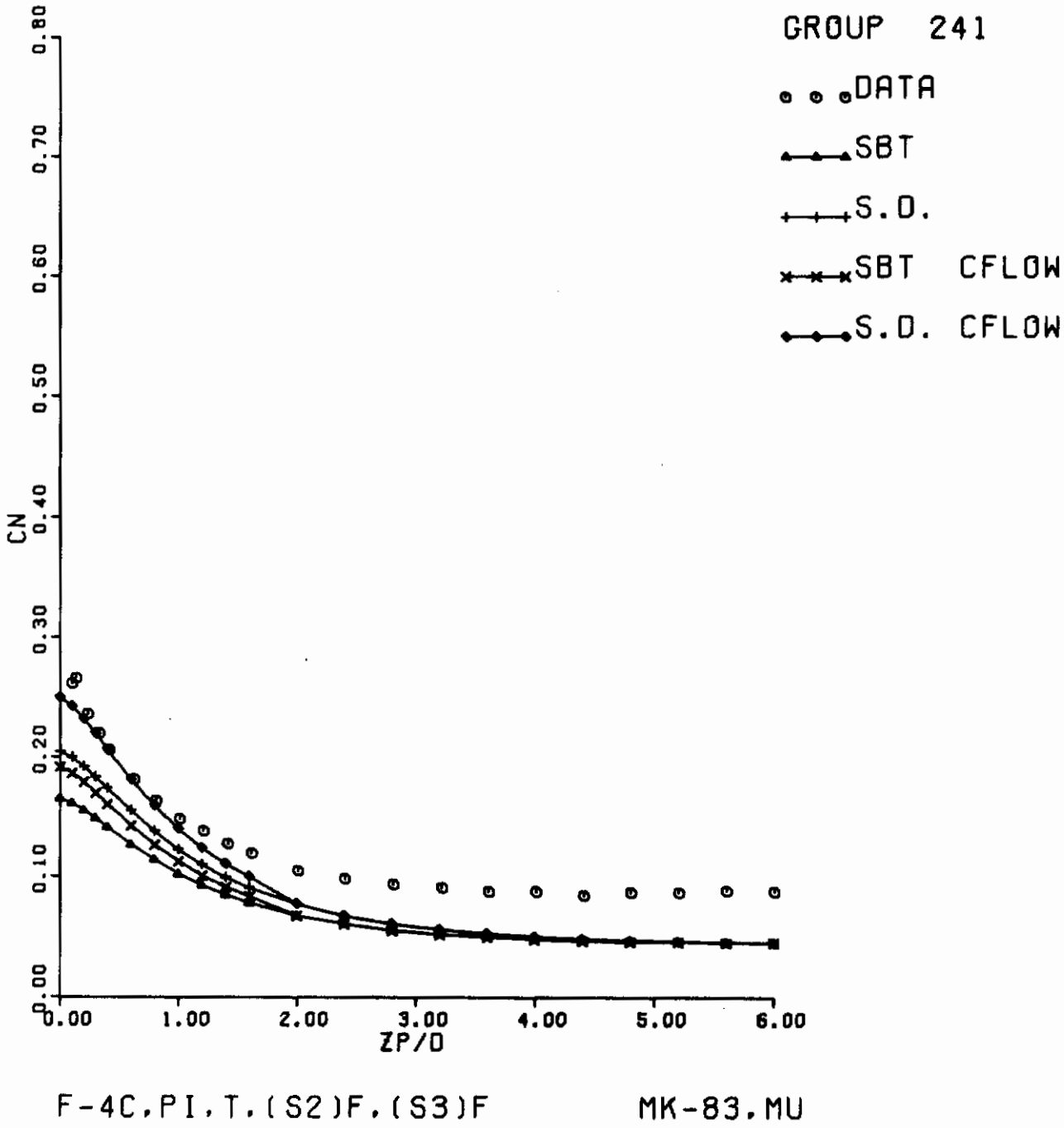

Figure 19. F-4C-Inboard Pylon-TER-2 Finned MK-83 Shoulder Stores Loads at $Alpha_{store}=4^{o}$ with the Modified Unfinned MK-83
(a) C_n vs $Z_{P/D}$

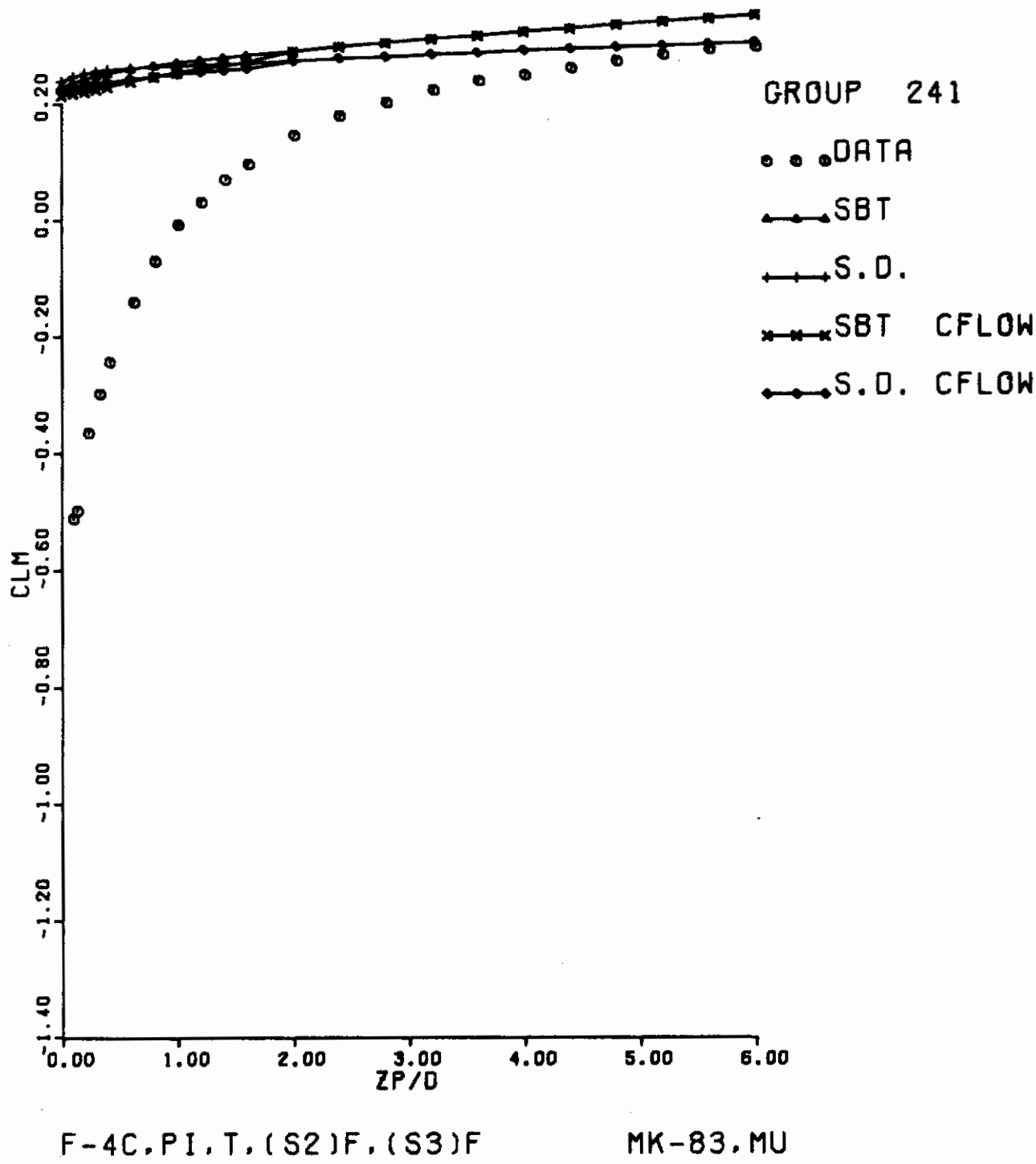

Figure 19. (Contd) F-4C-Inboard Pylon-TER-2 Finned MK-83 Shoulder Stores Loads at $Alpha_{store}=4^{o}$ with the Modified Unfinned MK-83
(b) C_{ℓ_m} vs $Z_{P/D}$

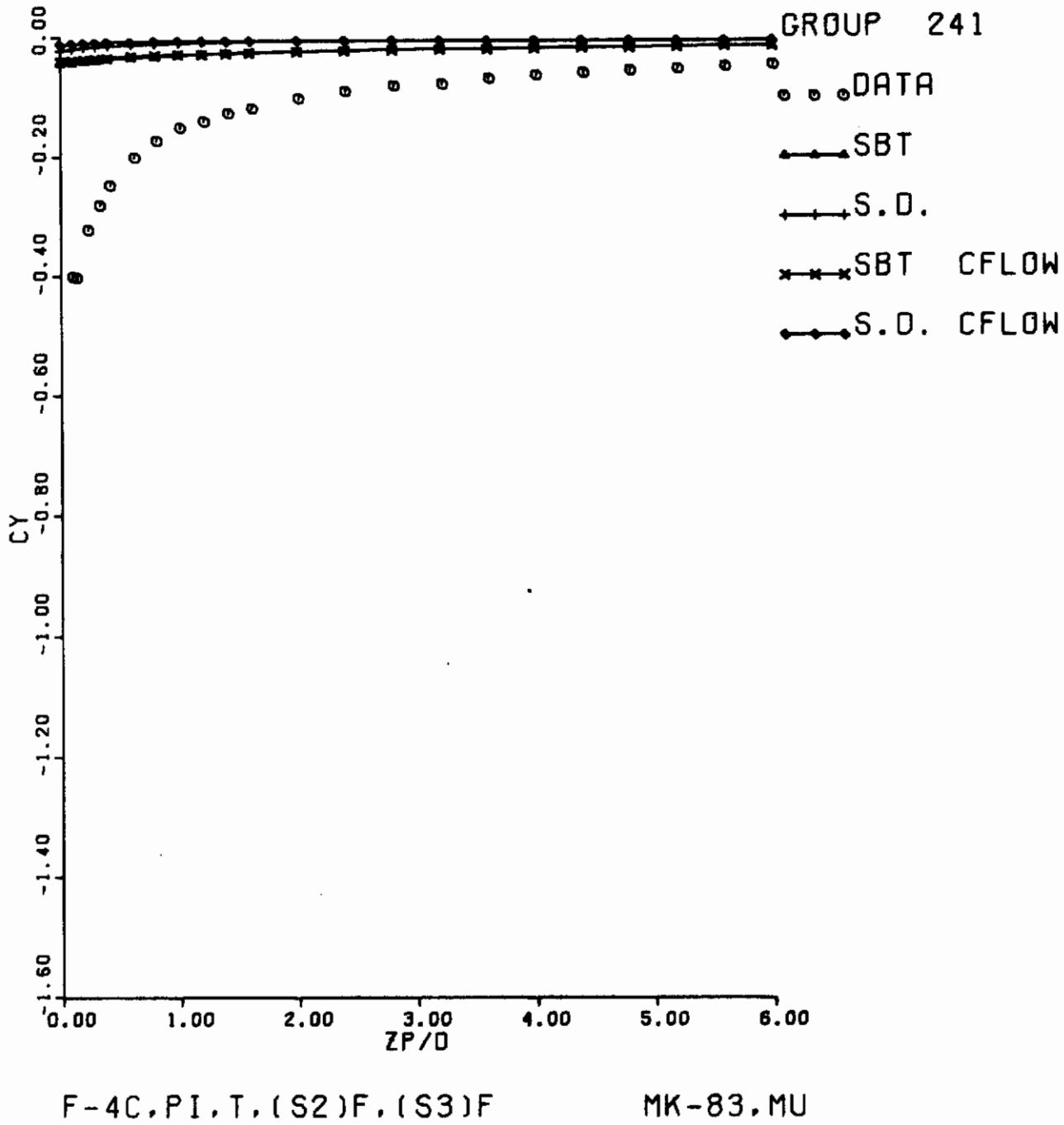

Figure 19. (Contd) F-4C-Inboard Pylon-TER-2 Finned MK-83 Shoulder Stores Loads at $Alpha_{store}=4^{o}$ with the Modified Unfinned MK-83

(c) C_y vs $Z_{P/D}$

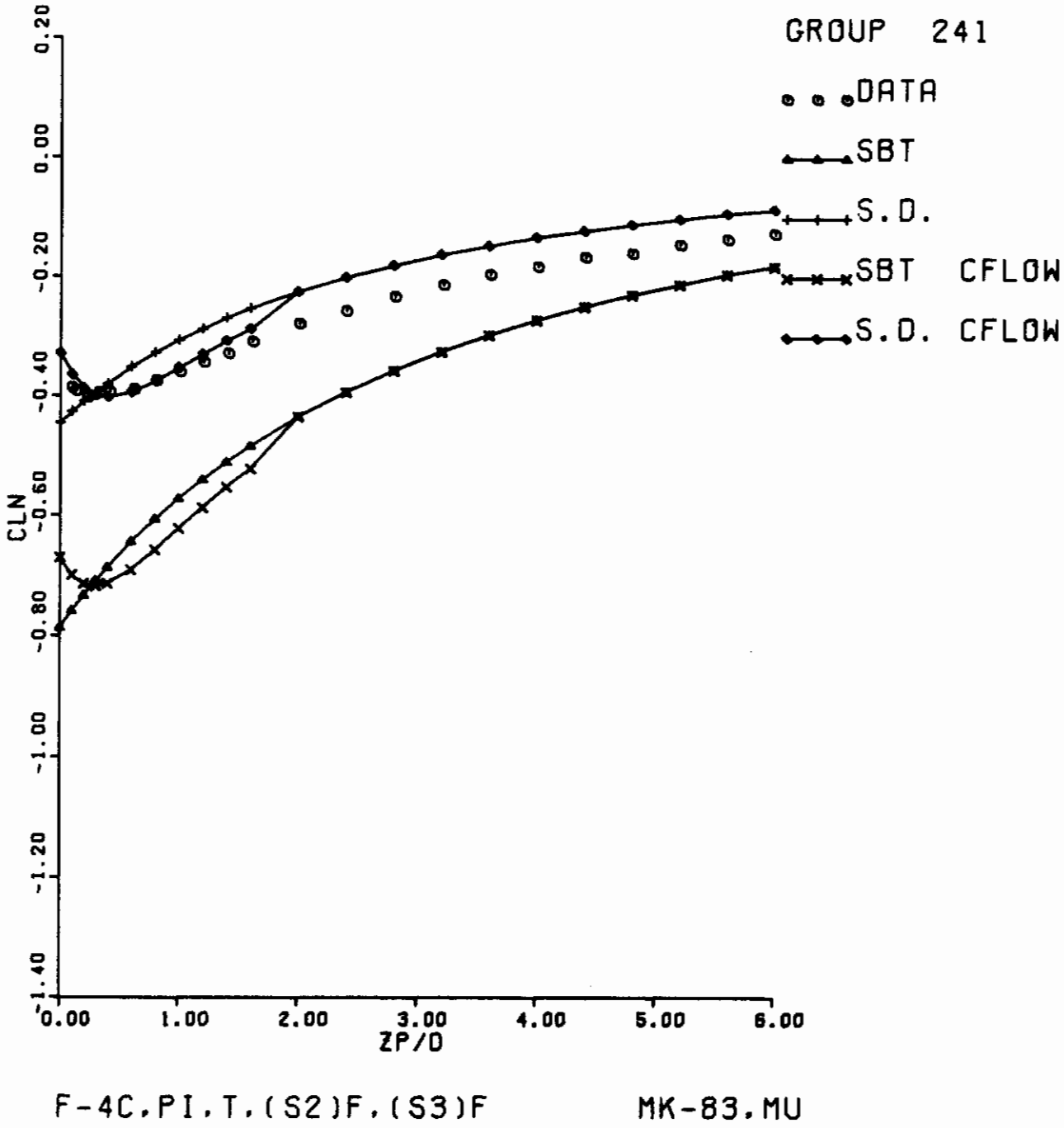

Figure 19. (Concluded) F-4C-Inboard Pylon-TER-2 Finned MK-83 Shoulder Stores Loads at $Alpha_{store}=4^{o}$ with the Modified Unfinned MK-83
(d) C_{ℓ_n} vs $Z_{P/D}$

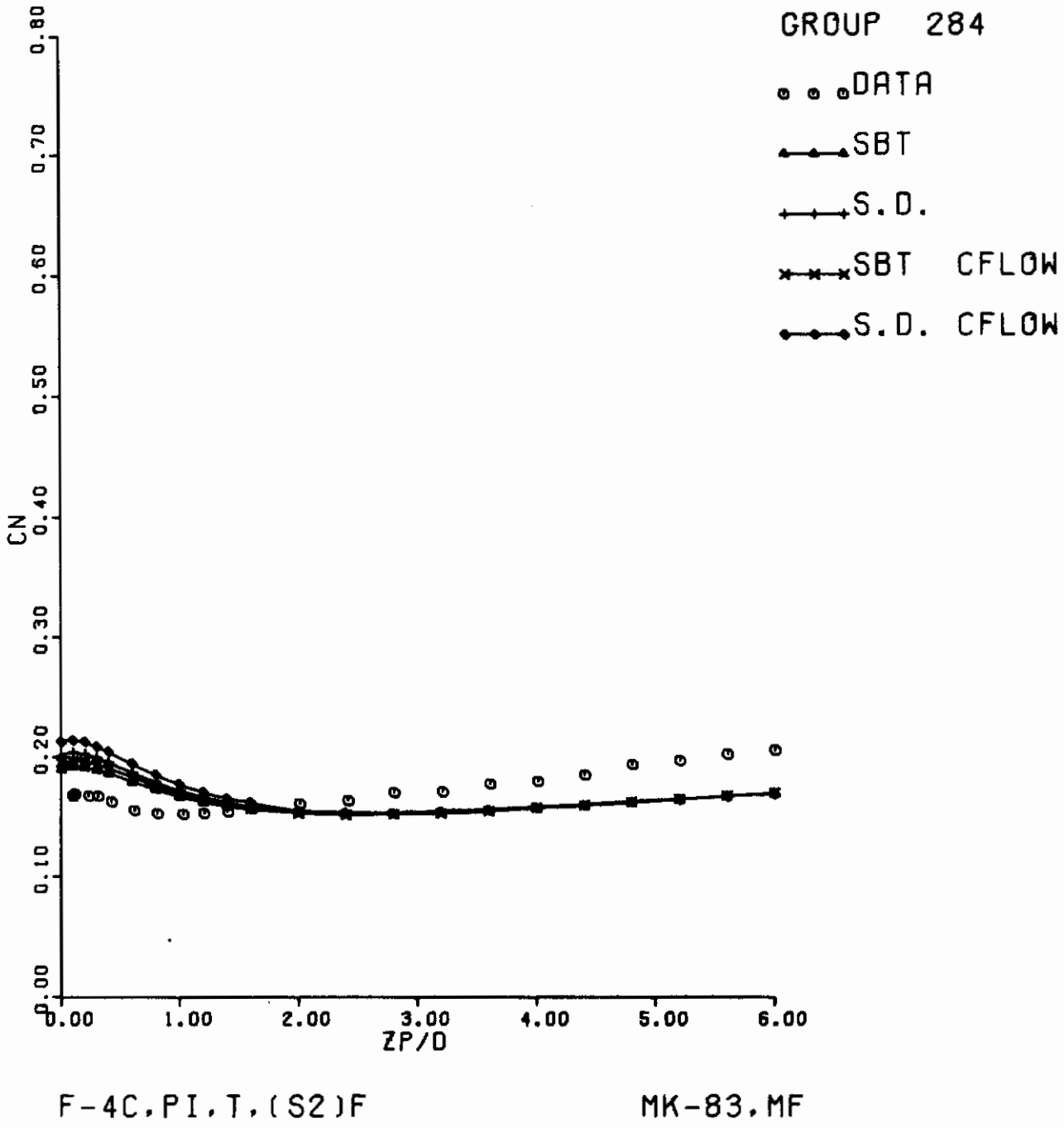

Figure 20. F-4C-Inboard Pylon-TER-Finned MK-83 at TER Station 2 Loads at $Alpha_{store}=5^{o}$ with the Modified Finned MK-83
(a) C_n vs $Z_{P/D}$

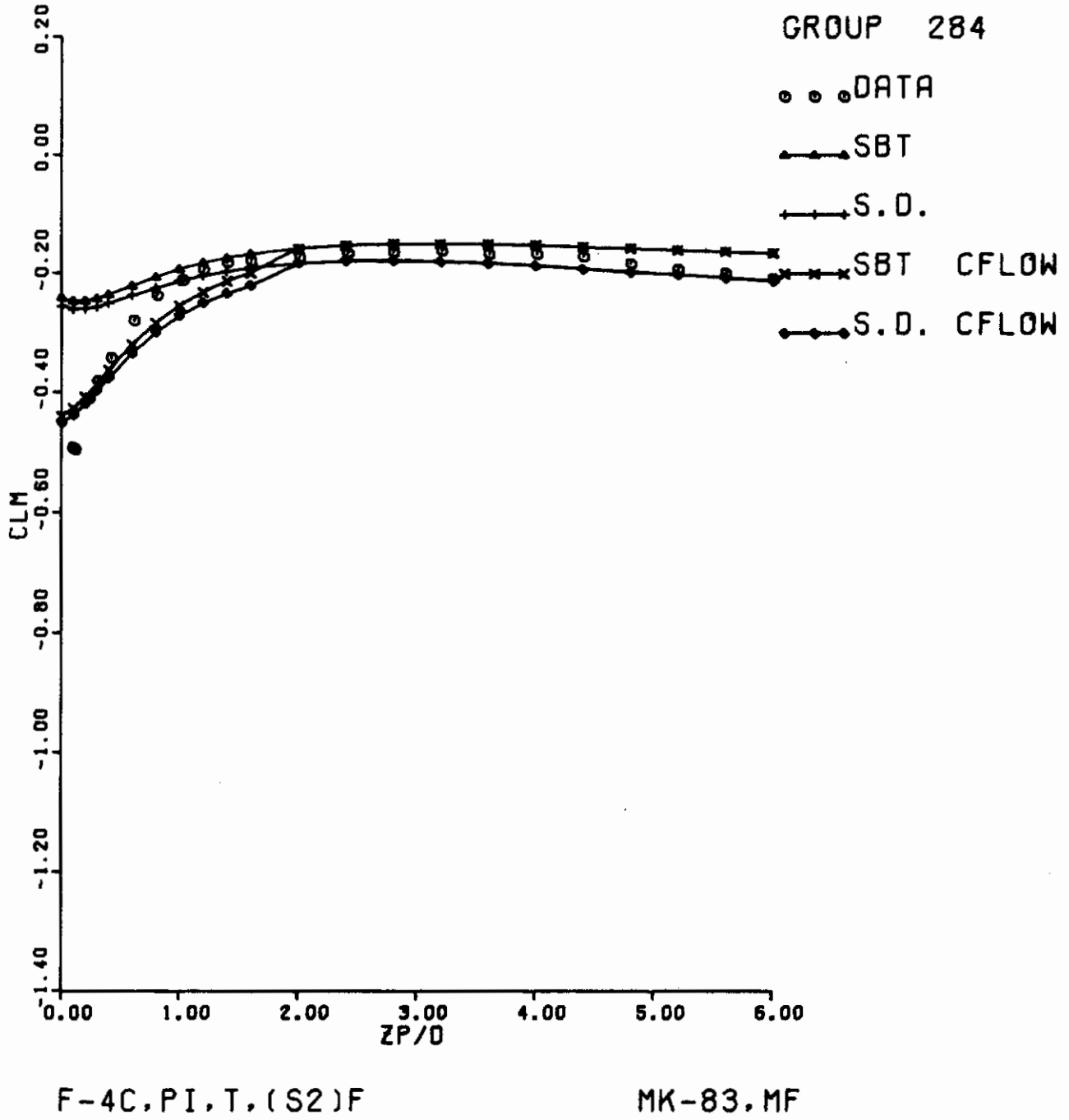

Figure 20. F-4C-Inboard Pylon-TER-Finned MK-83 at TER Station 2 Loads at $Alpha_{store}=5^{o}$ with the Modified Finned MK-83 (Contd)

(b) C_{ℓ_m} vs $Z_{P/D}$

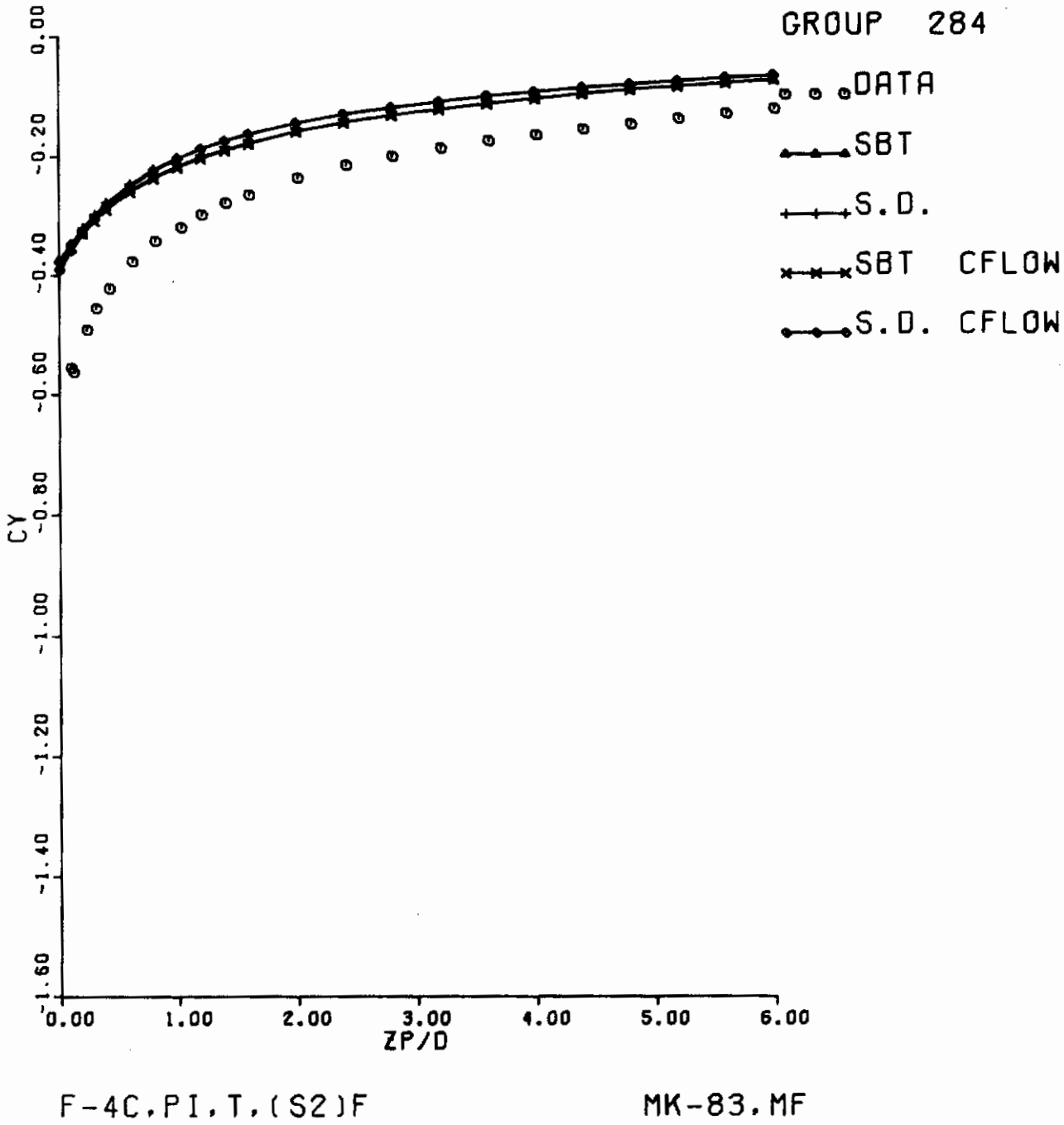

Figure 20. F-4C-Inboard Pylon-TER-Finned MK-83 at TER Station (Contd)
2 Loads at $Alpha_{store}=5^{o}$ with the Modified Finned MK-83
(c) C_y vs $Z_{P/D}$

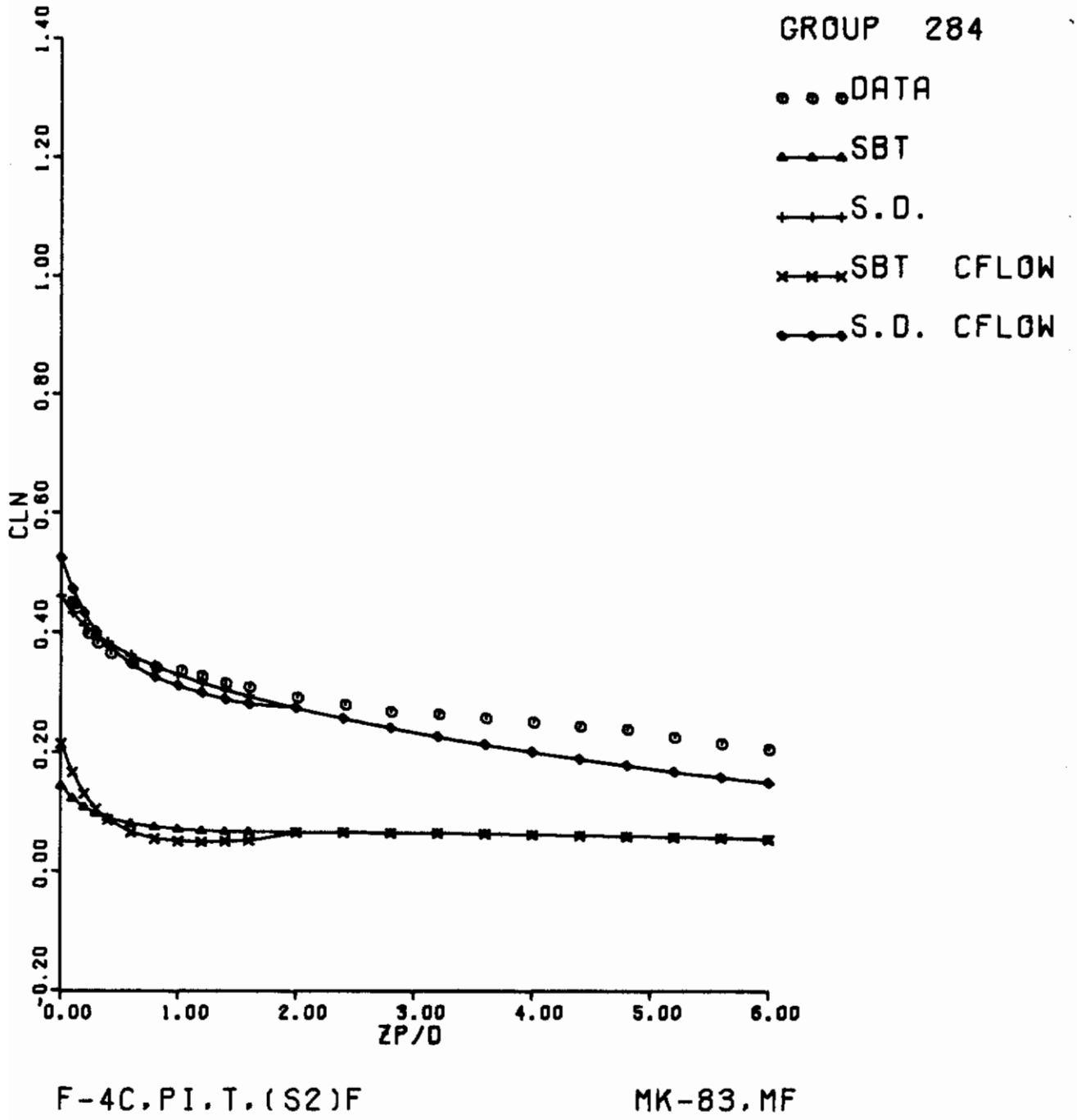

Figure 20. (Concluded) F-4C-Inboard Pylon-TER-Finned MK-83 at TER Station 2 Loads at $Alpha_{store}=5^{o}$ with the Modified Finned MK-83 (d) C_{ℓ_n} vs $Z_{P/D}$

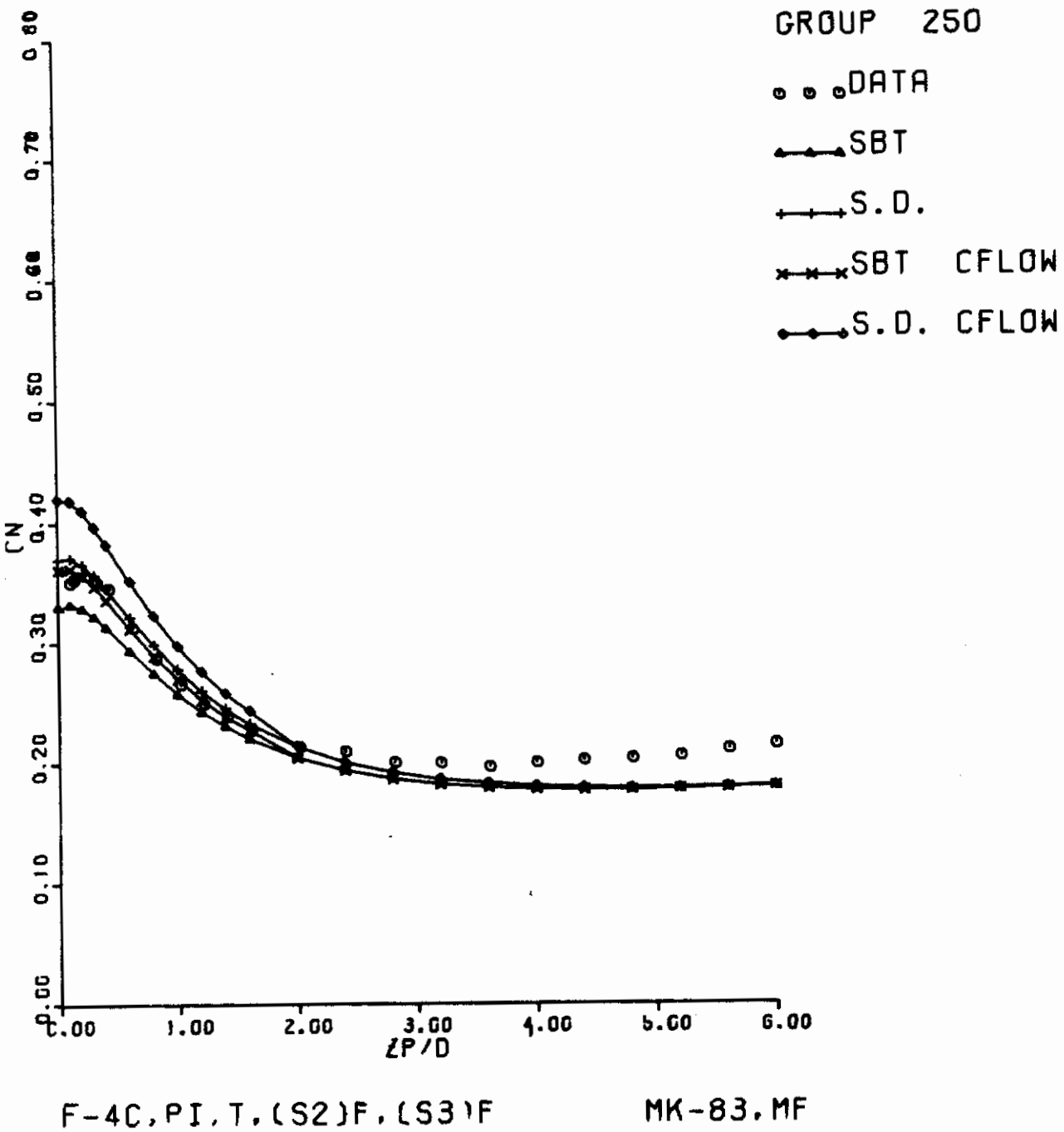

Figure 21. F-4C-Inboard Pylon-TER-2 Finned MK-83 Shoulder Stores Loads at $Alpha_{store}=4^{o}$ with Modified, Finned MK-83
(a) C_n vs $Z_{P/D}$

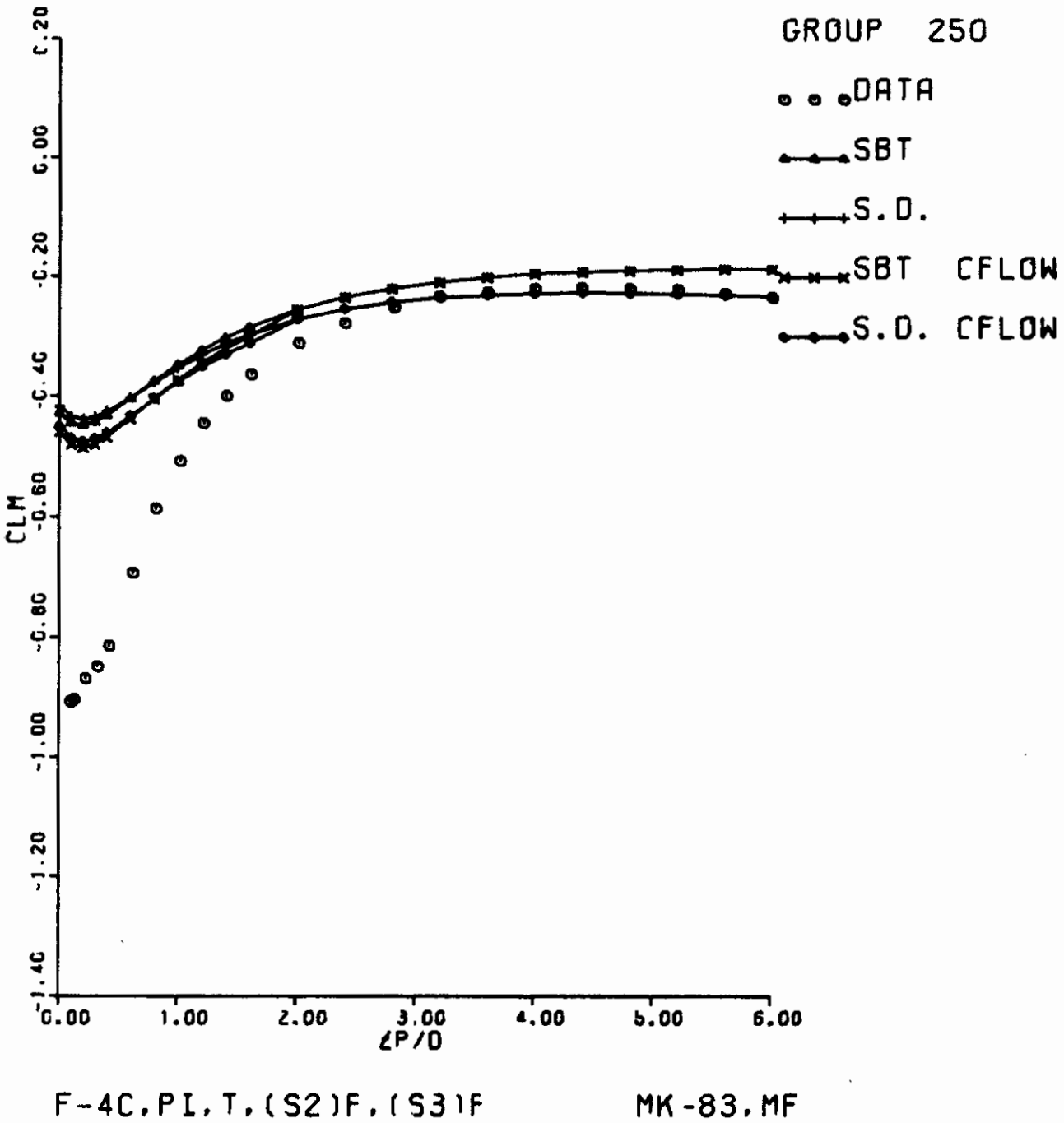

Figure 21. (Contd) F-4C-Inboard Pylon-TER-2 Finned MK-83 Shoulder Stores Loads at $Alpha_{store}=4^{o}$ with Modified, Finned MK-83
(b) C_{ℓ_m} vs $Z_{P/D}$

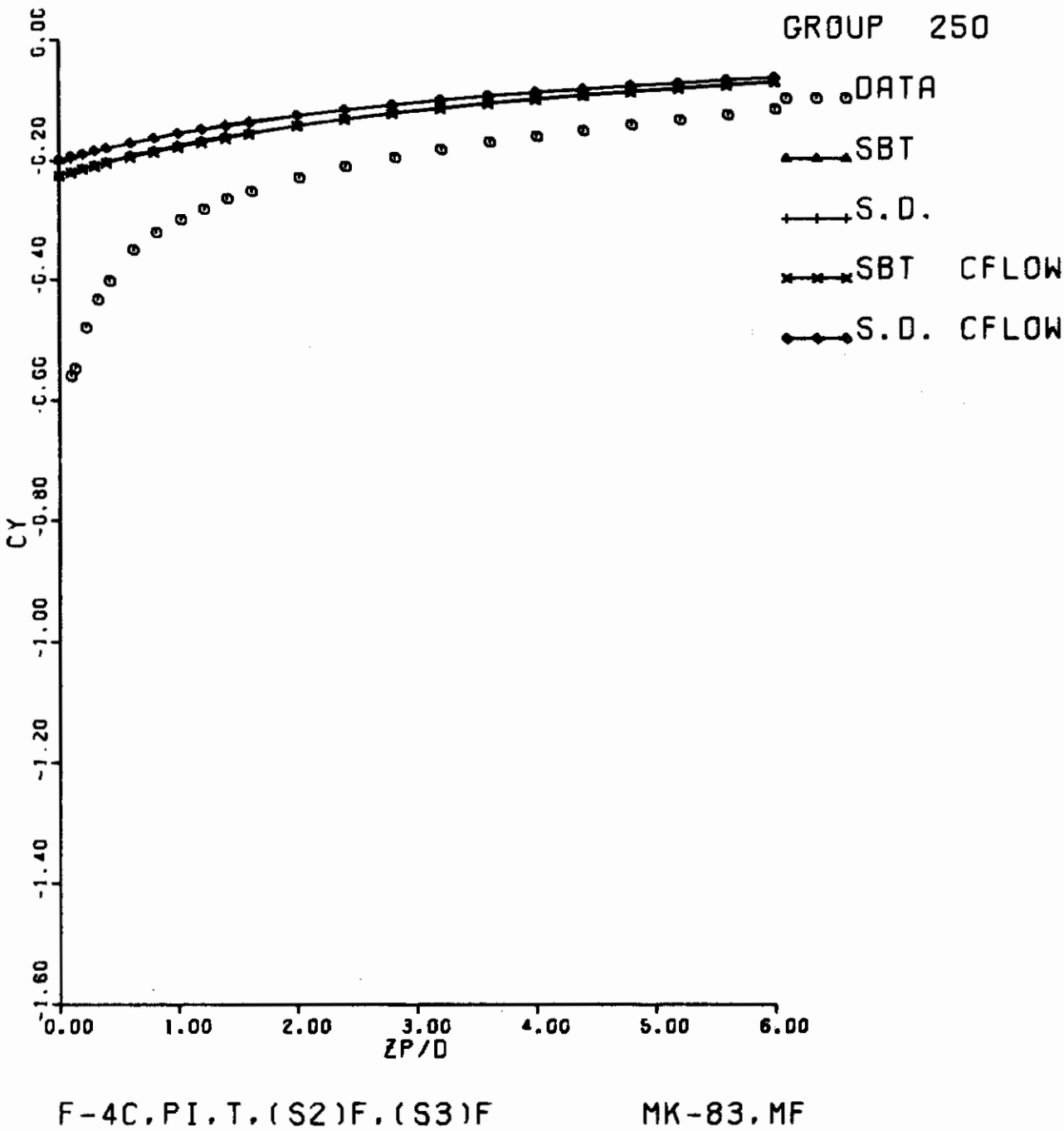

Figure 21. (Contd) F-4C-Inboard Pylon-TER-2 Finned MK-83 Shoulder Stores Loads at $Alpha_{store}=4^{o}$ with Modified, Finned MK-83

(c) C_y vs $Z_{P/D}$

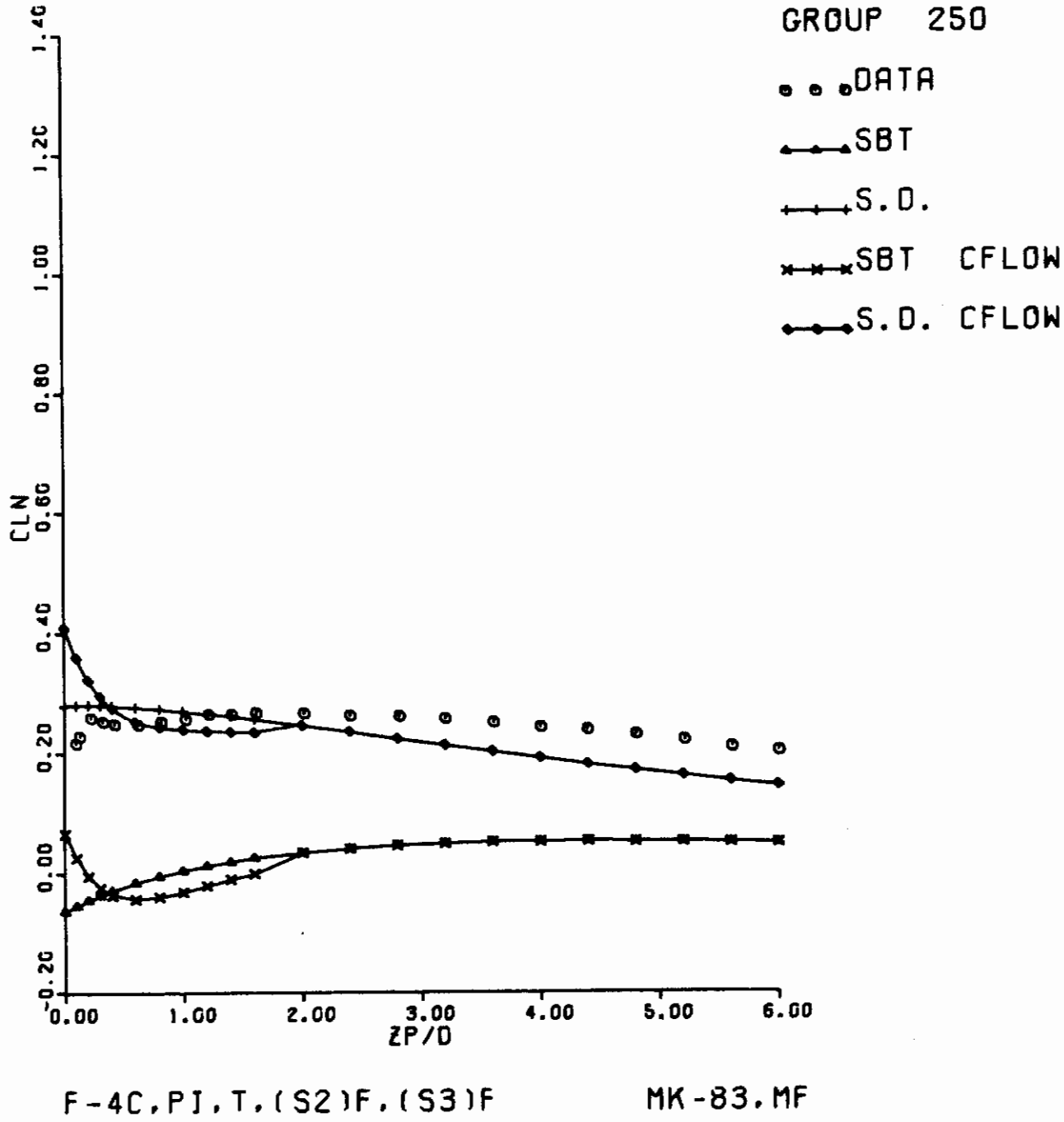

Figure 21. F-4C-Inboard Pylon-TER-2 Finned MK-83 Shoulder Stores (Concluded)
Loads at $Alpha_{store}=4^{o}$ with the Modified, Finned MK-83
(d) C_{ℓ_n} vs $Z_{P/D}$

REFERENCES

1. Goodwin, F.D., Dillenius, M.F.E., and Nielsen, J.N.: Prediction of Six-Degree-of-Freedom Store Separation Trajectories at Speeds up to the Critical Speed. Volume I - Theoretical Methods and Comparisons with Experiment, Air Force Flight Dynamics Laboratory, Wright-Patterson AFB, Ohio 45433, Technical Report AFFDL-TR-72-83, Vol. I, October 1972.

2. Karamcheti, K.: Principles of Ideal-Fluid Aerodynamics, Wiley and Sons, Inc., New York, 1966, Chapt. 20.

3. Goodwin, F.K., Nielsen, J.N., and Dillenius, M.F.E.: A Method for Predicting Three-Degree-of-Freedom Store Separation Trajectories at Speeds up to the Critical Speed, Air Force Flight Dynamics Laboratory, Wright-Patterson Air Force Base, Ohio 45433, Technical Report AFFDL-TR-71-81, July 1971.

4. Goodwin, F.K., and Dillenius, M.F.E.: Extension of the Method for Predicting Six-Degree-of-Freedom Store Separation Trajectories at Speeds up to the Critical Speed to Include a Fuselage with Noncircular Cross Section. Vol. III - Users Manual for the Computer Programs, Air Force Flight Dynamics Laboratory, Wright-Patterson Air Force Base, Ohio 45433, Vol.III, November 1974.

5. Dillenius, M.F.E. and Nielsen, J.N.: Prediction of Aerodynamics of Missiles at High Angles of Attack in Supersonic Flow. Office of Naval Research Annual Report October 1975.

6. Liepmann, H.W. and Roshko, A.: Elements of Gasdynamics. John Wiley and Sons, Inc., New York, 1957, p. 55.

7. Bergrun, N.R. and Goodwin, F.K.: Data Report for the External Stores Test Program. Volume II - First Tunnel Entry Force and Moment Data. Nielsen Engineering and Research, Inc., NEAR Rep. TR 24, Oct 1970.

8. Bergrun, N.R. and Goodwin, F.K.: Data Report for the External Stores Test Program. Volume III - First Tunnel Entry Pressure and Load Distribution Data. Nielsen Engineering and Research, Inc., NEAR Rep. TR 24, Oct 1970.

9. Bergrun, N.R. and Goodwin F.K.: Data Report for the External Stores Test Program. Volume IV - Second Tunnel Entry Flow Field Survey Data. Nielsen Engineering and Research, Inc., NEAR Rep TR 24, Oct 1970.

10. Dix, R.E.: Influence of Sway Braces and Mounting Gaps on the Static Aerodynamic Loading of External Stores. AEDC-TR-77-117, February 1978.

REFERENCES (Concluded)

11. Goodwin, F.K. and Nielsen, J.N.: Experimental and Theoretical Study of Flow Fields and Store Forces in Close Proximity to a Triple Ejection Rack at Transonic Speeds, Naval Weapons Center Technical Report, to be published.

12. Hesketh, A.A.: A Wind Tunnel Test to Study the Mutual Interference of Multiple Bodies in the Flow Field of the F-4C Aircraft in the Transonic Speed Range, AEDC-TSR-79-P79, December 1979.